A Discrete Model of Oil Recovery

G. González-Santos
Departamento de Matemáticas, ESFM-IPN
Unidad Profesional Adolfo López Mateos
Col. San Pedro Zacatenco 07738 México D. F.
e-mail:gsantos@esfm.ipn.mx

C. Vargas-Jarillo
Departamento de Matemáticas, CINVESTAV
Av. Instituto Politécnico Nacional 2078
Col. San Pedro Zacatenco, 07000 México D. F.
e-mail:cvargas@math.cinvestav.mx

Abstract

We propose the simulation of a oil recovery by means of a molecular type approach. By using a finite set of particles under the interaction of a Lennard-Jones type potential we simulate the behavior of a fluid in a porous media, and we show under certain conditions the fingering phenomena appears.

Introduction

In this work we propose the simulation of oil recovery by means of a molecular type approach. This means that we consider the materials to be composed of a finite number of particles, which are approximants for molecules. Porous flow is studied qualitatively under the assumption that particles of rock, oil and the flooding flow interact with each other by means of a compensating Lennard-Jones type potential. We also consider the system to be under the influence of gravity. We study miscible displacement in an oil reservoir from various sets of initial data. The velocity and the rate of injection of the ingoing particles proved to be among the most important parameters that can be adjusted to increase the rate of production. It is noted also that the fingering phenomenon is readily detected. The influence of gravity is important, since it affects fingering and increases the time that the oil particles take to go out.

Model formulation

Consider a rectangular region *R*, which is a porus medium. We assume that in this region we have a resident fluid or oil. We shall introduce a different kind of fluid which, as a matter of convenience, will be called water, although it is an aqueous solution which could be a polymeric solution, surfactant solution or a brine. The physical system consists of

$N = N_1 + N_2 + N_3$ particles

$$P_1, P_2, ..., P_N,$$

With masses

$$m_1, m_2, ..., m_N .$$

The particles

$P_1, P_2, ..., P_{N_1}$, Represent rocks,

$P_{N_1+1}, ..., P_{N_1+N_2}$, Oil, and

$P_{N_1+N_2+1}, ..., P_N$, Incoming water

For purposes of injection of water and production of oil, two wells are opened, one in the bottom left corner of *R*, for injection, and other in the diagonally opposite corner for production.

At time $t = k\Delta t,$

$\bar{r}_{i,k}$ Coordinates of the particle P_i,

$r_{i,j,k}$ Distance between the particles P_i and P_j,

$\bar{v}_{i,k}$ Velocity of the particle P_i,

$\bar{a}_{i,k}$ Acceleration of the particle P_i,

$\overline{F}_{i,j,k}$ Local force exerted on P_i by P_j,

$\overline{F}^*_{i,k}$ Local force acting on P_i due to the other particles

$\overline{f}_{i,k}$ Long range force acting on P_i (like gravity),

$\overline{F}_{i,k}$ Total force on particle P_i

for i=1,2, . . . , *N* and *k* 0, 1, …

The local force $\overline{F}_{i,j,k}$ exerted on P_i by P_j is

$$\overline{F}_{i,j,k} = m_i m_j \left[\frac{H_{i,j}}{r_{i,j,k}^{q_{i,j}}} - \frac{G_{i,j}}{r_{i,j,k}^{p_{i,j}}} \right] \frac{\bar{r}_{j,k} - \bar{r}_{i,k}}{r_{i,j,k}} \quad \ldots(1)$$

where the values of the parameters $H_{i,j}$, $G_{i,j}$, $q_{i,j}$ and $p_{i,j}$ depends on the particles which are interacting. The total local force $\overline{F}*_{i,k}$ acting on particle P_i due to the other particles is given by:

$$\overline{F}*_{i,k} = \sum_{j=1, j\neq i}^{N} \overline{F}_{i,j,k}$$

So the total force acting upon the particle P_i is

$$\overline{F}_{i,k} = \overline{F*}_{i,k} + \overline{f}_{i,k}$$

The aceleration of P_i is related to the force by Newton´s Law

$$\overline{F}_{i,k} = m_i \overline{a}_{i,k} \qquad \text{....(2)}$$

In general system (2) can not be solved analytically from given initial positions and velocities, therefore it must be solved numerically. For economy, simplicity and relatively numerical stability we use the" leap frog" formulae, which is second-order accuracy in time.

$$\overline{v}_{i,1/2} = \overline{v}_{i,0} + \frac{1}{2}\overline{a}_{i,0}\Delta t$$

$$\overline{v}_{i,k+1/2} = \overline{v}_{i,k-1/2} + \frac{1}{2}\overline{a}_{i,k}\Delta t$$

$$\overline{r}_{i,k+1} = \overline{r}_{i,k} + \frac{1}{2}\overline{v}_{i,k-1/2}\Delta t$$

For *i=1,2,…,N*, and *k=1,2,…*

The number of calculations required to evaluate (1) at each iteration is $O(N^2)$. However this number is much smaller if the potential is truncated after a distance r_c.

Boundary conditions

We assume the when the particles of the fluids interact with the walls of the region *R*, a velocity damping factor, δ_i, will be necessar**y** to model the hardness of the wall relative to the reflection of the interacting fluid. This is done by using the following parameters:

$$\delta_i = 0.4 \text{ for } i = N_1 + 1,..., N_1 + N_2$$
$$\delta_i = 0.8 \text{ for } i = N_1 + N_2 + 1,..., N$$

Initial conditions

The rock and oil particles were set up at the initial time in sucha way that they satisfied an equilibrium state, as shown in Fig. 1.

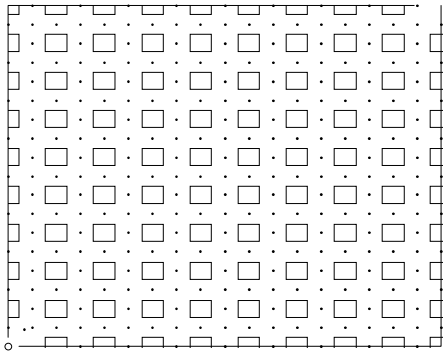

Fig. 1. Initial configuration

Numerical results

The figures 2 to 4 show the system evolution. All the examples were run with time step $\Delta t = E-5$ on the Sun workstation Ultra 60, the distance between particles of water before going to into the well was $d = 0.5$ and their velocity was $v = 15.0$. The gravity constant was equal to $g = 9.8$.

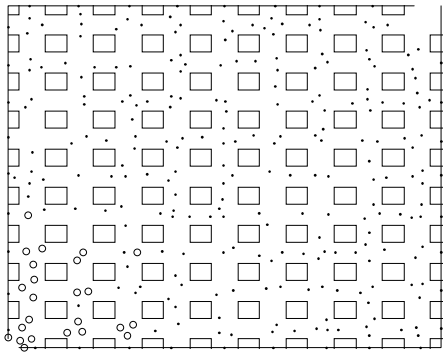

Figure 2. Time=0.8

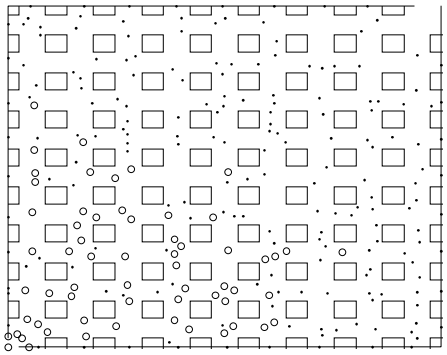

Figure 3. Time=2.0

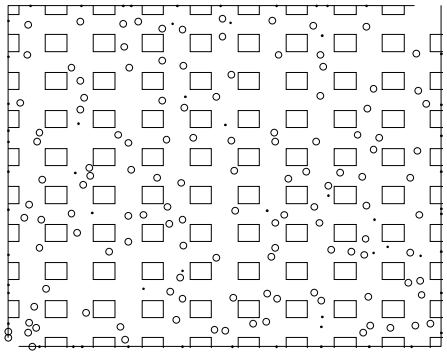

Figure 4. Time=4.8

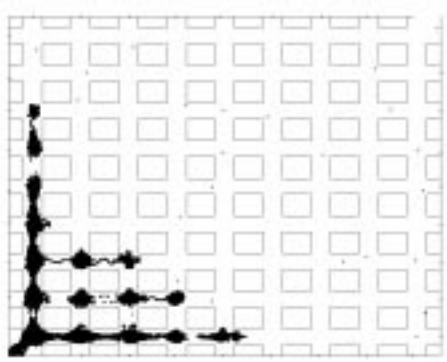

Figure 5. Advancement of the water for d=1, v=5 and Time=1.2.

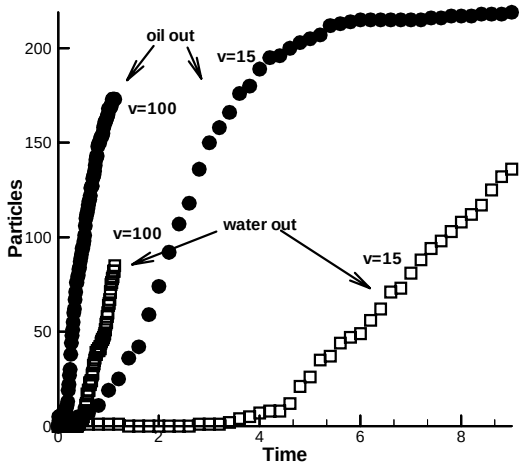

Figure 6. Comparison of the effect of the velocity of the water particles on the oil and water production.

AN INTEGRATED STUDY TO EVALUATE FLUID MONITORING CAPABILITY OF TWO TIME-LAPSED 3D SEISMIC DATA SET AT MARLIM FIELD

Carlos Eduardo B. de S. Abreu, Petrobrás-E&P,
ceduardoabreu@petobras.com.br
Ricardo Tarabini Castellani, Petrobrás-Cenpes,
tarabini@petrobras.com.br

ABSTRACT

Since 1997, with acquisition of a new seismic detector 3D for studies of reservoirs, Marlim Field has become the unique oil field at Campos Basin with two seismic surveys. In view of the natural congestion by production equipment, geometry and acquisition parameters were different from those used in the first survey (old volume), acquired in 1986 by the exploration of the Company. This project was to respond if the anticipated production of oil and the total volume of injected water would have been sufficient to generate seismic marks that could stand out concerning the expected noises associated with such unequal acquisitions.

In this work a multi-disciplinary study based on simulation of fluid flow and seismic modeling incorporating characteristic features of the Marlim field based on the reinterpretation of Marlim pseudo 4D showed that a major part of the differences encountered on the maps, is probably associated to artifacts generated by remarkable geologic events such as the fault that limits the field at the east board and Marlim Canyon. The unsuccessfulness of this new-old pair is associated to the small volume of injected water and the proximity of the injecting area with the major fault on the field board. In view of the nature of the reservoirs (bright spots of oil), the continuity of efforts to monitoring water fronts should be held in this field and the year 2003 was considered ideal for a new acquisition, regarding the water volume and the difficulties of reduction or elimination of the fault artifacts.

INTRODUCTION

While the secondary recovery process through water injection was initiated already 2 years before this new survey and due to the fact of behavior of the reservoir as oil bright spots, it was decided to check the possibility of using two quite different surveys for monitoring of the water injection. As an additional motivation, the recovery process through water injection is used in the earlier stages in the majority of the Companies large oil fields and the survey of new seismic activity is becoming a standard for studies of reservoirs.

The detection feasibility is analyzed by Dillon and others (1998) showing that an addition of up to 7% can be expected in the acoustic impedance in the case of substitution of oil with water. Although considering these chances as not very relevant, challenge for the success of this attempt would be undoubtedly the 1997 data processing in order to minimize the differences of the earlier acquisition. Gomes and others (1998) concluded that the considerable differences of the 2 seismic surveys did not disable the performance of the 4D studies, but caused additional difficulties. Besides presenting the data processing and equalization stages for the 4D studies, criteria were defined for the preparation of indicative maps of fluid moving. Based on such maps the authors concluded that monitoring of fluid content in Marlim reservoir through 4D analyses is feasible and they believe that the quantification of the secondary gas cover thickness, as well as the delimitation of the injected water front only depends on the performance of systematic studies of seismic models.

Although these results signalized in a positive way, the final maps based on other attributes present countless ambiguous features, even with no intervention or with amplitudes contrary to the foreseen in areas where the intervention would have been maximum at the time of the survey. According to Gomes and others use of the same stacking and migration velocities in different surveys can cause minor distortions of positioning of the seismic reflections and thus, these features could impregnate the maps of differences with artifacts. Castellani and Abreu (2000) present in detail the steps followed for the 4D modeling, which intended to check the variation of various seismic attributes such as oil-water contact rise and thickness reduction, which occur at Marlim field due to the presence of an extensive canyon. Figure 1 shows the differences maps transposing the original interpretation for the new volume On the right portion of this figure is shown the result when the data has been picked following subtraction of the traces.

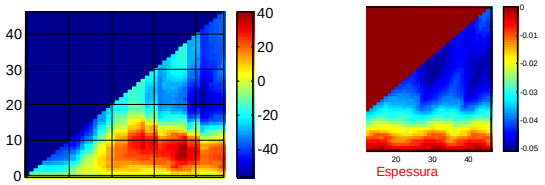

Figure 1. *Variation of the amplitude of the bottom reservoir zone in function of the thickness and height of the oil-water contact. On the left side transposing the picking (percentual variation) and on the right side the volume of differences, where the variation is always negative.*

What is noted is that the ambiguous behavior, where both positive and negative differences can be

expected occurs in the case of the simple transposition of the surface mapping the positive peak of the amplitude of the base on the wedge model based on real well. However, when you map on a wedge of differences this ambiguity ceases and the differences encountered for the reflection at the base are integrally present with the negative signal, showing the decrease of acoustic impedance contrast at the outlet of the reservoir in function of the substitution. Although in practice the latter way of mapping presents the major difficulty of performance, it is the one which more approaches the foreseen based on acoustic impedance variation.

We submit here below the main conclusions of model 4D which directly affect the work of the 4D interpretation:

- In function of the tuning of the oil-water contact and of not deterministic internal heterogeneities to the reservoir the interpretation of a 4D is not trivial as suggested by the analysis based on the variation of impedance and some attributes such as the ones related to the top of the reservoir and the time of zero-cross present rather limited efficiency.
- The chances of detecting water fronts increase with the increase of data resolution.
- Concerning the attributes relative to the bottom of the reservoir the thicker the reservoir the better for the detection of water fronts. The use of more than one attribute is highly advisable, mainly the ones related to the variation with the offset as Ro, Gradiente and the product of both.
- The use of models is fundamental to interpret data of this nature. To expect locally differential response in function of the distinctive characteristics of each well.

3- INTERPRETATION

The maps of differences obtained presented values with both polarities. This occurred in the proximity of the injection area, but also at distant locations where the occurrence of differences was not expected, clearly indicating the influence of countless other factors not related with substitution of fluids. A good exercise which shall precede any interpretation of maps of differences 4D is to attempt in getting an idea of the dimensions of these areas candidates for water fronts. At least one data is known by engineering, that is the total volume of water injected in each well. This amount reached the value of 1,200,000.00 cubic meters in one or two wells. Considering that the average thickness in the injection areas is approximately 80 meters, we come across some values of the possible expansion areas of the water front, as shown in Table 1. In the light of the exercise and of the modeling presented showing that when the contacts meet less than 10 meters above the base, the chances of detection of water fronts with data sampled in 4 meters are reduced, a sort of guide is created to distinguish what may be effect of substitution and what may be the result of the acquisition and/or processing artifacts. For different rises of the contact we have different areas associated to the water fronts, whose diversity based on the size of the field and the area of substitution of both volumes is illustrated in Figure 2. Figure 3shows the comparison of some of these areas with the sizes of the anomalies checked on the map of differences of the arnp1.itude of the base. Thus, we are interested in variations whose area on the map of differences present a size similar to the one shown by the red square in said figure.

Vh = Vr x phi x (1-Sor)
Vr = 1.200.000 / [0.3 x (1 - 0.4)]
espessura média = 80 metros
Sr = Vr / e ; Sr = 6.700.000 / 80
Sr = 84.000 m2 ; Lr = 289 m

O/A	S	L (m)	%	CDP	Linhas
80	8.33E+04	289	2.6	12	4
20	3.33E+05	577	5.2	23	8
10	6.67E+05	816	7.4	33	11
5	1.33E+06	1155	10.4	46	15
1	6.67E+06	2582	23.3	103	34
3D	1.05E+08	10247	92.4	410	137
Campo	1.23E+08	11091	100.0	444	148

Table 1: *Possible areas (S) of expansion of water fronts for different rises of the oil/water contact (O/A} for a stationary thickness of the reservoir (e = 80 meters}. Vr is the volume of rock associated to volume of pores which received the 1,200,000 m3 of water. Sr and Lr are respectively area and sides of a parallelepiped with 80 meter thickness. CDP and lines refer to the number of cdps and llines for each value of L. Sor is the saturation of residual oil.*

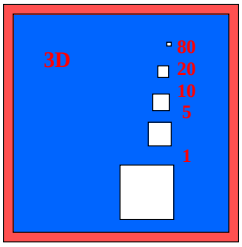

Figure 2: *Areas based on Table 1 and positions of the oil/water contact related to the base of the reservoir. The non- residual oil is totally substituted.*

In order to investigate the efficiency of the equalization of the new volume with the old one, a level pertinent to the equalization window, however above the reservoir, has been mapped, we have tried to capture artifacts affecting equally the volume of differences. Assuming such areas as of global character it would be possible to correct the maps to the level of the reservoirs. The confection of the map of the differences of amplitude of the base shown below, has been performed taking into account the interpretations in the two volumes and the result of the subtraction has been submitted to this additional correction. Figure 4 shows the map of reason of amplitude obtained through mapping of the referred level above the area of the reservoir in the

two volumes. The prevalent green color on the map of reason signifies values around the ideal value, i.e., the unit, from 0,5 to 1,5.

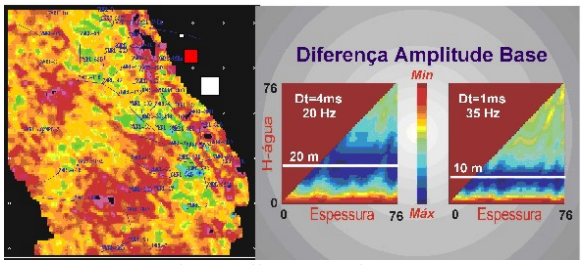

Figure 3: *Map of the differences of amplitude at the base and the squares representing contacts 80, 20 and meters from the base. Note that the modeling has shown 9 a better possibility of detecting substitution, when the contact reached the 20 meters (red square), considering the new-old pair, in other words for 4 meters of sampling (graphs on the right). The map of differences of the amplitude of the base has undergone a correction (see text). Note that differences with positive and negative signals persist in situations near and distant from the injection area (central part of the east board of the field).*

In the upper left portion of the map appears a large blue area where the amplitude of the new data is approximately 2 times the one checked in the old seismic data. On the right side of the figure is shown the indicative map of fluid moving, generated from the differences of the reason of amplitudes between top and base taken in the new reprocessed and old volumes by Gomes and others (1998). According to the authors, such attribute would characterize the anomalies with reflex of the presence of gas covers. Note the great geographic coincidence of these anomalies with the areas of reason 2. Such fact suggests that these anomalies have also great chances to be an artifact, and accordingly do not have any relation of the substitution of fluid.

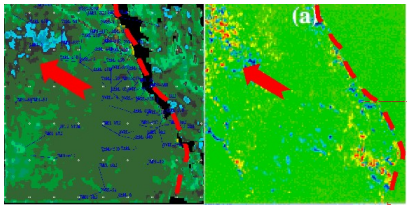

Figure 4: *Map of reason of amplitude (left) on a level above the reservoir for detection of a global standard of differences not associated to the replacement of fluids. Note the geographic coincidence between the blue area (reason = 2) at the upper left position of this map with an area interpreted as indicating the presence of gas (right). The traced lines show the contour of the failure of the board. Note that the scale of colors used on the map (right) only emphasizes great differences.*

Figure 5 shows a seismic line where the two principal features can be seen, one of structural and the other of stratigraphic character, generators of artifacts. They are respectively the failure of the board and Marlim Canyon. As the surveys were obtained in rather distinct directions, the trajectories to image the failure and points below its surface were also obtained. This has generated another artifact in the computation of the differences. Thus, on any map of differences of any attribute will be possible to note a range of differences exactly accompanying the tracing of the failure of the board and the area of the canyon. As engineering has positioned the great majority of important injectors, exactly over this noisy range associated to this failure without reducing this problem of the failure of the board, any and all effort to treat these two volumes as a 4D becomes practically useless. If the problem of migration and/or use of the same speed has been critical to generate a range of noises exactly if the extension of the failure in its high block generated a shade over the reflections in the area of the reservoir, a similar problem occurs along the Marlim Canyon. This figure shows the map of the differences of the first zero-cross above the reflection of the base, also from Gomes and others report modified herein with the introduction of an arrow indicating the anomalous area interpreted as moving of fluid, in this case water.

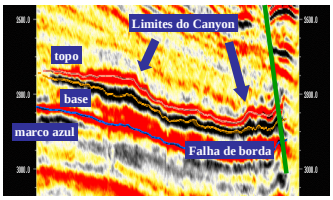

Figure 6: *Seismic line with the principal structural and statigraphic features of Marlim field (see location of the line on the map of Figure 7).*

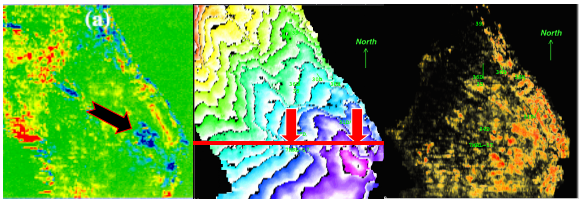

Figure 7: *Map of the differences of the first zero-cross above the reflection of the base (left) extracted from Gomes and others (1998). In the center, the structural map in time of the top of the reservoir shows the Marlim canyon. The red line shows location of the seismic line illustrated in Figure 6 and the arrows indicate the limits of the canyon. On the right side, there is the visualization of the negative differences symmetrical to the reflection at the base of the reservoir made with the VoxeoGeo program of Paradigm.*

Figure 7 presents on the right side the substraction of the two volumes with opacity for negative differences above a certain value, made with VoxeoGeo software of Paradigm. Comparing this map with the map of the center it is noted that the great variations are associated to the failure of the board and the Marlim canyon. The logical conclusion is that it would be necessary to minimize very much the possible

artifacts described herein. So that any interpretation intended to monitor substitution of fluids can be attempted with this pair of surveys. Finally, the real possibility that the volume of injected water at the time of the second survey was still incipient to enable its detection does not justify the assertion that no more effort shall be involved in order to minimize these artifacts through new processing or other treatment. This step is very important for a future acquisition because the same features will be present there and probably no even one could repeat today exactly the same geometry of acquisition of 1997.

4- COMMENTS ON A NEW ACQUISITION

Regarding a new survey it is important to decide the optimum time of performance thereof. This question may be answered in various way, but the estimate shown herein is mainly grounded on aspects exclusively connected to seismic and the experience with models and data of this nature in the field. The extrapolation of the flow simulation based on petrophysical models and fluids with updated responses well adjusted to the production histories is the unique supply available to make this forecast, this also may seem conflicting since the seismic monitoring proposes correction of possible errors carried in the simulator. Considering an injection well and a horizontal producing well, the flow simulator shows the formation of cones over the wells, With major saturation at the base of the cone. Only later on occurs the occupation of the "tank" which is formed between the cones. The water saturation maps show an expansion around the wells,
with areas which reduce with the deviation of the base (L12 and top Ll). Figure 8 shows this behavior for 3 different times on the upper part, with start of the injection in December 1996 and October 1999. Observing such, we have noted that the distribution of the original aquifer hardly did not change up to December 1996 and that the same is practically concentrated along the failure of the board due to the dive in this direction. For this reason and due to the larger thickness of the major part of the injectors is located adjacent to the failure. The average thickness of each .layer is 10 meters and it is noted that the areas with contact of approximately 20 meters would be insignificant, leaving remote chances of detection of the water fronts. The distribution of the fronts up to October 1999 shows a larger expansion of the overlying layers, however, the question is the fact that this expansion is not sufficient to dominate other areas apart from the failure. On the lower portion of Figure 8, we have some sceneries of the evolution of the water injection in the basic layer for three occasions in the future by extrapolation of the simulation for the month of December of the years 2000, 2003 and 2015. Undoubtedly considering all the factors discussed in this report it would be more advisable to think of a new acquisition in the year 2003.

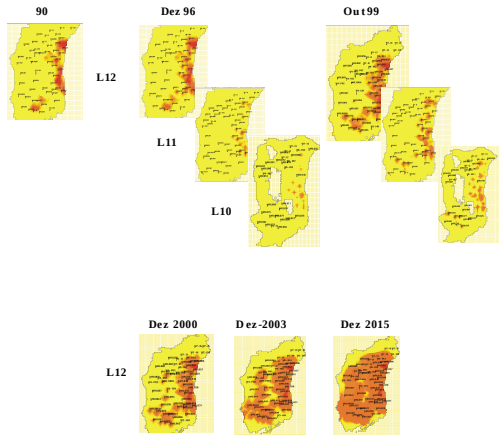

Figure 8: *Above, simulations for 3 layers in 3 occasions including the one of the second survey. Below, extrapolation of flow simulation at the basic layer (number 12) for the month of December of the year 2000 (above and left), 2003 (above and right) and 2015 (below). Note that the expansion of the water fronts occupies enormous areas distant from the failure of the east board as of 2003.*

CONCLUSIONS

The unsuccessfulness of the new-old pair is associated to the small volume of injected water and the proximity of the injecting area to artifacts generated by remarkable geologic events such as the fault that limits the field at the east board of the Field. In view of the nature of the reservoirs (bright spots of oil) in countless other fields, the monitoring studies of water fronts shall continue in this basin. Thus, new acquisition is suggested directed to the monitoring problem with similar resolution to the one considered on 1997. The year 2003 is considered ideal for a new acquisition.

BIBLIOGRAPHIC REFERENCES

Dillon, L., Vasquez, G., Bastos, A., Soares, J. A, Lira, J. E., 1998, Análise de Viabilidade Técnica para Monitoramento Sísmico 4D: Enfoque Petrofísico, II Seminário de Reservas e Reservatórios.

Gomes, A., Gerhardt, A, Filpo, E., Aquino F, Ritter,G., Schmidt , J. e Pimentel , M.,1998, Relatório 4D do Campo de Marlim, Relatório Interno da Petrobrás.

Castellani, R., T. e Abreu, C., E., B., S., Interpretação de dados sísmicos 4D – Campo de Marlim, Simpósio de Geofísica, 2000

An Interpretative Model for Naturally Fractured Reservoirs using Borehole Electrical Images

Gonçalves, C.A., LENEP/UENF, carlos@lenep.uenf.br
Drumond, E.R., LENEP/UENF, erica@lenep.uenf.br

Abstract

Structural features in a borehole have been target of reservoir analysts for over many years. Features such as naturally open fractures help interpreters not only to delineate the main structural characteristics of a reservoir, but can also help the interpretation of the main flow patterns during its characterisation.
Fractured sandstones are producing reservoirs in many giant oil and gas fields around the world. Recent hydrocarbon discoveries have evidenced that these features can create a producing reservoir even in rocks with very low primary porosity.
Detailed analysis of naturally fractured reservoirs shows that most of those reservoir rocks have anisotropic nature with regard to the fracture patterns. This may be due to different stress regimes suffered during deposition or after that. Mapping and quantifying these heterogeneities are critical for precise reservoir characterisation.
Most open-hole logs can indicate fractures, but do not provide any in-depth quantitative analysis in terms of their geometrical and petrophysical aspects. In the past, standard logging tools were able to identify some of these structural features, based mainly in the dipmeter and sonic log curves. Today, a complete characterization of these features can be obtained by borehole electrical devices. This article shows the use of this tool and discusses a tentative interpretative model for naturally fractured reservoirs with the quantification of the main reservoir geometrical and petrophysical parameters.

Introduction

Electrical borehole devices allow the mapping of sedimentary and structural features using several microresistivity measurements, and thus produce an image of the borehole wall. Featured in four, six or eight pads, the tool uses a series of electrodes to send a low frequency alternate current into the formation. The vertical resolution is as low as 5mm in modern tools, thus allowing the mapping of very low scale features in the borehole wall.
In conductive muds, these tools provide microresistivity measurements almost totally insensitive to borehole conditions and can offer quantitative information, particularly for fracture characterisation. They combine high-resolution measurements with almost fullbore coverage for standard diameter boreholes. The processed borehole images allow for the investigation of formation features such as structural dips, naturally open, healed and mechanically induced fractures, and also other sedimentary features (Gonçalves, 1999).
Recently, high-resolution borehole electrical images are obtained from the FMI* (Formation MicroScanner Imager). This tool uses arrays of small electrodes (192) pressed against the borehole wall. Sucessive and small vertical increments of the formation are examined while the tool moves up into the borehole during logging. A triaxial accelerometer helps determine tool position and three magnetometers help determine its orientation.

Naturally Fractured Reservoirs

Fractured reservoirs are generally thick, with very low primary porosity. The distribution of porosity (mainly secondary) and permeability is very irregular. They generally occur in brittle rocks, but take into account several factors such as rock type, cementation, confining pressure and strain rate.
Natural fractures usually exhibit common characteristics. They generally present a perpendicular orientation related to the formation bedding planes, although it is not always necessarily true. Some naturally open fractures are parallel to the fomation bedding planes. These features are less frequent and usually present a less areal extension than the vertical ones, but can play an important role in reservoir characterisation.
Naturally open fractures also present distinct characteristics when compared with induced fractures, mainly originated from drilling operations. Induced fractures are also open fractures, but show relatively less extension from the borehole wall than the naturally open ones.
Fracture detection and characterisation has been done by geologists and log analysts for a long date, mainly using logs such as gamma-ray with high uranium or other radioactive mineral concentration, the litho-density log recognizing thick mudcakes or borehole enlargement in front of these zones, separation between resistivity curves in front of non-permeable zones. However, any of these techniques are not able to clearly identify the presence of fractures without the help of other petrophysical or geological information. Today, electrical borehole devices

provide an effective way of solving some of the aspects of fractured reservoirs.

The Interpretative Model and their Results

The main goal of this work is to set a tentative interpretation model for fractured reservoirs using microresistivity images from borehole electrical devices. This is presented here by using data from a fractured reservoir in South America, and made available through the use of Hole A (Figure 1). This example shows an interval of 70 meters of low porosity sandstone with high fracture density in some zones. Fractures are generally open. Microresistivity images show these fractures as dark brown colors (conductive) compared with the the host rock in light yellow (more resistive).

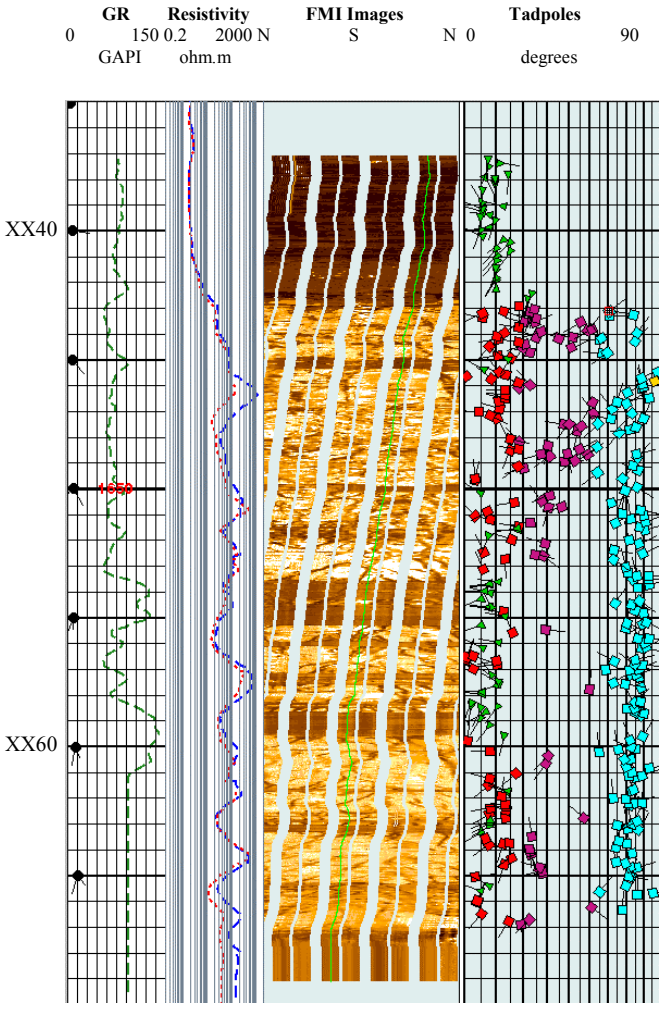

Fig. 1 – Log display of borehole electrical images for an interval of about 70 meters in Hole A with an associated interpretation.

Our interpretative model started as picking the main sedimenary features as bed boundaries and other internal bed features. Figure 1 shows on the right track green tadpoles with the orientation of bed boundaries along the interval. Bed boundaries are clearly marked as changes in the microresistivity response along the interval. Their planes (sinusoids patterns in unwrapped borehole images) are usually regular features. Bedding planes in the example of figure 1 are all low angle (dips from 0^o to 15^o) features with azimuth varying from 180^o to 300^o. Very few measurements are observed between 320^o and 360^o of azimuth (figure 2).

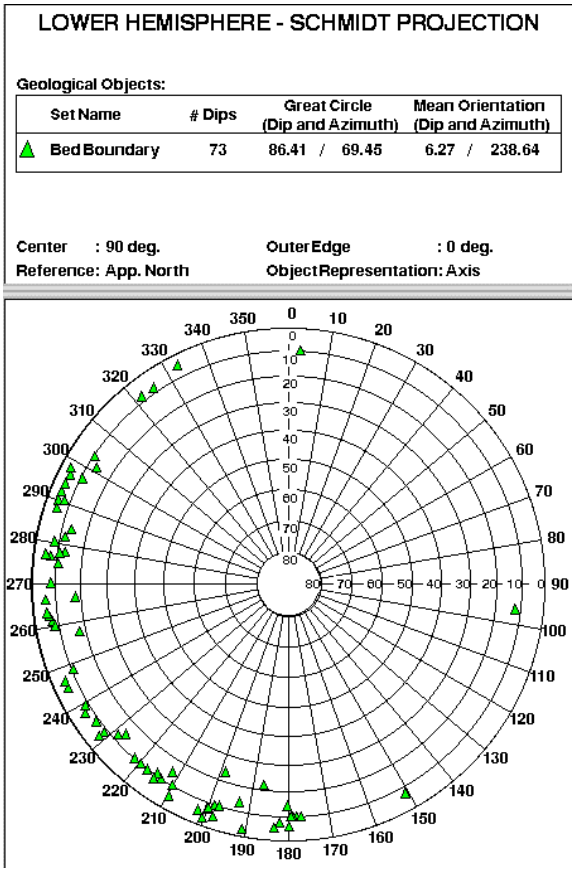

Fig. 2 – Schmidt projection showing main orientation of bedding in Hole A.

After defining the layers within the whole interval in Hole A, the second step is the characterisation of naturally fractures. These features, mainly dictated by the stress regime applied to the host rock, are mapped

in accordance with their geometrical and petrophysical aspects, such as orientation and aperture. In the example of figure 1, Hole A shows mainly naturally open fractures. These features were interpreted based on their microresistivity patterns, usually showing dark brown color. The fractures were classified in high angle open fractures (blue tadpoles in figure 1), medium angle open fractures (magenta tadpoles in figure 1) and low angle open fractures (red tadpoles in Figure 1). These fractures also show different behaviour along the whole interval.

Low angle fractures dip between 0^o and 20^o between XX42 and XX49 meters (fig. 1 and fig. 3) with main azimuth between 260^o and 290^o . Between XX49 and XX70 meters, dip magnitude is still 0^o to 20^o, while azimuth changed to a range of 250^o to 285^o, with some dispersion to 180^o-240^o and 330^o to 20^o . This type of fracture is associated to bedding and features are parallel to them.

Medium angle open fractures are characterized by dip magnitudes between 20^o and 50^o (fig. 3) and a very scattered pattern in azimuth direction along the interval.

High angle open fractures are the most common feature along the whole interval in Hole A. Dip magnitudes vary from 55^o to 80^o between XX42 and XX49 meters, with azimuths also varying from 40^o to 70^o, 220^o to 240^o and 260^o to 270^o (fig. 1 and fig. 3). From XX49 to XX70 meters, dip magnitudes range from 60^o to 85^o with azimuths mainly from 340^o to 10^o and 70^o to 110^o, with very low or almost no dispersion.

These fracture patterns are also related to fracture aperture and consequentely fracture porosity. Low angle open fracture are generally very tight compared to medium and high angle open fractures (Gonçalves, 1999), and the porosity computed from these three sets will show dramatic differences.

Conclusion

This work has show how effective can be the use of an electrical borehole device in imaging the borehole wall and quantifying the geometrical and petrophysical aspects of both sedimentary and structural features present in a borehole. Sedimetary features such as bedding planes defined the ruptile and ductile characteristics of each one, showing how some fracture suddenly stop when reach this feature (fig. 1 at XX55.5 and XX59.5). Open fractures were also characterized both in qualitative and in quantitative ways. The distinction between high angle, medium angle and low angle open fractures can be used to better characterize fracture porosity, avery important parameter in very low primary porosity reservoir such as the sandstones shown in Hole A.

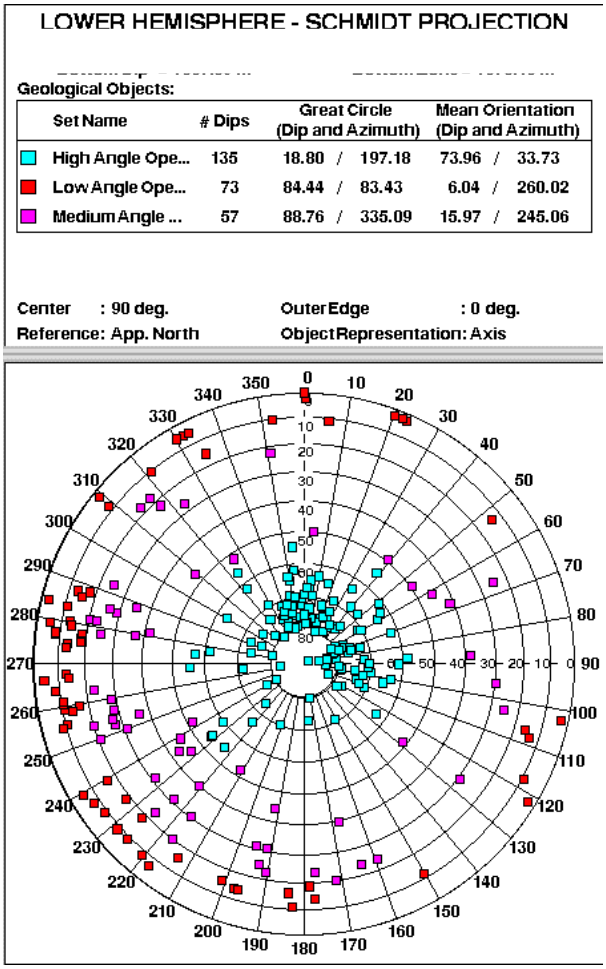

Fig. 3 – Schmidt projection showing main orientation of open fractures in Hole A.

References

Gonçalves, C.A., Sanguinetti, M. and Glorioso, J.C., 1999, Interpretation of fractured reservoirs using borehole electrical images and dipole sonic data: a bolivian case. VI International Congress of SBGf, Rio de Janeiro, Brazil.

Comportamento Excêntrico do Efeito Tuning em Sísmica 4D

Marco C. Schinelli, PETROBRAS S/A, Brazil

Resumo

A análise da viabilidade técnica para monitoramento do fluxo de fluidos em reservatórios através de levantamentos sísmicos do tipo "time- lapse", ou 4D, deve envolver não apenas a avaliação laboratorial das modificações provocadas no reservatório pela substituição de fluidos com a consequente variação dos parâmetros elásticos mas, principalmente, uma fase prévia de modelagem sísmica cuja importância é, dentre outras, quantificar o impacto do efeito tuning que pode afetar as esperadas variações de amplitude após o time-lapse. Neste particular tal efeito precisa ser investigado com profundidade, pois, devido a substituição de fluidos ao nível dos reservatórios a variação do tuning pode introduzir um fator modificação das amplitudes sísmicas que inviabilize a correta interpretação da sísmica 4D

Introdução

Muitos são os requisitos técnicos necessários para assegurar o sucesso de uma aquisição sísmica do tipo time-lapse, ou 4D, como é normalmente referenciada. Os elevados investimentos necessários para aquisição de sucessivas imagens 3D sobre uma mesma área, necessárias à monitorização do movimento de fluidos no reservatório, é técnica bastante dispendiosa o que por si só justifica quaisquer esforços para seu perfeito planejamento. Vários são os autores como Lumley, Behrens e Wang, que já empenharam esforços na identificação de instrumentos para quantificação da viabilidade técnica de levantamentos deste tipo. Dentre os vários fatores de risco para um levantamento 4D está a capacidade de discriminação temporal do reservatório a ser monitorado. Neste contexto a resolução sísmica e espessura do reservatório são, conforme este trabalho pretende apresentar, elementos fundamentais a considerar.

Com base na análise de modelagens podem ser feitas predições sobre o efeito do tuning e a capacidade de monitoramento do 4D, e obtidas informações importantes para a estratégia de aquisição, processamento e interpretação dos resultados do time lapse.

Etapa de Análise da Viabilidade Técnica

O Campo de em foco, cujo mapa estrutural sísmico ao nível do topo do reservatório, está mostrado na figura 1, foi escolhido para um estudo da viabilidade técnica de monitoramento da injeção de CO^2, através do uso de sísmica 4D. Dentre as etapas desta análise constou a estimativa da eficácia do monitoramento sísmico usando técnica de ranqueamento segundo critérios sugeridos por técnicos da Chevron (ver bibliografia) e apresentado na tabela 1. Observar que os valores da escala variam de 0 a 45 (valor máximo correspondente ao prospecto ideal). Nesta classificação o 4D analisado situou-se no grau 27, um valor acima da média para prospectos 4D, entretanto a metodologia usada desconsidera a importância de fatores altamente críticos que podem até mesmo inviabilizar o sucesso do time-lapse.

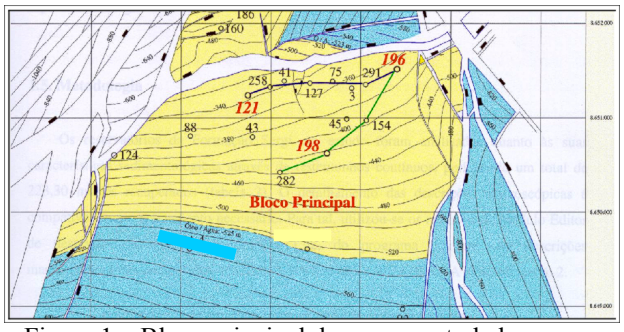

Figura 1 – Bloco principal do campo estudado

TABELA TOTALIZADORA DO RISCO					
Reservatório					
módulo de bulk					1
contraste da compressibilidade de fluidos(%)					5
mudança da saturação do fluido(%)					2
porosidade(%)					3
mudança de impedância(%					3
mudanca de tempo de traansito(no de amostras)					1
Total do reservatório					**15**

Sísmica					
razão sinal/ruido					boa=4
resolução média(ft)					35=3
visibilidade do contato de fluidos					1
repetibilidade					4
Total da sísmica					**12**

Escore Total **27**

Tabela 01 – Quantificação dos fatores de risco para o 4D proposto

Modelagem do efeito tuning

O poço usado na análise, (121) encontrava-se, na época da aquisição dos perfis, na área do campo dentro da capa de gás para o intervalo do reservatório a ser estudado. Para efeito da modelagem foi então

usada a substituição inversa, isto é, adicionou-se óleo ao intervalo compreendido entre o topo da Fm. Sergi e o paleosolo subjacente que funciona como selo limitador daquele intervalo em relação as outras zonas do reservatório. É também na porção superior deste intervalo que esta sendo injetado o CO^2. Como para efeitos práticos o gás associado e o CO^2 a ser injetado tem diferenças de gravidade que pouco influenciam os resultados foram usados os parâmetros do gás do reservatório.

A figura 2 mostra o trecho analisado no poço 121. Observar que o intervalo tem espessura em torno de 15 m. Atentar também para a presença da camada de paleosolo cujo aparecimento marca o limite inferior da primeira zona do reservatório Sergi na área. Este paleosolo, que tem expressão regional, é constituído de pacotes sílticos argilosos e tem espessura de até 3 m. Seu comportamento sísmico é marcado por um alto valor de impedância, superior ao do arenito sobrejacente o que normalmente resulta num alto coeficiente de reflexão na interface, que devido a proximidade da reflexão do topo da zona superior do Sergi provoca forte interferência das duas reflexões. O objetivo da modelagem foi investigar o comportamento de amplitudes no topo do reservatório e principalmente a interferência provocada pelo paleosolo .

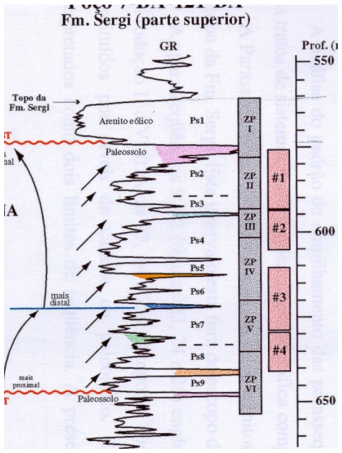

Figura 2 – O Paleosolo- Tem expressão regional e espessura média de 3 m , sendo constituído de pacotes síltico-argilosos com alto coeficiente de reflexão. Posiciona-se entre 15 a 30 m do topo da Fm. Sergi

Para maior fidelidade durante a modelagem foi extraído do próprio dado sísmico o pulso a ser usado na modelagem. Nos casos em que não se tenha ainda adquirido o 3D base a análise poderia ser feita com um pulso extraído de uma linha 2D da área com parâmetros aproximados aos que se pretende usar no 4D. A importância dessa etapa é a de trabalhar na modelagem com a resolução sísmica real que é um dos requisitos fundamentais para análise do efeito do tuning. A fase do pulso sísmico pode ser estimada por correlação entre o sismograma sintético e a sísmica disponível.

Para avaliação da relação Vp/Vs no reservatório foi usada a fórmula empírica de Greenberg/Castangna .

Apesar das aproximações decorrentes, desde que se conheça a litologia e porosidade com certa precisão os valores são aceitáveis para uma estimativa dessa natureza.

Parâmetros	Densidade	VP	VS	Amp. Stack	Amp. 0º	Amp. 20º	Amp. 40º	Variação %
Fluido/tipo	2.14	2868	1294	-481	-604	-500	-302	0
Amplitude	2.49	3722	2028	611	801	639	336	2.5
Gás- 100%				-452	-611	-475	-225	8.5
Amplitude	2.21	2949	1252	-353	-484	-377	-147	
Óleo- 100%	2.59	3846	1980	611	783	636	367	
				-543	-689	-564	-363	
Imp. elást.				-1282	-1654	-1351	-681	11.5
Gás- 100%				1451	1927	1509	835	37
				-447	-638	-487	-114	18
Imp. elást.				-937	-1324	-1015	-283	
Óleo- 100%				1767	2175	1801	1312	
				-680	-884	-772	-324	

Tabela 2 – Valores de amplitude para diferentes saturações, medidos em amplitude convencional e impedância elástica. Os 3 valores em cada coluna correspondem à amostragem dos lobos superior, principal e inferior da wavelet correspondente a reflexão no topo do reservatório .

Análise dos resultados

A tabela 02 mostra a variação de amplitude estimada ao nível do topo da Fm. Sergi, para o poço 121 para diferentes saturações em amplitude e impedância elástica . Nas situações extremas de saturação observar que a variação da posição do paleosolo provoca reduções de até 20% nas amplitudes.

A figura 3 mostra os perfis sintéticos, baseados nas propriedades médias reais dos intervalos e nas diferentes espessuras entre o topo da Fm. Sergi e o topo do paleosolo usados na modelagem do efeito tuning, usando a wavelet extraída dos dados sísmicos .

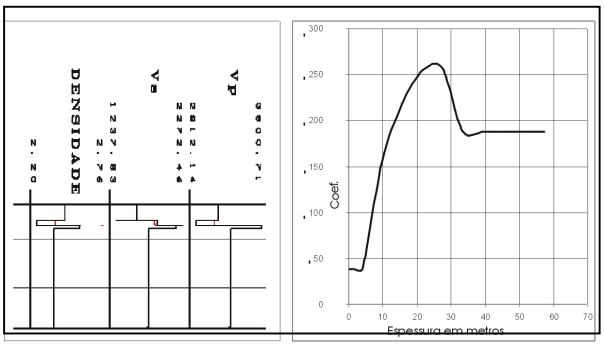

Figura 3 (página anterior – canto inferior direito) – Perfis modelados para situação original e após substituição de fluidos (esquerda) e função tuning correspondente para várias espessuras(direita).

Usando então as resposta de amplitude modelada para os perfis sintético com variadas espessuras foram gerados mapas de amplitude através de modelagem convolucional simples Nos mapas da figura 4 temos a distribuição dos valores que seriam obtidos na interface correspondente ao topo da Fm. Sergi, com base na modelagem do tuning. Neste mapa os valores de amplitude já estão influenciados pelo tuning com a condição de saturação original do reservatório e

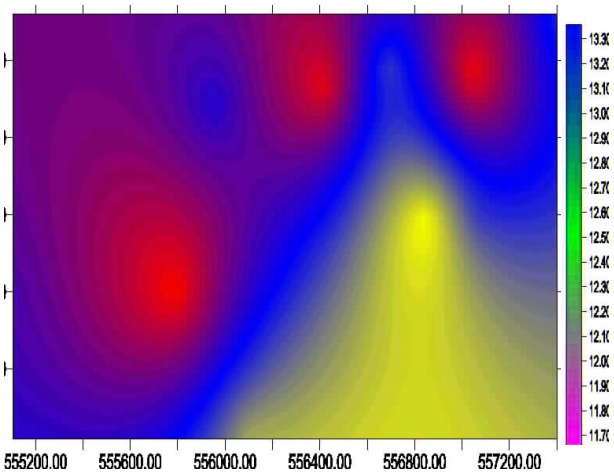

Figura 04 – Mapa de amplitudes modelado para a situação original de saturação do reservatório

poderiam, numa análise precipitada, ser correlacionados com a presença de hidrocarbonetos no intervalo. Nos mapas seguintes são simuladas as diferenças de amplitude que seriam observadas após a injeção, em duas situações distintas: saturação total de óleo de 100% para todos os poços(figura 5) e 50% apenas para os três poços mais a nordeste da área(figura 6). Observar que os mapas são influenciados pela variação do efeito de tuning e portanto não refletem fielmente as variações de saturação consideradas o que pode dificultar a interpretação dos resultados do time lapse, falseando a predição da anisotropia do fluxo e consequentemente influenciar negativamente a estratégia da injeção.

A variação no efeito do tuning após a substituição de fluidos se deve a variação dos atrasos na reflexão no topo do paleosolo , que é diferente para cada poço, ocasionada pela variação de saturação e consequentemente variação de Vp.

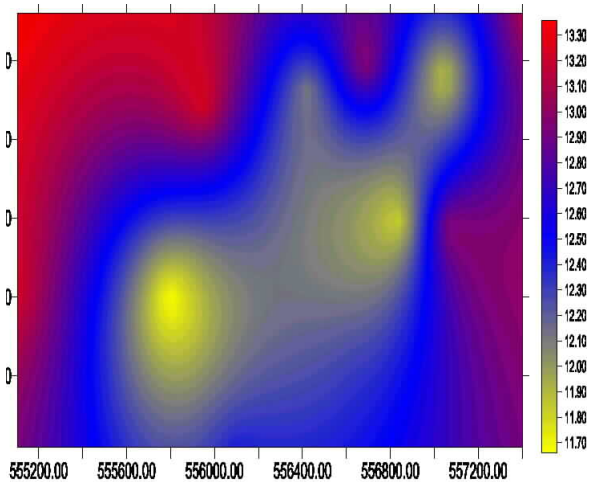

Figura 5 – seção anterior- Mapa de amplitudes para 100% de óleo em todos os poços

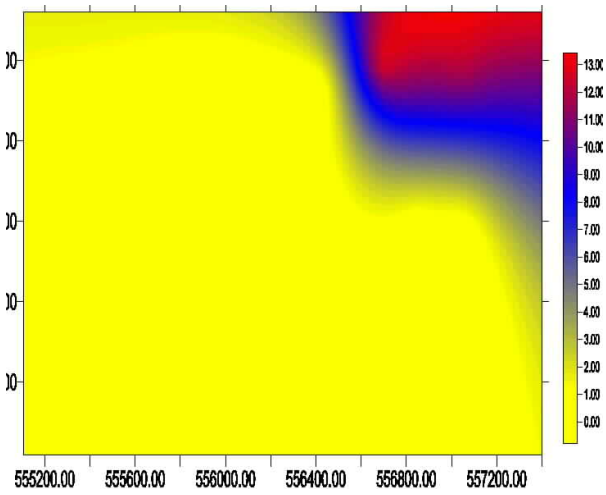

Figura 6 – Mapa de amplitudes para 50 % de saturação de óleo apenas para três poços mais a NE da área

Conclusões e Recomendações

Fica evidente que o efeito tuning tem comportamento excêntrico em situações onde o reservatório passe por substituição de fluidos e tal variação do efeito pode

até mesmo impedir a interpretação da sísmica 4D ou correlação fiel dos mapas de diferenças de amplitudes com a variação de saturação ao nível dos reservatórios. Assim sendo é importante, especialmente para reservatórios delgados, onde a variação de tempo de transito devido as modificações de velocidade de propagação no reservatório são imperceptíveis, restando apenas a variação de amplitudes como ferra-

menta de interpretação do 4D, que se avalie profundamente o efeito tuning. Esse tipo de análise oferece ainda, informações adicionais que podem ajudar nas etapas de aquisição, processamento (por exemplo recomendando diminuição do intervalo de amostragem, maior atenção na recuperação de altas frequências através de algorítimos de deconvolução, inversão para IE, etc) e mesmo na interpretação onde o uso de atributos "não tradicionais" como frequência instantânea que é boa indicadora de efeitos de tuning assim como análise do comportamento de AVO e outras técnicas que podem ajudar na estimativa e remoção da influência do efeito de tuning na resposta do 4D e finalmente permitir correlacionar de forma mais confiável variações de amplitudes com anisotropia do reservatório e diferenças de saturação.

Referencias

David E. Lumley, Ronald Behrens, and Zhijing Wang, Chevron Petroleum Technology Company, La Habra,California,1998, Assesing the technical risk of a 4-D seismic project .The Leading Edge, September 1997.

R. Savini, Flávio M. de Oliveira, Petrobrás, E&P-BA/GEXP,GELAB, Análise faciológica e Estra´gráfica da Porção Superior da Formação Sergi no bloco principal do Campo estudado na, Bacia do Reconôncavo

T.L.Lin and R. Phair, Texaco Exploration & Production, Inc., AVO Tuning, 63Rd Annual meeting International, expanded abstracts, 1993, pages 727-730

Zhijing Wang, Chevron Petroleum Technology Company, 1998, Feasibility of time-lapse seismic reservoir monitoring:The physical basis.The Leading Edge, September 1997.

Agradecimentos

Gostaria de agradecer a Petrobrás pela oportunidade de apresentação deste trabalho e aos colegas Aurino Aragão, Benildo Casanova, Alcides Aggio e Eduardo Ferrer pela contribuição para diversas etapas dessa análise .

Controls of Oilfield Compartmentalization

Dayse Daltro, Carlos Stank, Alberto Barroso, Mauro Mihaguti, PETROBRAS S/A, Brazil

Abstract

Ultra-deepwater exploitation requires strategies to optimize production-injection well distribution. Seismic 3D data can help to analysis the interaction between interpretation of depositional environment and structural pattern. This knowledge in conjunction with optimally placed wells have a high impact on the potential depletion of a given reservoir, could improve the production system with cost reduction. The primary objectives of this paper is present the geometry of high-continuity amalgamated channelized sand fan reservoir systems based on a series of attributes extracted along reservoir seismic horizon and its relationship with mapped faults to define the controls of oilfield compartmentalization.

Introduction

The Roncador Field is located in ultra-deepwater Campos Basin, Brazil between 1,500 to 1,900 m depth. The reservoir was divided in three main blocks: north, southeast and southwest area. This paper focus on the north area of the field with circa 120 millions cubic meters of recoverable hydrocarbon from the Maastrichtian RO-200 turbidite reservoir. The RO-200 reservoir encompasses amalgamated sand lobes encased within surrounding non-reservoir lithologies (shales). This study has shown that detailed seismic attribute analysis and classification is able to provide the distribution of reservoir rocks in this depositional system and some faults suspected to compartmentalize the reservoir.

Methodology

We extracted about thirty 3D seismic attribute from an area of twenty square kilometers area. These attribute maps contains a large amo unt of information that needs to be classified and validated. After first validation analysis, seven maps were chose: amplitude (fig.1-A), phase response, amplitude from Variance Cube (fig.1-B) (ref. 1), dip (fig. 1-C), edge-detection (fig.1-D), integrated-reflection strength and heterogeneity (volumetric attributes). Maps B, C and D (fig. 1) are very good indicators of subtle faults and flexures for further delineation of fault patterns.

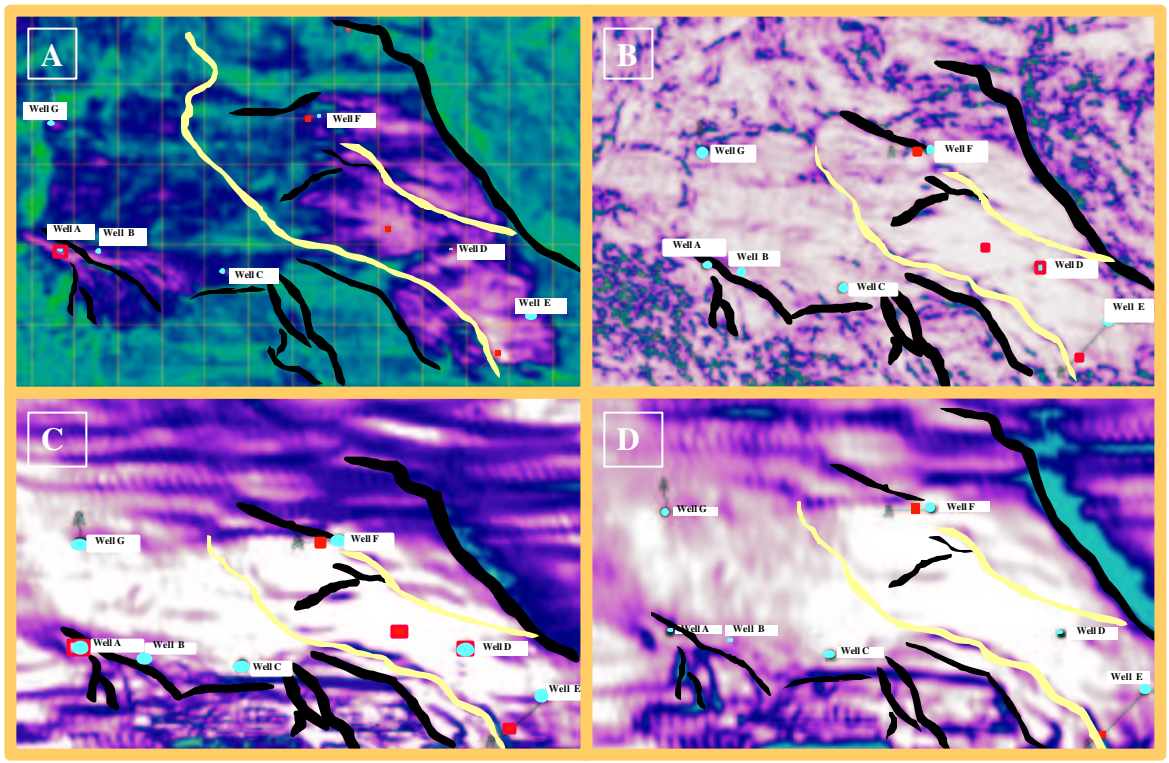

Fig 1 – Seismic attribute maps used to validation analysis; A- amplitude map ; B- amplitude map from Variance cube; C- dip map; D- edge-detection map

All of these seismic attributes were used in the classification without prior knowledge of the reservoir characteristics (very powerful in new frontiers areas) with Unsupervised Classification Method – Competitive Learning (ref. 1) and by multi-attribute statistical and neural network classifier. This last case combines the seismic attributes with prior knowledge, using well data as control points (training data) – Supervised Classification Method (Back Propagation, Ref. 1).

In the first method, Unsupervised Classification, the main challenge was to produce classification maps that discriminate between sand bodies and shales (fig.2 - C). In the supervised approach the prior information (training data) is used to calibrate the classification (fig. 2 - D). The well properties, such as fluid type, saturation or lithology were assigned in a given class. In the supervised classification we try to refine two facies class (fig.2 - C sand bodies), creating six classes. The facies in yellow and red (fig. 2 - C) were split into five – yellow, red, blue, green and lilac (fig. 2 - D). For both classification methods, facies maps can be quality controlled with crossplot in 3D attribute space (fig. 2 – A and B).

The unsupervised and supervised classification methodology was applied in Roncador field following a regional approach (ref.2).

Geological Setting

The ultra-deepwater Roncador Field was discovered in 1996 and the pilot system production starts on January 1999 in the southeast area of the field.

In this field two main factors controlled reservoir distribution: rate of subsidence related with halokinesis and preservation of sediments from erosion (ref. 3). In the north area, where the same amount of subsidence was more regionally distributed it was possible to spread turbidite reservoir, depositing similar thickness of sandstones and capping shales (ref. 4).

The stratigraphic zonation from well logs divided the reservoir in three main sequences, with internal sub-division in five main zones (ref. 5). The RO-200 Zone (the youngest) is treated in this paper. Based on Bruhn's classification (ref. 6), which divided the Brazilian Eastern deep-water reservoir in eight major types, the Maastrichtian turbidite reservoir RO-200 is Type 3, unconfined, sand-rich turbidite lobes filling wide depressions developed by downslope gliding of underlying evaporites.

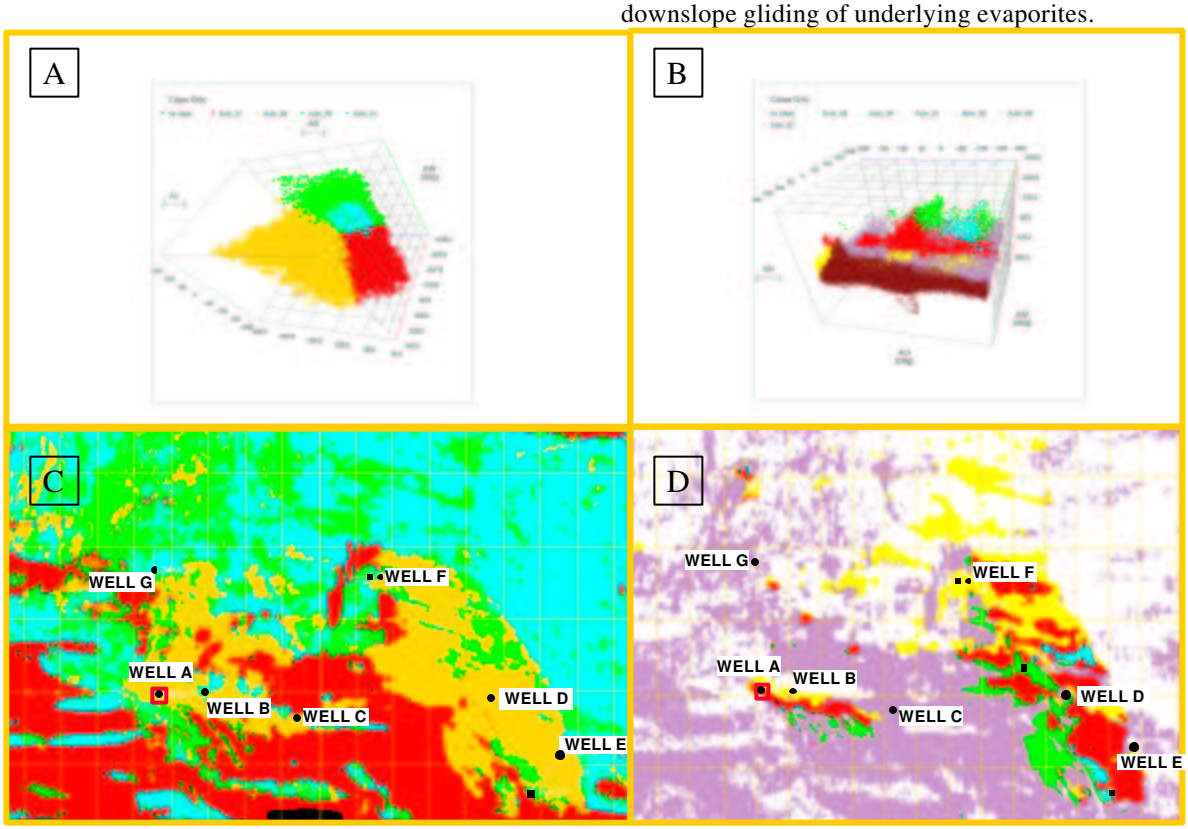

Fig. 2 – Facies analysis; A and B - 3D cross-plot; C – facies map (unsupervised method); D – facies map (supervised method).

Results

Seismic sequence interpretation using all of attribute maps and facies maps shows a vertically stacked series of channelized fan depositional systems. Structurally, the north area is bounded by NW-SE normal faults. A series of minor faults are almost parallel and conjugate to the main structural trend (fig. 3).

The stratigraphic series was divided into three zones. The oldest zone (I) trends towards the NE-SW with SW source (fig. 3). The fan system is partially eroded and is difficult to see its lateral continuity in seismic maps. The next zone (II) trends the opposite direction NW-SE with NW source and is stacked above de zone I. It is comprised of confined sinuous channel and its associated channelized fan (fig.3). The series of pre-existing faults superimposed the system fan pathway (fig. 3). The youngest zone (III) is characterized mainly of amalgamated lobes (fig. 3). One of the feeder channels, N-S trend, cut the upper part of channelized fan (zone B) and some of feeder channels are partially eroded (fig. 3).

In a qualitative approach, together amplitude map (A– fig. 1), seismic structural attributes such as amplitude map from variance cube (B – fig.1), dip map (C - fig. 1) and edge-detection map (D –fig. 1) were used to validate the structural framework. These attributes proved very helpful in delineating the major fault pattern trends. According the mapped channelized fan systems, the NW-SE normal faults are pre-depositional and were superimposed on channelized fan II and III (fig. 3). The yellow faults cut and modified the shape of some channelized fan III (fig. 3). Considering the same preferential trend NW-SE, these faults represent, probably, old reactivated faults. Locally, they enhanced and compartmentalized these channelized fan systems.

In a quantitative approach, looking for facies maps from unsupervised and supervised classification (fig. 2), the both was unable to fault classification, we couldn't discriminate the structural framework. The external geometry of channelized fan systems was discriminate in the unsupervised classification method (A and C – fig. 2). In the supervised class facies map, the internal geometry of channelized fan systems was better emphasized (B and D – fig. 2). The yellow, red, green, blue and lilac facies represent different fan systems. The blue facies, according well information delineate gas cap. The lilac facies couldn't separate old zone (fan system I) from other sand facies with thin thickness.

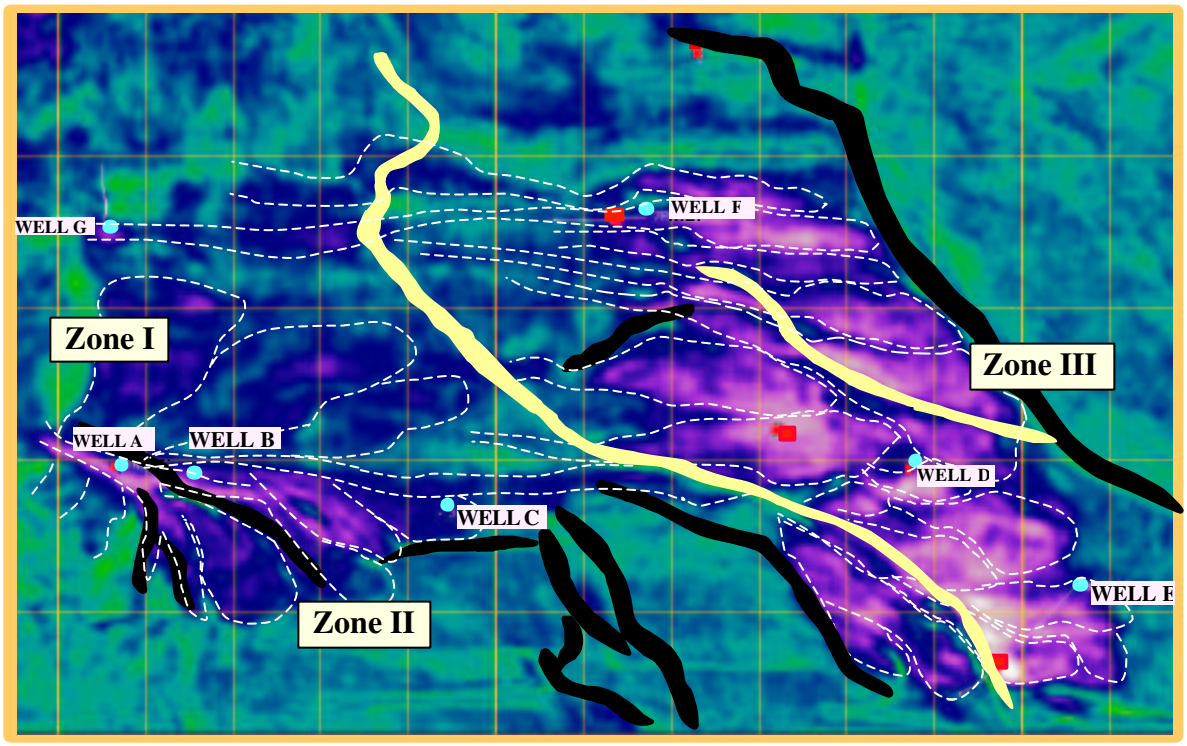

Fig. 3 – Channelized fan depositional system with structural framework. Faults in yellow disconnect the Turbidite fan system.

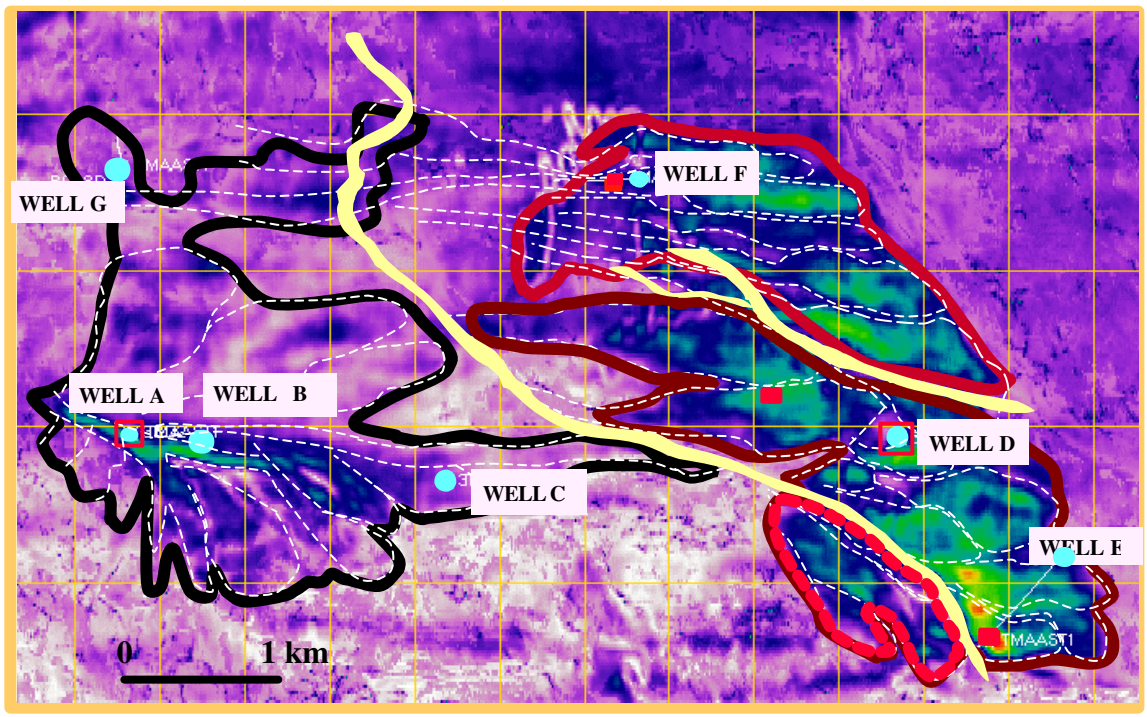

Fig. 4 – Compartimentalization of the north area.

To better understand and maybe solve uncertainties like bed continuity, connectivity and vertical and lateral facies variability, we analyze all of results, in a qualitative and quantitative approach together wells information (GOC, OWC and pressure data). The result of this comprehensive work was the compartmentalization of the north area of Roncador Field in three main blocks (fig. 4). Considering the gaps in yellow faults, these faults may disconnect the reservoir in that portion of the area in order to determine one extra block (red dotted area – fig. 4). This effort provides the framework for optimal placement of wells to maximize reservoir production performance .

Conclusions

The stratigraphic/structural patterns affected the distribution of reservoir rocks and seals. Reactivated faults or new ones controls the reservoir compartmentalization. Predictive capability of geological behavior, net reservoir distribution and hydrocarbon type, has been systematically refined to optimize well placements and, as a result, improve the production system with cost reduction.

References

1- Geoframe, 2000, Technical Documentation.
2- Johann, P., Daltro, D., Barroso, A., 2001, "Reservoir Geophysics: Seismic pattern recognition applied to ultra-deepwater oilfield in Campos Basin, offshore Brazil", SPE.
3- Rangel, H.D. et al., 1998, "Roncador Field. A New Giant in Campos Basin, Brazil", OTC, Houston: 579-587.
4- Santos, P.R. et al., 1999, "Geophysical and Log Characterization of Roncador Field, Campos Basin, Brazil" SBGF Rio'99.
5- Barroso, A. et al., 2000, "Roncador Giant Oilfield: Exploration and Production from a heterogeneous Maastrichtian turbidite reservoir in ultra-deepwater Campos basin, Brazil", AAPG.
6- Bruhn, Carlos, 1998, "Major Types of Deep-Water Reservoirs from the Eastern Brazilian Rift and Passive Margin Basins", AAPG.

.

Acknowledgments

We thank Petrobras for permission to publish this paper. Special thanks to Darci José Sarzenski and Luciane Bonet for the support in the geological and simulation reservoir discussions.

Fluid fill and Lithology from seismic using Elastic Inversion

Helgesesen Jan, CGG Oslo, jhelgesen@cgg.com
Buran Haavard, CGG Oslo, hburan@cgg.com
Lafet Yves, CGG France, ylafet@cgg.com

Abstract

Post-stack inversion is by now a mature tool for extracting information on lithology, fluid fill and porosity from seismic. The inversion is often done in two steps. In the first step, acoustic impedance (AI) is estimated from the seismic, using wells as calibration for the wavelet and for getting some a priori information on the model (impedance trends, impedance variability etc.). In a second step, the reservoir parameter (porosity or lithology) is estimated or modeled from the acoustic impedance. Alternatively, the inversion result may be interpreted directly and qualitatively, bearing in mind the relationship between AI and the reservoir parameter. Again, in this second step, well data may be used to condition the model, and to establish the relationship between acoustic impedance and the reservoir parameter at the proper scale.

Elastic inversion of angle stacks is a relatively new approach to inversion where the goal is to estimate both Poisson's ratio and acoustic impedance from the seismic data. The use of angle stacks allows us to get access to AVA (Amplitude Variation with Angle) information in the data. This is extra information compared to the traditional post-stack inversion, where only normal incidence data are used. This extra information is precisely what is needed to estimate the Poisson's ratio. From acoustic impedance and Poisson's ratio, other elastic parameters may be estimated, such as the shear impedance.

Introduction

CGG has used its proprietary inversion package (TDROV) in numerous case studies around the world. The inversion results are routinely used in the evaluation of exploration targets and for planning of production wells. However, In many situations, acoustic impedance does not provide enough information to determine fluid fill and lithology uniquely. In the present case history from the North Sea the task for the inversion was to delineate a gas-bearing sand that is penetrated by a well, and to identify other prospects in the same area. Logs at the well show that the acoustic impedance values in the gas sand are similar to those of the water-bearing sands and shales above and below the reservoir. Thus, it would be hard to identify the sands based on acoustic impedance only. However, the gas sand can easily be identified from Poisson's ratio. With the combined estimates of acoustic impedance and Poisson's ratio, lithology and fluid fills could be more reliably identified and mapped.

Data processing and pre-conditioning

In elastic inversion, the angle stack data should be identical to the angle-dependant reflection coefficient convolved with a seismic wavelet. All other amplitude variations should ideally be removed in the pre-processing of the data. More specifically, the following issues should be carefully attended to during the processing of the seismic:

- Multiples must be attenuated as much as possible without destroying primary energy.
- Amplitude variations that are related to geometrical spreading, transmission losses, absorption (Q) must be removed as well as possible. However, if necessary, some of these effects may partially be included in the angle-dependant wavelet at the inversion stage.
- Acquisition footprints and amplitude variations related to acquisition artifacts should be removed.
- The data should be pre-stack (time) migrated with an algorithm that preserves amplitudes.
- The data should be close to zero phase. If this is not the case, a residual zero-phasing is applied prior to the inversion.
- Any variations in source signature should be removed as much as possible.
- Angle stacks should be properly amplitude balanced. However, improper amplitude balancing may be repaired at the inversion stage by varying the amplitude level of the seismic wavelet at different angles.
- Angle stacks should have similar frequency content. This can be achieved through spectral balancing of the angle stacks. Often, the frequency content of the far angle stack can be increased somewhat while still keeping the noise at an acceptable level.

Well calibration and wavelet extraction

The concept of elastic impedance (EI) was introduced by Conolly . EI allows computing the earth reflectivity and synthetics (without moveout) at an

arbitrary angle, using formulas that are analogous to those of normal incidence seismograms. For normal incidence, we have for the reflectivity across an interface:

$$R(\theta=0) = \Delta AI / (2 \cdot \overline{AI}) \qquad (1)$$

where ΔAI is the change in AI across the interface, and AI is the mean value of the impedances above and below the interface. Similarly, for an arbitrary angle, we have:

$$R(\theta) \cong \Delta EI(\theta) / (2 \cdot \overline{EI}(\theta)) \qquad (2)$$

One useful expression for EI, which usually is a good approximation up to 30 degrees, is given by:

$$EI(\theta) = AI^{\cos 2(\theta)} (V_p/V_s)^{2\sin 2(\theta)} \qquad (3)$$

where V_p is P wave velocity and V_s is S wave velocity. The formulae for EI clearly show that elastic impedance depends on AI and Vp/Vs, the two parameters that we would like to estimate through elastic inversion. By using the EI logs, synthetics can be calculated for each angle, and an angle-dependant wavelet can be extracted by matching the synthetic to the real angle stacks.

Elastic Inversion

In the next step, each angle stack of the data is inverted. This inversion is carried out using the TDROV program with some modifications. In this layer-based approach to inversion, the earth is divided into micro-layers that are consistent with the seismic interpretation and the geological model. Thus, truncation and compaction effects can be taken into account. Typically the thickness of each micro-layer is 6-8 msec. In the inversion, both the thickness of each layer and its (laterally varying) EI is estimated. We attempt to use the same micro layering for all angles, and we therefore obtain information on how the EI varies with angle in each micro-layer. Also, the inversion of one angle stack is conditioned to the inversion result of another angle stack, and this stabilizes the inversion. Figure 1 shows the results of elastic inversion on a North Sea data example, together with the computed EI logs from the well.

The 30 degrees stack was first inverted, and the inversion result at 30 degrees was then used as initial model at 10 and 20 degrees. The layer model was kept fixed at these two angles, and only impedances were updated. Observe how well the AVA behavior of the elastic impedance in the target is recovered by the inversion. The gas sand can easily be identified at 30 degrees on the inversion result, but is not visible at 10 degrees. This is an expression of the Class 2 AVO anomaly related to gas-filled sand.

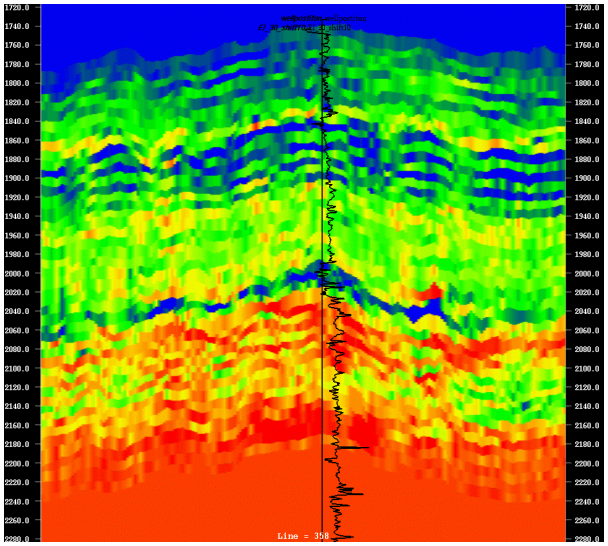

Figure 1 - Inverted elastic impedance at 30 degrees in a cross-section through the well position. The gas sand, just below 2000 ms at the well, can be seen as a low impedance region at 30 degrees

Conclusions

Using the estimated elastic impedances, it is now possible to estimate Poisson's ratio directly from seismic acoustic data, as well as the acoustic impedance and shear impedance by inversion of equation (3) or a similar equation.

The interpretation of elastic parameter cubes requires some experience and detailed knowledge of the petrophysics of the studied area. These cubes can however be transformed to lithology and fluid fill cubes, using empirical relationships derived from well logs. These relationships are functions that give the probability of a certain lithology and fluid, given the acoustic impedance and the Poisson's ratio. Using such probability functions, the AI and Poisson cubes can be transformed into lithology and fluid cubes. A geoscientist or reservoir engineer can easily use such cubes in exploration or well planning.

Geological and Geophysical Integrated Methodology for Reservoir Characterization

C.E.G. dos Anjos (GeoQuest), H. Zucchi, Schlumberger (GeoQuest) & Marcelo Martins Neto (UFOP/DEGEO)

Abstract

Well measurements and seismic attributes can be used to derive multi-dimensional calibration functions that are applied to seismic attributes to map reservoir properties. Estimation of various properties is guided by multiple seismic attributes simultaneously. The estimates fit the well measurements and are guided by seismic data away from the wells. Significance estimation and error mapping provide a quantitative measure of confidence.

Specific seismic attributes have been found to correlate well with individual reservoir properties, thus improving the ability to map them. For example, interval velocity and acoustic impedance often correlate well with porosity.

This mapping process was used to define effective porosity and water saturation along the reservoir.

Introduction

The small dimension of recently discovered reservoirs and the increasing cost of production has been demanding improvements in reservoir characterization. Porosity, permeability, fluid and gas saturation, as well as other reservoir properties are measured in well. But well data cover only the immediate enviroment of the boreholes, a very small fraction of the reservoir volume. Accurate high-resolution estimation of reservoir properties "near" the wells may be wasted if the estimation of these properties "away" from the well is poor.

Seismic waves propagate everywhere covering the whole reservoir, not limited to well. With the rising importance of reservoir characterization and stratigraphic exploration, seismic data acquisition, processing and interpretation have evolved to give more information about the reservoir properties. Seismic processing output is no longer a single image of reflectivity. In addition, seismic attributes can be generated. Some attributes are generated post stack by mathematical transformations (Taner *et al*, 1979; Sonneland *et al*, 1990) These include instantaneous phase and frequency, reflection heterogeneity, dip and azimuth.

Acoustic impedance estimated by inversion is an important seismic attribute. In **Fig. 1**, we show a cross section in which porosity is apparently related to acoustic impedance much better than is to the reflectivity image.

The mean problem in using seismic attributes for property estimation is that their relation to rock properties is not obvious. There are unknown local factors that may affect the data in unexpected ways. To solve this, we have to build a *familiarity* with certain sedimentary basin or reservoir to know how seismic attributes are related to reservoir properties. Comparing seismic and borehole data, region familiarity is built.

To build region familiarity, quantify its reliability, and subsequently use it to estimate properties, interpretation methods and tools are needed. In this paper we present a method to obtain correlation between seismic attributes and rock properties and then map these properties guided by those attributes (Ronen *et al*, 1993).

Data Base

To implement the proposed methodology some input data are required. For this work, the used input data is listed below:

1. Seismic Cube (in time);
2. Three seismic horizon and related fault segments (in time);
3. Stack velocity analysis;
4. 15 wells with logs (acoustic impedance, interval velocity, sonic, DT, Density, Neutron porosity, water saturation, effective porosity, volume of shale, etc.);
5. 8 geological markers and fluid contacts.

Hardware and Software

Integrated 3-D modeling requires workstation capability to provide the 3-D graphics speed and the computational horsepower to run multiple mathematical operations in a single day. This section is not an endorsement of any item, but is intended to illustrate the class hardware and software that was used to construct this 3-D model. Other equivalent products are available.

The 3-D model was built on a desktop workstation using an ultraSPARC-II with a 250 MHz CPU, 512 Megabytes RAM, creator 3-D graphic board, and 18-Gigabyte data disks.

Methodology

The interpretation process, as implemented on the reservoir modeling workstation, is divided into a few steps.

Checking and editing geomarkers locations. Relating seismic reflectors to geological markers seen in boreholes is a critical step. Inaccuracy of a few meters may completely change the results. After well tie, based on synthetic seismogram and time to depth conversion, based on velocity model, it is important to be able to fine-tune the intersections interactively.

Scaling over geomarkers. Borehole data has much more vertical resolution than seismic data. Averaging borehole data can simply be the arithmetic averaging of the well logs in a certain zone, or use cutoff values and average schemes that account for the effect on seismic wave propagation.

Seismic attributes x rock properties. After attribute mapping has taken place it is possible then to try the correlation of petrophysics with available seismic attributes. **Fig. 2** shows that there is a high correlation between net time thickness/ acoustic impedance/ amplitude/ depth and effective porosity and between thickness/ acoustic impedance/ amplitude/ depth and water saturation.

In **Figs. 3** a linear regression is performed on the available correlations.

Calibration Function. Using correlation values between attributes and properties, a linear calibration function, $F(A_1, A_2, \ldots, A_n)$ is determined. Here, A_i is an attribute value. Then if the interpreter wants, non-linear terms can be calculated with artificial neural networks.

Linear calculation is adequate when relationships are linear, for example porosity guided by slowness (1/velocity) (Gassman, 1951; Biot, 1956). Non-linear calibration is important when these are more complex. This paper discusses only linear calibration.

The calibration function is estimated at well locations. It is then applied everywhere the attributes are given.

3-D Model Generation. Besides log property mapping, the interpreter can make a 3-D structural model, which is able to receive those maps and generate a volumetric model for the reservoir by averaging tools. Then, this volumetric 3-D model can be send to reservoir simulation software.

Integrated 3-D reservoir characterization and reservoir simulation modeling offers a self-consistent method to insure that available field data are honored in the same 3-D model (Clayton et al, 1992).

Results

The following results although not representative of a complete field study, are rather a set of tests of the technique.

In order to show how seismic attributes can be used as a petrophysical property guide over the area of a 3-D survey, we have taken the effective porosity (PHIE) log property, and guided it, simultaneously, with the seismic amplitudes plus acoustic impedance, under linear adjustment on the oslo_demo layer which showed 85% and 93% significance, respectively. According to linear regression (**Fig. 3**) and calibration function (**Fig. 4**) the following PHIE map was obtained from those attributes above (**Fig. 5**).

In this particular case, as it can be seen in correlation matrix (**Fig. 3**), depth and net time thickness could also guide the PHIE mapping. Since the significance factor of the average velocity and instantaneous phase were only 62% and 34% we did not apply this procedure.

The map in **Fig. 5** arises from the interaction of 2 different disciplines (seismic data and well logs), and adds real value to a 3-D structural interpretation. By comparing this map, which represent the PHIE for oslo_demo in each well preserving the seismic amplitude and acoustic impedance attribute trends between and outside of them, with a map that only shows PHIE value for the wells location, without seismic guided mapping, you can realize this added value.

An optional step is predicting the properties at a planned well location using all previous results. The properties one would expect to find for such a well based on our model are shown in **Fig. 6**.

Conclusions

1. In this paper we present a practical and reliable method for the determination of the existence of any meaningful correlations between sets of attributes and properties.

2. On finding a significant correlation, we have suggested a method of calculating functional relationship between geophysical attributes and well measurements, and use it for seismic guided mapping of reservoir properties.

3. Three-dimensional models provide better integrated reservoir descriptions, improving reservoir management decisions, data quality control, volumetric calculations and integration between disciplines.

4. The main advantage of a log property mapping guided by seismic attributes is the high resolution mapping between and outside well locations, giving more reliable measurements in these areas.

5. The control of log properties along the reservoir can give to interpret data to plan a new well location, which contain properties values based on your previous model.

6. 3-D analysis requires the same input data as 2-D methods and does not add significantly to reservoir characterization costs and time spent.

References

1. Clayton, C. A., Dobin, M. W., *et al.*: "3-D Visualization for Reservoir Description and Development." SPE 24511 (ADSPE 1003), 5th ADNOC/SPE Abu Dhabi Petroleum Conf., Proc. p340–346 (April 1992).

2. Biot, M. A.: "Theory of Propagation of Elastic Waves in a Fluid-Saturated Porous Solid." J. Acoust. Soc. Am. (1956) p168-191.

3. Gassmann, F.: "Elastic Waves Through a Packing of Spheres." Geophysics (1951) p673-685.

4. Ronen, S., *et al.*: "Mapping Reservoir Properties From Well Measurements Guided by Seismic Attributes." paper OTC 7086 presented at the 25th Annual OTC in Houston, Texas, 3-6 May 1993.

5. Sonneland, L., Barkved, O. and Hagenes, O.: "Construction and Interpretation of Seismic Classifer Maps." paper presented at the 1990 EAEG meeting in Copenhagen.

6. Taner, M. T., Koehler, F. and Sheriff, R. E.: "Complex Trace Analysis." Geophysics (1979), p1041-1063.

Acknowledments

We would like to thank Schlumberger GeoQuest for permission to publish this work.

Appendix

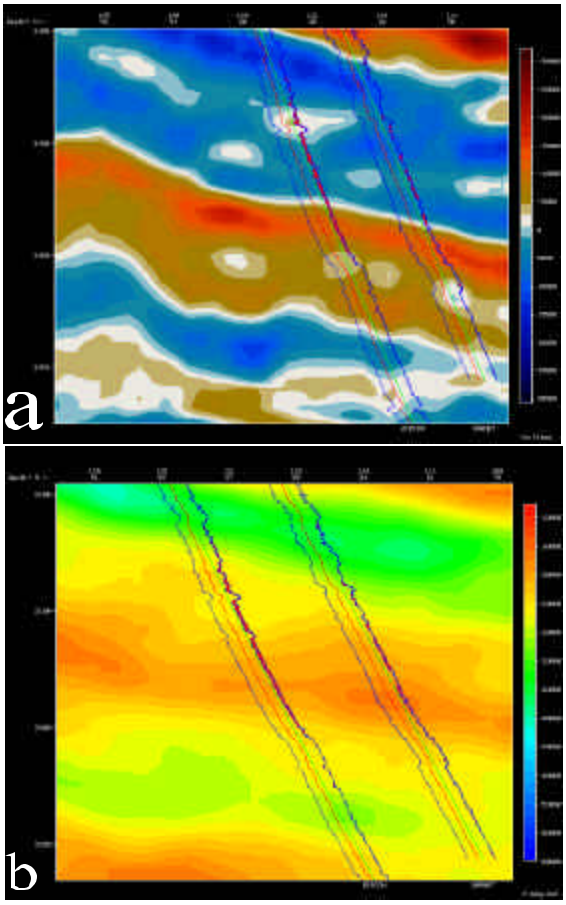

Fig. 1 – Cross Section display of (a) seismic data and (b) acoustic impedance with porosity logs on wells projects on the cross section. Section (a) was extracted from a 3-D seismic cube of time migrated seismic data. Section (b) is from a 3-D cube of acoustic impedance (AIMP) from the inversion module of reservoir modeling software. The zero crossing of the strong reflector at 1115 milliseconds (approximately) coincides with a high porosity layer, but it is difficult to estimate porosity from these seismic data without further processing. On section (b) the relations between AIMP and porosity are more evident and will be used for seismic guided porosity mapping.

	BulkDensity	EffectivePorosity	NeutronPorosity	VolumeOfClay	WaterSaturation
AVGV	71,19	61,76	50,64	30,47	66,69
DEPTH	85,01	82,15	78,91	14,50	85,01
Net_Time_Thickness	92,33	90,63	80,58	34,29	88,62
Avg_Acoustic_Impedance	93,09	93,09	89,66	51,92	89,66
AMPLITUDE	83,36	84,91	78,03	31,63	86,34
Instantaneous Phase	30,47	34,29	18,58	13,86	30,47

Fig. 2 – A quality matrix is generated to indicate how expressive is the correlation between an attribute/property pair. The highlighted values shows that there are high correlations between net time thickness/ acoustic impedance/ amplitude/ depth and effective porosity and between thickness/ acoustic impedance/ amplitude/ depth and water saturation.

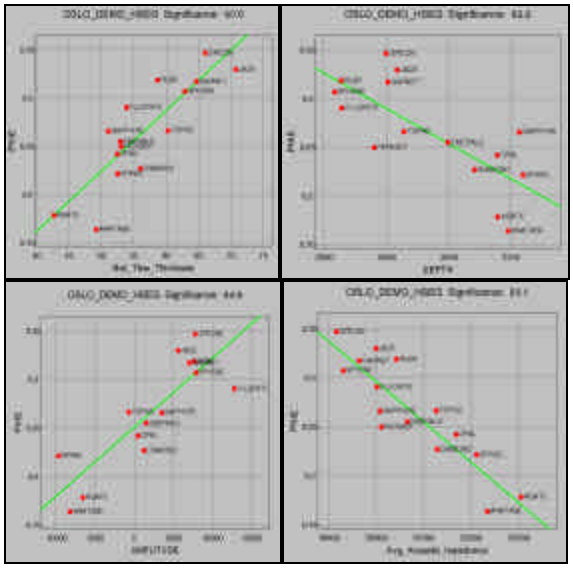

Fig. 3 – Regression line cross plot between selected attributes (net time thickness, depth, amplitude and acoustic impedance) and effective porosity.

	Constant	Avg_Acoustic_Impedance	AMPLITUDE
EffectivePorosity	0,977518	-3,43856e-05	1,67771e-06

Fig. 4 – Calibration function used to map effective porosity guided by acoustic impedance and amplitude. In this paper a linear function was used.

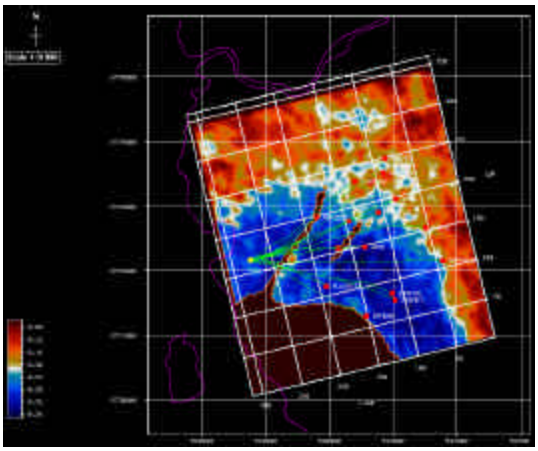

Fig. 5 – Effective porosity map obtained from well measurements and seismic attribute (amplitude and acoustic impedance).

TOURMALINE	OSLO	PARIS	MILAN	TOKYO	RIO	LAGOS	DALLAS	Summation
Drainage Geometry	Circle	Circle	Circle	Circle	Circle	Circle	Circle	Circle
Drainage Radius	0,0	0,0	0,0	0,0	0,0	0,0	0,0	0,0
Top	-3014,0	-3020,8	-3039,3	-3065,2	-3092,7	-3121,8	-3136,3	-3014,0
Bottom	-3020,8	-3039,3	-3065,2	-3092,7	-3121,8	-3136,3	-3213,3	-3213,3
X Top Coordinate	540853	540853	540853	540853	540853	540853	540853	540853
Y Top Coordinate	8772547	8772547	8772547	8772547	8772547	8772547	8772547	8772547
X Bottom Coordinate	540853	540853	540853	540853	540853	540853	540853	540853
Y Bottom Coordinate	8772547	8772547	8772547	8772547	8772547	8772547	8772547	8772547
DIP	4,109	4,025	4,495	3,172	2,735	7,389	7,154	-
AZIMUTH	107,530	104,504	102,571	121,280	134,034	66,209	68,904	-
THICKNESS	6,8	14,5	25,9	27,5	29,3	14,5	77,0	195,5
Gross Thickness	6,8	18,6	25,9	27,5	29,1	14,5	77,0	199,3
Net Thickness	6,7	18,6	25,8	27,4	29,1	13,9	76,8	198,4
True Bed Thickness	6,8	18,5	25,8	27,4	29,0	14,4	76,5	198,4
Gross Gas Pay Thickness	0,0	0,0	0,0	-	-	-	-	0,0
Gross Oil Pay Thickness	6,8	18,6	25,9	27,5	29,1	14,5	76,5	198,9
Net Gas Pay Thickness	0,0	0,0	0,0	-	-	-	-	0,0
Net Oil Pay Thickness	6,0	18,5	25,6	26,6	28,8	3,7	51,7	160,8
Net Pay Gas Pore Thickness	0,0	0,0	0,0	-	-	-	-	0,0
Net Pay Oil Pore Thickness	1,1	4,7	5,1	5,1	8,2	0,4	6,6	31,1
Net to Gross Ratio	0,992	1,000	0,998	0,999	1,000	0,961	0,997	0,995
Effective Porosity	0,246	0,310	0,255	0,237	0,322	0,155	0,165	0,226
Horizontal Permeability	34,614	133,817	91,3832	64,7688	311,96	3,52689	35,9185	94,4867
Vertical Permeability	34,614	133,817	91,3832	64,7688	311,96	3,52689	35,9185	94,4867
Net to Gross Ratio Gas Pay	0,959	1,000	1,000	-	-	-	-	-
Net to Gross Ratio Oil Pay	0,886	0,995	0,987	0,969	0,988	0,252	0,675	0,808
Net Pay Gas Saturation Ratio	0,771	0,822	0,886	-	-	-	-	-
Net Pay Oil Saturation Ratio	0,634	0,809	0,779	0,785	0,871	0,202	0,519	0,696
Water Saturation	0,334647	0,209229	0,332594	0,323102	0,134929	0,615254	0,540551	-

Fig. 6 – Table showing reservoir properties calculated to the proposed well (TOURMALINE), based on previous modeling results.

Incorporation of seismic intermediate-scale data for improving reservoir description

Ricardo Tarabini Castellani -Petrobras/Cenpes
tarabini@cenpes.petrobras.com.br

ABSTRACT
A description of reservoir heterogeneities in all scales is crucial for improvements in reservoir characterization. In this work a multi-scale approach was developed to integrate seismic intermediate-scale data and the conventional short and large scale data, represented by logs and surface seismic data respectively. Intermediate-scale data obtained by short and far-offset crosswell surveys, vertical seismic profiles and high resolution seismic lines can be geostatiscally incorporated in this approach in order to provide more complete reservoir descriptions. The approach employs the available seismic data as reference data in two post-matching steps. An interwell model is the final product of the first step using crosswell data. Such upscale and post-matching is then repeated to the larger-scale seismic traces, using logs and the interwell image as hard data to feed simulations. The final product is an optimal acoustic property model constrained by all logs and seismic surveys.
This multi-scale incorporation was applied using field and synthetic data, showing that the main impact in modeling is caused by the incorporation of crosswell images obtained by shooting short distance surveys. Since such data provide a tool to map and recover a very fine layered lateral framework, which can be extrapolated under the constraint of conventional seismic data, the integration must prioritize data with higher frequency content, i.e., should follow two steps: only short-crosswell data are used in the first post-matching, and additional seismic data during the second.

INTRODUCTION

The incorporation of profiles and seismic data has become more and more frequent in geostatistical methodologies used in the characterization of reservoirs. Among the reasons for a major integration are distinguished the following: 1) major covering of possible scales presented by heterogeneities which can play an important role in reservoir flow properties as a whole; 2) the need of restricting stochastic models to a major volume of data with different scales of observation and accuracy.
Although such methodologies present advantages concerning those based only on the use of well data, important features of intermediate size which can control the fluid flow standard; in the range of tens to a few hundreds of meters, are not correctly recovered with the use of these two tools. An alternative to make the description more complete have been the studies based on outcrops of the proper reservoir or in reservoirs considered analog to same. Another alternative would be incorporating seismic data of intermediate scale, such as seismic interwell VSPs and high resolution lines.
The present work shows the development and application in real and synthetic data of a geostatistical process to integrate acoustic properties (propagation speed and acoustic impedance) measured in multi-scales and volumetric supports. The algorithm of geostatistical inversion presented by Bortoli and others (1993), referred in the literature as post-matching approach has been redesigned to incorporate data proceeding from other sources. Incorporation of all data occurs step by step with prioritization of major resolution data initially generating intermediate models with vertical resolution of the well which will condition, the final model which corresponds to a downscaling of seismic data. The final product is a model of acoustic property, conditioned by wells and all the seismic available occupying all the points of the seismic grid and with vertical resolution of the profile.
The advantages of incorporating seismic data of intermediate scales, as interwell seismic, for the generation of 2D geological models has already been demonstrated in some works, with emphasize of Bashore and others (1995), Tucker and others (1996) and Castellani (1998). This type of survey presents a large potential because it is possible to image layers with quite reduced thickness, allowing for a stratigraphic recognition of high resolution in the interwell area. However, its application for 3D modeling presents as principal limitation the fact that this type of seismic data, at best, would only be available for a rather reduced number of wells. In order to better evaluate the potential of this tool, relevant questions such as the extrapolation to other areas of the field and use thereof to calibrate and reduce the uncertainty of conventional seismic data are presented in this work.

POST-MATCHING METHODOLOGY TO INCORPORATE SEISMIC DATA OF INTERMEDIATE SCALE

Bortoli and others (1993) described the seismic post-matching methodology, where successive traces of acoustic properties are stochastically modeled based only on well data and following the optimization described below:
1. Define a random trajectory over all the knots (x, y) to be simulated.
2. Carry out the local optimization for each knot (x, y) as below:

- Determine the conditional cumu1ative distribution (CCDF) resolving the equations of the simple kriging system.
- Simulate accomplishments from this distribution.
- Retain the beast trace and make it conditional data (pseudo- log).

3. Pass to the next knot until all knots are complete.

The original method was changed to accept other data in addition to the conventional seismic 3D. The modification consists in the introduction of an additional step in the case of integrating interwell seismic data and other additional steps according to the number of seismic surveys with distinct and better resolution than the conventional seismic. For the following discussion we are going to consider the case of integration of wells, interwell seismic and seismic 3D, as shown in Figure 1. This case represents a way of extrapolation of interwell seismic data to other areas of the field without this type of survey. Data derived from surveys are called twice during the whole process. During the first step the interwell seismic data are used as reference data for the post-matching of simulations of a synthetic tomogram in the area between the wells. In the final step we obtain an optimum interwell velocity model at the vertical resolution of the well profiles. This occurs because the post-.matching is made between filtered simulated traces and traces of the tomogram or of the section of reflection amplitudes, but the accepted traces are retained in their original version i.e. not filtered version.

In the second step this bidimensional model will be the conditioning data for 3D simulations following the optimization process of Bortoli. Figure 1 shows the complete process with emphasize of the two steps discussed above. This procedure can be seen as a succession of scale reductions of geostatistical downscaling of the seismic data available, oriented from the data from major to minor vertical seismic resolution.

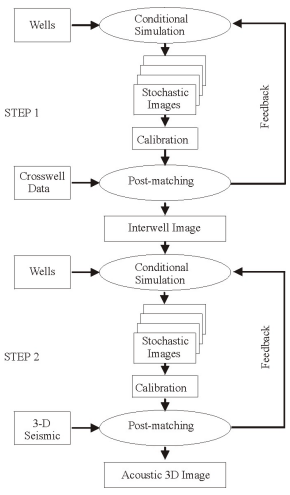

Figure 1: *Flow chart of the method of Bortoli modified to incorporate seismic data of intermediate scale.*

Another modification was made in the original method and was intended to perform filtrations in 2D using filters derived from geotomograpy. Harris (1993) introduced those operators to mimic the lateral effects of the seismic filtration. To perform such filtration the simulations 2D and 3D have to be performed at once. In the 2D case the image is filtered and departs to the trace by trace post-matching. In the case of 3D modeling, the volume is sliced in the direction of the lines of the survey, prior to the filtration. Figure 2 shows these filters in the K_x-K_z domain. The interval of source-diffractor, diffractor-receiver angles, respectively, can meet the ideal conditions of infinite aperture or nearer of real surveys of conventional seismic, VSP and crosswell profiles. In order to copy the frequency bands arrived at in these experiments such operators can be constructed by means of filter staking with different angular frequencies. Figure 2 shows the construction of one of these operators for the case of surface seismic, where the angles vary in an 30º to 150º interval.

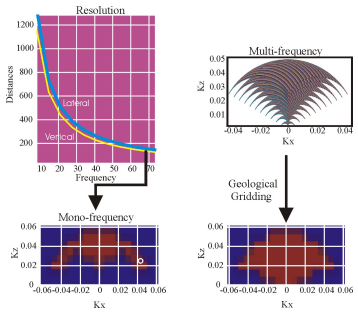

Figure 2: Filter *construction with multi-frequencies used in the seismic filtration 2D of simulated data. The frequency band used goes from 8 to 72 Hz according to the recovered field data*

The multi-frequency filter is the result of staking of various filters obtained in the discretization of the band above. The final. filter is obtained following transfer to a grid K_x-K_z related to the dimension of the cells of the geological model. The blue area marks the dominion below the specific lateral. and vertical resolutions, acquisition and any geological. feature with dimensions over this area will not be correctly imaged. For the filtration it is necessary that the model is in depth and not in time. This results in facilities in the case of interwell seismic, however it is necessary to convert the conventional seismic lines to depth. Once a model is simulated coincident with the crosswell survey, it is required to transform it to the domain K_x-K_z and multiply it by the filter. Thereupon the results brought to the X-Z domain post-matching. The multiplication is made in all points K_x-K_z pertinent to the transformed geological grid, because the discretization in this domain is related to the lateral and vertical dimensions or by the cell-size of the final geological model. For this reason each pair of orthogonal components of the filter must be repelled to this grid. This transfer separates the geological cells containing or not pairs (K_x-K_z) of the filter, assigning value 1 or 0 respectively (or the brown or

blue color in Figure 2). In the case of that, figure, the surface-seismic will not be able to image geological structures whose coordinates in the dominion K_x-K_z are over the blue area.

APPLICATION IN REAL DATA (STEP 1: INCORPORATION OF WELLS AND INTERWELL SEISMIC

In this section step 1 of the process described above is applied to data of the McElroy Field in Texas, USA. As reference data we have a speed tomogram derived from a crosswell survey between the wells 1068 and 1202 spaced 185 feet. The tomogram is sampled each 2.5 feet in both directions. In this application each iteration consists in the simulation of a set of 5 accomplishments of speed interwell models, in the calibration or filtration of each of these models in the post-matching, in the separation of the approved traces and in the preparation of a new conditional data for the following iteration. Iteration number 1 commences with data proceeding only from well 1068 and 1202.

The upper part of Figure 3 shows the speed profiles of these wells at the extreme positions of the area to be modeled, filled with blue color. Only these two profiles feed the Gaussian simulations of the first set of five simulations. The final object is to completely fill the blue area with speed data with the same vertical resolution of the wells, in other words generate 72 pseudo-profiles of speed sampled in minimum dimensions up to 2.5 x 0.5 feet (horizontal and vertical) between the two existing real profiles. The form of obtaining this final model is through a geostatistical downscaling of the diffraction tomogram or reference data shown in the Figure under the title of post-matching. The transformed Fourier 2D of the tomogram determined the maximum value of K_z , which with an interval of angles from -90º to 90º (ideal case of infinite opening), has been used for the construction of the filter applied in the convolution. Prior to the proper filtration vertical direction form 0.5 to 2.5 feet and thereupon the transformed Fourier 2D are taken form each one. The filtration is supplied by the multiplication with the filter and the filtered models in the dominion K_x-K_z are brought back to the dominion X-Z. The post-matching is accomplished taking the value of the correlation between coincident traces of the real and simulated tomograms.

For each iteration, the process of acceptance has been designed to only retain traces pertinent to a same accomplishment, assuring lateral continuity for the final model. The passage from the first to the second iteration occurs with the separation of the new conditionant data of the following simulation, in other words, the accepted pseudo-profiles plus the profiles of original wells. Returning to Figure 3, the best simulated tomogram is number 4 for presenting a major number of traces with maximum correlations superior to 0.85. The accomplishment number 4 (left) provides the new profiles for the next simulation. Approximately 7 iterations are required to complete the interwell space with the average value of correlations of all traces always increasing.

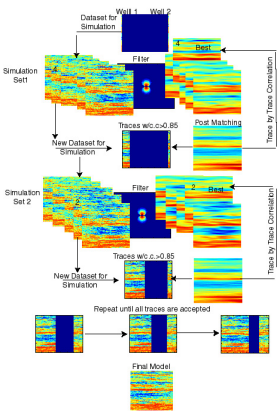

Figure 3: *Field data application. The target is to fill the interwell space (blue color) with pseudo-logs with higher resolution than the tomogram. The cutoff value of 0.85 was determined measuring the correlation between synthetic sonic and the well positions tomogram traces. This calibration reflects the good quality of the seismic data used to the establish a strong geostatistical connection between the different tools.*

EXTRAPOLATION FOR OTHER AREAS OF THE FIELD

In view of being impracticable and economically prohibitive throw crosswell profiles to each pair of wells of a field, but since such data is available it Is important to be possible to extrapolate this information for other areas of the field. This extrapolation has been carried out using synthetic data based on real data of the oil field already mentioned with the already described methodology and has stochastic character and at this approach the main object is to reduce the uncertainty. In Figure 4 we have a real model and various seismic surveys which will be sequentially used in the post-matching such as; one section of amplitudes of a crosswell with reduced interwell distance, another one with major distance and two lines thrown from the surface, the upper one in high resolution and the lower one in the conventional form. The data conditioning the simulation are impedance profiles. In the modeling of the principal area of the reservoir we note a gain obtained In an analysis of uncertainties when we know in more details the feasibility of the reservoir. The minor uncertainty Is evident whenever the equiprobable realizations show great similarity and this is only found in the case with multiscale data. The models based on wells on1y or on we1ls and conventional seismic drive to a great diversity of sceneries, encumbering an optimization of the development of the field. Although the resolution of

the crosswelll and sonic differ considerably, only with the first ones it is possible to observe lateral discontinuities which can be important in the characterization of the reservoir. From all seismic surveys of intermediate scale, the highest impact caused in modeling is undoubtedly due to the narrow crosswell. The incorporation of this tool, in addition of showing a thinned layered stratigraphy, results in an enormous reduction of uncertainties which cannot be resolved by the conventional seismic, only able to detect variations of lower frequency in the profile.

A second application has been carried out with the seismic data available in this field. In addition of a crosswell with 185 feet interwell distance, there are three other surveys of this kind but with distances varying between 600 and 800 feet and two perpendicular seismic lines of high resolution each with approximately 1500 feet over the area of crosswell surveys. The modeling consists in designing an impedance cube comprising the total area of seismic surveys. Obviously the post-matching has only been carried out at the points of coincidence with seismic data. The procedure adopted to initially carry out the first step until completion of the 185 feet tomogram and thereupon continue the process to fill with data of high resolution all the points of the other seismic grids. This application mainly intended to show that extrapolation 3D is practicable, since there is no enough coverage of seismic data. Figure 5 shows the result of the correlations obtained for one of the lines of high resolution. In function of the quality of the quality of this data, not all correlation values were so high as in the first example shown herein, but there has been a reasonable increase from the first to the last iteration, showing that the methodology may be applied, even in adverse conditions as this one.

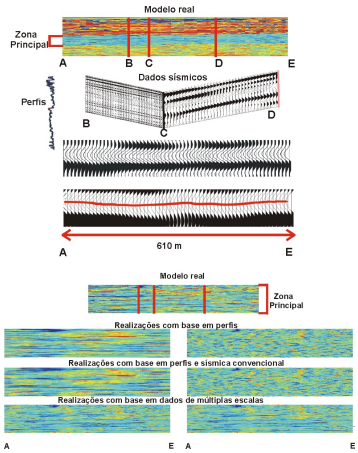

Figure 5: Results of the post-matching in the first and last iterations for one of the seismic lines used in extrapolation 3D.

Figure 4: *Attempt to build the real model constrained by only logs and/or surface seismic and multi scale data. Models carried out based on data of various scales are very similar due to the uncertainty reduction*

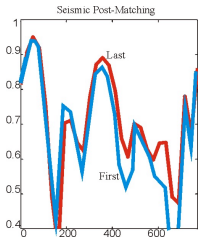

CONCLUSIONS

Seismic data of average scale can be integrated to data of well profiles and conventional surface seismic through the post-matching methodology introduced by Bortoli and others (1993). From these tools the one that has generated the highest impact on models has been the crosswell with not distant wells. This occurred because it has been possible to recover a stratigraphic piling of highest resolution and its lateral variation in a short distance, not detectable features with the conventional tools. The process corresponds to the geostatistical downscaling of the seismic data available, what occurs from the data from major to minor resolution. As in general it is possible to establish relations between acoustic properties and the reservoir, the reduction of uncertainties found with the integration of a larger volume of data is transferred for a better volumetric characterization of the reservoir. The reduction of uncertainties occurs because the post-matching performed based only on conventional seisn1ic is only efficient for vertical features of low frequency. The feasibility of extrapolating surveys of intermediate scale for other areas of the field discovered by this information has been demonstrated herein and shall be understood in its geostatistical sense and shall be preceded by studies of the reservoir which indicate the extension of the area and the pertinence of the operation.

BIBLIOGRAPHIC REFERENCES

Bashore, W. M., Langan, R. T., Tucker, K.E., and Griffith, P.J., Geostatistical integration of *crosswell* data for carbonate reservoir modeling, McElroy Field, Texas: in Stoudt, E.L. and Harris, P.M., Eds, Hydrocarbon reservoir characterization - Geologic framework and flow unit modeling: SEPM Short Course N0.34, SEPM, 199-226, 1995.

Bortoli, L. B., Alabert, F., Haas, A., and Journel , A, "Constraining sthocastic images to seismic data". In Soares. Editor. Geostatistics Troia, volume 1, pages 325-338, Klumer&Dordrecht, Holland, 1993.

Castellani, R. T., High resolution interwell acoustic models based on crosswell reflection image, STP Annual Report, Paper Z, Volume 9, 1998.

Harris, J.M., Diffracted projections in geotomography, STP Annual Report, Paper P, Volume 4, No.1, 1993.

Lo, T. and Inderwiesen, P. L., Fundamentals of seismic tomography, SEG-Geophysical Monograph Series no. 6, ed. By David V. Fitterman, 1994.

Tucker, K. E., Harris, P. M., and Nolen-Hoeksema, R. C., Geologic investigation of vertical and lateral *crosswell* seismic response in a carbonate reservoir -

McElroy Field, West Texas, presented at SEG Develop.Prod. Forum, Vail, Co, 1996.

Integrating 2D reservoir parameters by indirect seismic spatial information updating

Paulo Sérgio LUCIO, ICEx-UFMG - Brazil, lucio@est.ufmg.br*
Manuela MENDES, IST-UTL - Portugal, d1865@alfa.ist.utl.pt

Abstract
Stochastic imaging is the process by which alternative and equiprobable images of the spatial distribution of the interest variable are generated. All such images must honor at their locations not only the principal variable but also the related indirect information.
Probability computation is a key component of statistical analysis on imaging structures. In the probabilistic approach to expert systems, relationships between variables are depicted as conditional probabilities. It is not an uncommon practice, before feasible computational methods were developed, to divide the image into nuclear characteristics and analyze the data as if the set of images were independently sampled. Such analysis fail to utilize part of the geophysical information provided by some interrelated variables, and hence may not be powerful enough to infer the underlying geophysical mechanism correctly.
The purpose of this research is to explore the spatial Markov Chain Monte Carlo (MCMC) method, by means of the Bayesian methodology, to provide practical geostatistics solutions on geophysical extended and complex structures. In reality, for geostatistical problems, reliable implementation of MCMC is not straightforward. The Bayes+Markov algorithm proposed in [4] and developed here, allows a full updating of soft information (*a priori* distribution) by distinguishing the spatial structure of the soft data and it requires no more modelling effort than a traditional multiple indicator kriging. This approach allows generating a *posteriori* probability distribution for any unsampled value, conditional to both local hard and soft data.
A case study on a synthetic realistic data set that concatenates the joint distribution in 2D space shows that this methodology can yield excellent results.

Keywords: Amplitude; Bayesian Modeling; Geostatistics; Impedance; Markovian Calibration.

Introduction

Methods for solving geophysical problems have been greatly influenced by modern statistics and computer methods. These new approaches and methods require few distribution assumptions and can be applied to more complicated estimators. This greatly enhances the practicality for exploring spatial data and drawing valid statistical inferences without the usual concerns for mathematical tractability. The quality of the interpolation or spatial prediction can be measured by non-parametric assessment of local uncertainty.
A common problem in reservoir characterization is that of spatial interpolation from data of different types and different accuracy. Seismic data can provides indirect information on local hard values through *a priori* calibration statistics. The key idea is to model spatial correlation patterns as observed on the calibration scheme (indirect versus direct) and exports this model to other locations allowing inference of unsampled hard data from sampled seismic values. The efficiency of this inference process depends on several considerations, as the decision of "*stationarity*".
In practice of reservoir characterization, the decision of "*stationarity*" corresponds to the traditional split of the reservoirs into zones deemed homogeneous enough by the geologist. Of course, that split should not be so fine as to retain one zone per datum, for then no statistics is possible.
The aim of this algorithm is to export not only the mean of each conditional distribution that is the regression or conditional expectation, but the entire conditional distribution. Based on this approach, the Bayesian framework within which an information, such as the conditional distribution, can be extracted from calibration data and utilized. So, using more effectively indirect sources of information, such as seismic data, is not a mere statistical methodology; it impacts directly our imaging of reservoir heterogeneity in situations where hard data (core or logs and data combinations) are exceptionally sparse and expensive. By the Markovian approximation and calibration, whereby hard information screens all collocated soft information, allows a fast updating of *a priori* distributions without requiring the tedious modeling of numerous cross-covariances between hard and soft data. The objective of this work is to study and implement the proposed algorithm in [4], which is statistically light to the critical problem of data integration.

The Bayesian modeling

Bayesian inference deals with parameter uncertainty by treating parameters as random variables and expressing inferences about parameters in terms of their conditional distributions, given all correlated

observed data. The general idea for prediction is to formulate a model and make inferences based on the conditional distribution.

Consider a stationary (or quasi-stationary) spatial function [3], modeling the variable of direct interest. Its stationary cumulative distribution function is independent on the location (the minimum information available at all location- global *a priori* distribution). The joint bivariate cumulative distribution function depends only on the separation vector, which can be modeled as a series of indicator covariances and cross-covariances ([1] and [2]).

A local *a priori* or *a pre-posteriori* cumulative distribution function of the random variable at this location can model *a priori* local information at a particular location. It represents the local information available at *a priori* to any correction or updating based neighboring information. Availability of any pieces information specific to some location results in a first updating of the global *a priori* into the local *a priori* or *a pre-posteriori*.

The following step consists in a second updatingof the *a pre-posteriori* distribution by the other local *a priori* information available at neighboring locations resulting in a final posterior distribution, characterizing the uncertainty about the hard value at location.

A hard direct sample value can be interpreted as a local *a priori* distribution with null-variance. Such null-variance distribution is a unit-step (indicator) function and should not be updated. A constraint interval can be coded, as an incomplete unit-step function where the hard step location is unknown.

Local *a priori* information specifics to each data location are processed under *a priori*-model of spatial dependence into a *posteriori* distribution functions, different for each location. The model of spatial dependence allows a Bayesian updating of any local *a priori* or of the cumulative function by neighboring related data. The basic idea is to interpret the local *a priori* distribution function values as realizations of corresponding random functions, with their specific covariances and cross-covariances.

Markovian calibration

Under the hypothesis that the hard information indicator always prevails over any soft collocated information, the cross-covariance (soft versus hard-indicator) and the auto covariance (indirect) can be deduced directly from the indicator covariance model and a few calibration parameters. Hence, the inference required for cokriging approach reduces to that of the indicator covariances a task equivalent to that required for indicator kriging (*non-parametric geostatistics*) [2]. The calibration parameters inform the system about the soft information accuracy. For each cutoff value, the moments of the conditional distributions of the soft information, given respectively their indicator function, provide a calibration of the soft information. Under the Markovian approximation, the covariance of the soft data is assumed proportional to the hard indicator data covariance except for an additional nugget measuring the imprecision of the soft data.

The information content of the soft data is better understood if expressed in terms of standardized correlograms. The loss of information content due to the softness of the soft data can be measured by a relative loss of correlation.

Modeling (Block Indicator Cokriging)

Consider a modeling of the empirical a posteriori distribution function obtained from some hard indicator values at different locations and some others soft indicator data (Fig.2), obtained at different locations (not necessarily the same of the first variable group).

The cokriging of the indicator random variable provides a posteriori distribution function model. In the general case, the cokriging system would require the inference and modeling of three covariance functions for each cutoff value (auto-covariance of the indicator, cross-covariance of soft versus indicator and the auto-covariance of the soft).

The Markovian approximation reduces that inference to the single indicator covariance and the other two covariances are deduced from their relations with the calibration parameter [4]. With the indicator variogram models of Fig. 3 (range is approximately 25.x8. meters), all the structural functions needed for determination of a posteriori *cdf's* (*cumulative distribution function*) using multiple indicator kriging are available. The calibration parameters of Tab.4 allows determining the additional structural functions [4] needed to apply the proposed Bayes+Markov (or Markov-Bayes, following [4]) formalism.

Application

The ability and accuracy of the proposed algorithm was checked using pseudo-synthetic data. Here we present a test run over 2D data sets, which comprise a regular $(nx = 50m) \times (nt = 500ms)$ rectangular grid sample location. This data set concerns the True Impedance (TI) and the True Seismic Amplitude (TSA), which is the seismic amplitude associated to

the impedance by convolution with a band-pass wavelet. Each grid node is under-sampled, in order to reduce the computing weight, for the variables $(nx = 100m) \times (nt = 1000ms)$. So the data sets become: the Impedance (Fig.1 (a)), the attribute focuses of the study providing the hard data and the Seismic Amplitude (Fig.1 (b)), the secondary variable providing soft information about the hard data. Their respective associated statistical distribution are showed in Fig.1 (c) e Fig.1 (d).

The goal is to recover the True Impedance, over the whole field, by using the reduced samples as hard data and using the collocated True Seismic Amplitude as a secondary or background variable (soft information). The data pairs are used strictly for deriving a number of conditional distributions of hard values given the indirect information, sometimes concerning the rock types or lithofacies coding. In this study, five classes were considered enough (Fig.2 (a) and (b)). According to the explained theory, several statistical amounts have to be computed. For providing the Markovian calibration, information about the Uniform Distribution constructed are computed and displayed in Tab.1 and Tab.2 for each percentile cutoff. The stationary *cdf* is presented in Tab.3 and the calibration parameters, for the spatial integration algorithm, are showed in Tab. 4. Finally, Tab.5 provides the cumulative conditional distribution of direct threshold value with classes given by the indirect information attribute (Fig.2).

The 2D indicator variograms (Fig.3) were calculated and standardized by the corresponding indicator variance. The final result delivers a stochastic image of the Impedance, presented in Fig.4 (a). The match between the Fig.1 (a) and Fig.4 (a) provides a good evaluation about the accuracy of our algorithm. It can be measured by the absolute error (mismatch) which is negligible, since it is almost everywhere less than 10%, as displayed on Fig.4 (b).

Conclusions

We have integrated seismic and well data to define the structure and to make an attribute-derived prediction about the distribution of Impedance. Our challenge is still to make the True Impedance and Estimate Impedance as close and robust together as possible, given the relatively small number of wells available for cross-correlation with seismic attributes.

Acknowledgements

The CAPES - Brazil, BEX0455/00-8, supported this Project. The GeoMS - Geostatistical Modelling Software was gently provided by the CMRP - IST – Portugal.

References

[1] David M. (1988). Handbook of Applied Advanced Geostatistical Ore Reserve Estimation, Elsevier.

[2] Journel, A. G. (1989). Fundamentals of Geostatistics in Five Lessons, Short Course in Geology, 8, American Geophysical Union, Washington D. C.

[3] Ripley, B. (1987). Stochastic Simulation, John Wiley & Sons, New York.

[4] Zhu, H. and Journel, A. G. (1993). Formatting and Integrating Soft Data: Stochastic Imaging via the Markov-Bayes Algorithm. Geostatistics TROIA'92, A. Soares, Ed., vol. 1, pp. 1-12, Kluwer Academic Publishers.

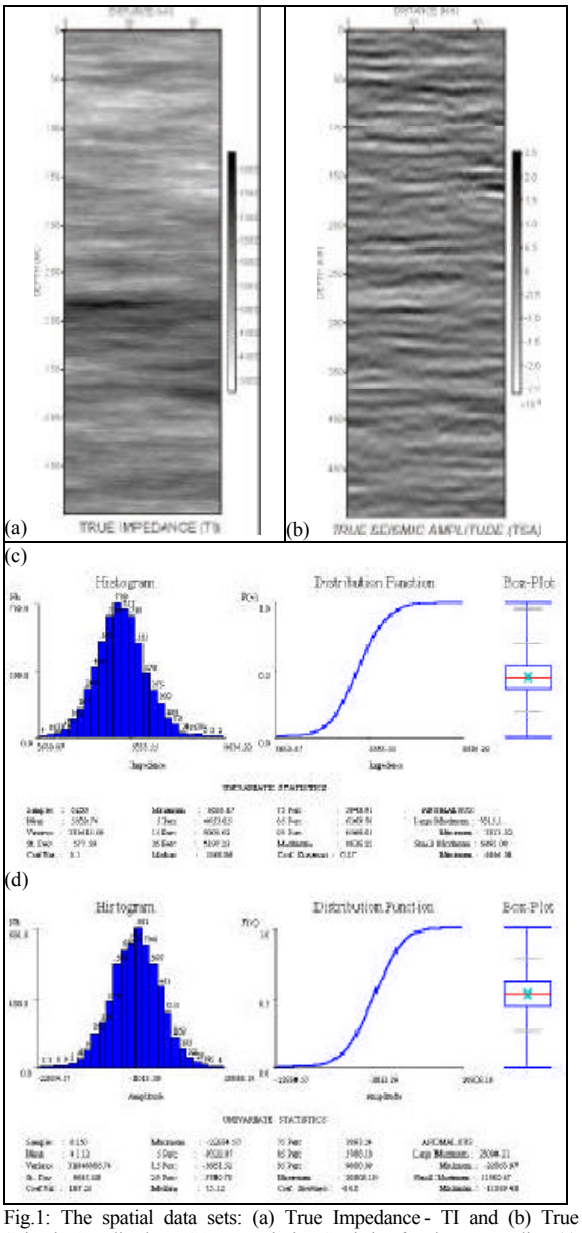

Fig.1: The spatial data sets: (a) True Impedance - TI and (b) True Seismic Amplitude - TSA. Descriptive Statistics for the re-sampling (c) Direct Impedance attributes and (d) Indirect Seismic Amplitude.

Amplitude		
Class	Cutoff-Point	N. of Samples
AC1	-4632.979980	1249
AC2	-1344.380005	1256
AC3	1488.420044	1247
AC4	4817.379883	1246
AC5	23119.31055	1252

Tab.1: The threshold of Soft(Seismic Amplitude) values.

Impedance		
Class	Cutoff-Point	N. Samples
IC1	5104.55	1253
IC2	5433.42	1246
IC3	5711.17	1246
IC4	6045.73	1250
IC5	8142.88	1255

Tab.2: The threshold of Hard(Impedance) values.

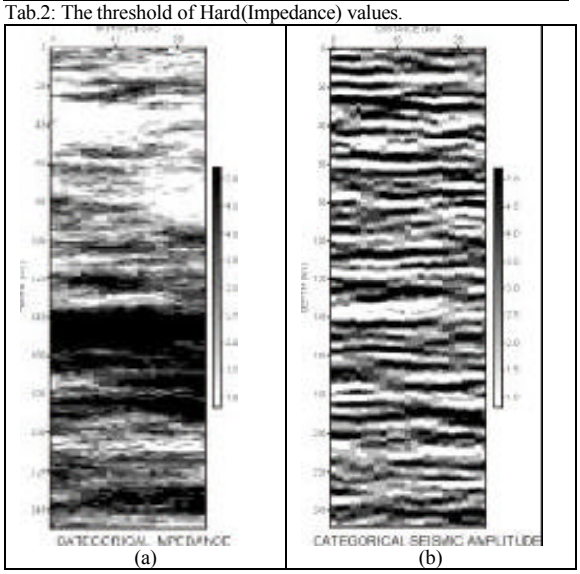

(a) (b)

Fig.2: Descriptive Statistics for the five thresholds (cutoff points) for the (a) indirect and (b) direct attributes, respectively– Spatial Uniform Distribution.

$Prob(Imp(x) \pounds z_{ClassIC})$	$Prob(Amp(x) \pounds z_{ClassAC})$
0.20048	0.19984
0.39984	0.40080
0.59920	0.60032
0.79920	0.79968
1.00000	1.00000

Tab.3: The stationary cumulative distribution.

Class	E[Y|I=1]	V[Y|I=1]	E[Y|I=0]	V[Y|I=0]
C1	.58714	.07854	.40976	.07807
C2	.60539	.07977	.39151	.07910
C3	.61012	.07430	.38977	.07428
C4	.62134	.12450	.38266	.12546

Tab.4: Calibration parameters for the Markovian algorithm modeling.

Y=F(I|A)	IC1	IC2	IC3	IC4	IC5
AC1	.2642	.4708	.6589	.8263	1.000
AC2	.1911	.3933	.5932	.8002	1.000
AC3	.1716	.3753	.5726	.7995	1.000
AC4	.1637	.3708	.5803	.7833	1.000
AC5	.2117	.3890	.5911	.7867	1.000

Tab.5: Cumulative Conditional Distribution (soft distribution: **Y=F(IC|AC)**) of the direct threshold value (Impedance) with classes given by the indirect information attribute (Amplitude).

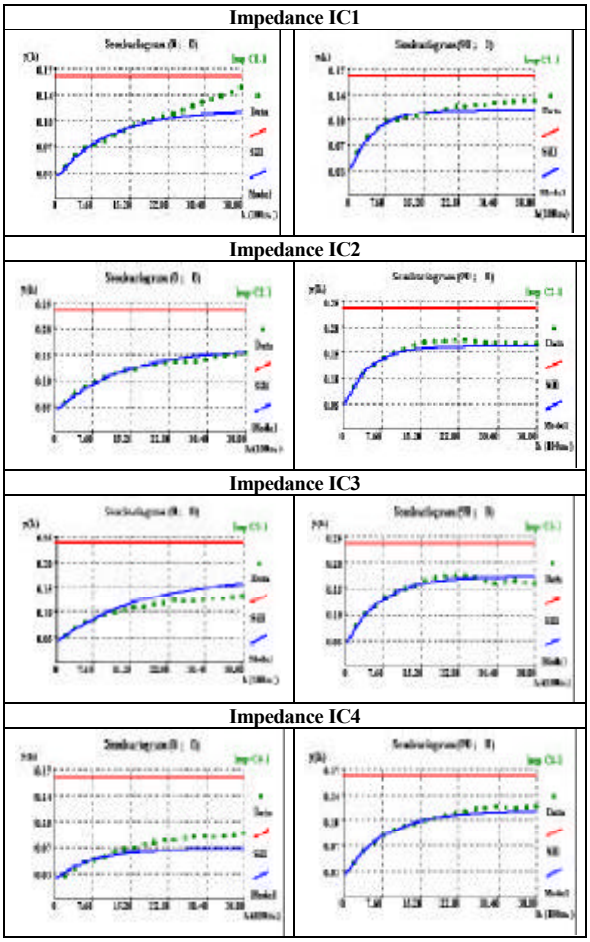

Fig.3: Variograms in the two (main = 90^o , minor = 0^o) direction of continuity for the four cumulative ranges of the direct indicator attribute. Geometrical anisotropy is detected in each class.

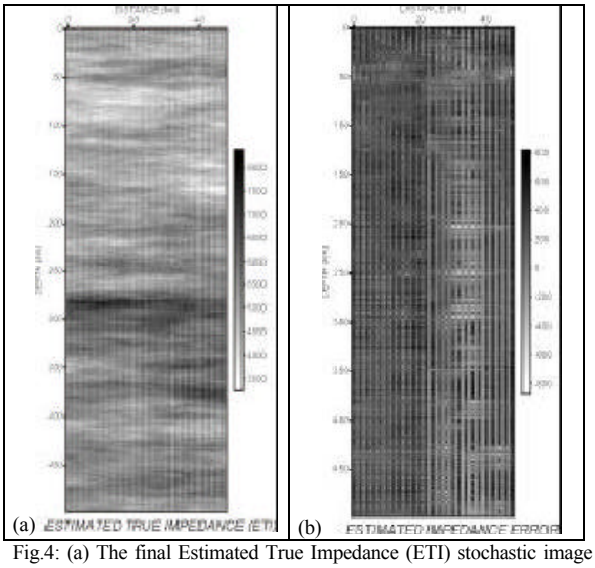

Fig.4: (a) The final Estimated True Impedance (ETI) stochastic image and (b) the associated absolute error.

Integration of Dynamic & Static Reservoir Models in Campos Base Field

Alcides Aggio, PETROBRAS S/A, Brazil and Scott Burns Geowell Inc., Paris, France

Abstract

Shared-Earth-Model is an efficient tool to characterize dynamic and static reservoir. The application to a Campos Base Field is shown in this paper. It was providing a rapidly integration of information that an asset time need to manage a reservoir. Addressing in the paper the matching of the flux-fluid simulator scale in geologic/seismic scale, providing a downscaling that is the main task to generate a synthetic data to analysis the 4D seismic analysis of legacy seismic data, in the same computational environment.

Introduction

An integrated reservoir model, or shared-earth-model, is a vehicle for rendering different data types with an effective property for visual comparison at different scales and in different domains. With the advent of integration ease—providing freedom for creative solutions by seasoned professionals—comes the potential of rapidly relating different inner- and cross-disciplinary data to help gain a better understanding of a reservoir's current "information state." This improved understanding allowing then the determination of the technology, cost & time appropriate for reservoir characterization using available data, and determining the need for additional data. This relational framework serves to highlight areas where more emphasis is needed, and to optimize and gauge the effectiveness of more sophisticated characterization, processing, imaging and inversion techniques that are implemented in subsequent phases.

In this context, our presentation focuses on the task of relating seismic information to geologic models and fluid-flow simulations. In our initial integration of a deepwater dataset, we address improved visualization of 3D seismic amplitudes for stratigraphic interpretation, saturation downscaling methodology for seismic modeling, and 4D seismic analysis of troublesome data. This study presents some of the results of a *Seismic Monitoring Technology for Deepwater Reservoirs* Project of the PETROBRAS/R&D research program for advanced oil recovery (PRAVAP).

Seismic Quantification

Utilizing sequence stratigraphy to build a high-resolution chronostratigraphic framework the reservoir is often essential for predicting vertical discontinuities and lateral variations in the rock matrix. Combined with the petrographic model this forms the basic work model for defining the control of fluid flow. Seismic information is used in constructing or updating the high resolution geologic model through the qualitative interpretation of the seismic signatures and through quantitative methods like inversion, multivariate statistics, and geostatistics. Rendering 3D seismic attributes in "stratigraphic space" helps to highgrade seismic interpretation and to validate the geologic model.

In addition to sharing some of the same problems of history-matching (upscaling assumptions, effective properties, domino effect) quantifying seismic information for reservoir characterization, which usually relies heavily on synthetic seismograms, requires transforms to estimate velocity and density as a function of the spatial distribution of rock

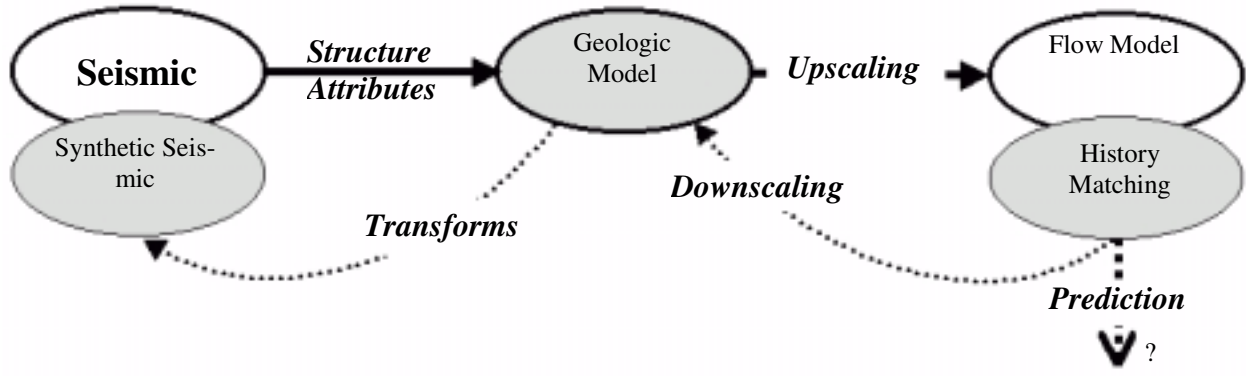

Fig. 1—Shared-Earth-Model: comparing multidiscipline data using effective properties and domain transforms facilitates static & dynamic reservoir characterization.

& fluid properties (**Fig. 1**). Synthetic seismic responses of the geologic model (updated with estimates of fluid distributions) is a very useful aid in quantifying and integrating seismic information into the reservoir model—it forms the basis for most seismic inversion algorithms. Limitations due to assumptions for theoretical modeling and practical aspects of seismic-to-well calibration can greatly decrease the confidence in seismic inversion results. Besides quality control of seismic inversion, seismic simulation of primary events and potential artifacts due to acquisition, processing & noise aids high-resolution interpretation, and the development of methodologies for quantifying seismic attributes.

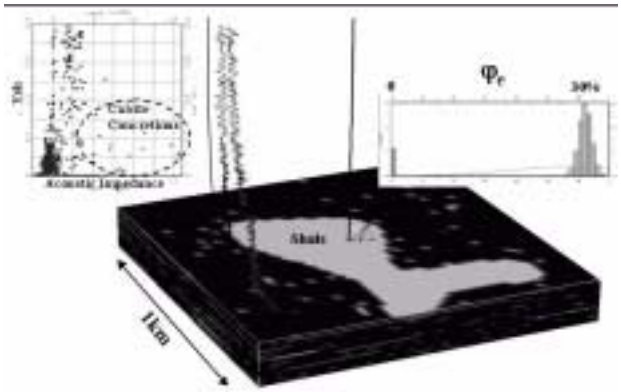

Fig. 2—High-Resolution Geologic Model centered at a well used For calibration shows a potential distribution of shale near top reservoir.

Static &Dynamic Reservoir Characterization

With the aid of seismic modeling and visualization within a high-resolution stratigraphic framework, we relate data from two, time-lapse 3D seismic surveys acquired in deepwater, Campos Basin, Brazil, to estimates of lithology and history-matched fluid distributions within a turbidite reservoir.

High-Resolution Geologic Model

The high-resolution geocellular model is the vehicle for visualizing both the relatively finer core/ wireline information, and the coarser seismic &production information. To relate seismic information to the other data types, the synthetic seismic response of the geocellular model is generated, which entails the downscaling of flow-simulator results.

To model expected heterogeneities of effective porosity, sequential gaussian simulation is used to distribute reservoir sandstone, shale and calcite concretions within a high-resolution stratigraphic framework. **Fig. 2** shows a realization centered on a well used for calibration (cell dimensions 20x20x2.5 m) – the histogram of this simulation shows 0 % effective porosity (φ_e) for shales & concretions and approximately 30% effective porosity for reservoir sands.

Saturation Downscaling

Accurate distribution of smooth simulated estimates of SW within a high-resolution geologic model requires a downscaling method – this method in turn can depend on the upscaling method employed for fluid-flow simulation. Our downscaling method is based on the premise that the smooth flow-simulator approximation can be distributed as a function of effective porosity, and that the porosity was not changed during history matching. The downscaled oil saturation, So' can be approximated with

$$So' = So(\varphi_e / \varphi_u)^{(1-\alpha)}$$

Which, when α = So, weights So' toward So as So approaches 100%. φ_u is the upscaled, volume averaged effective porosity. In **Fig 3** note on the results computed from the wireline logs that with So=80% the So' variation is less than at So=50%, and is approaching the 80% value.

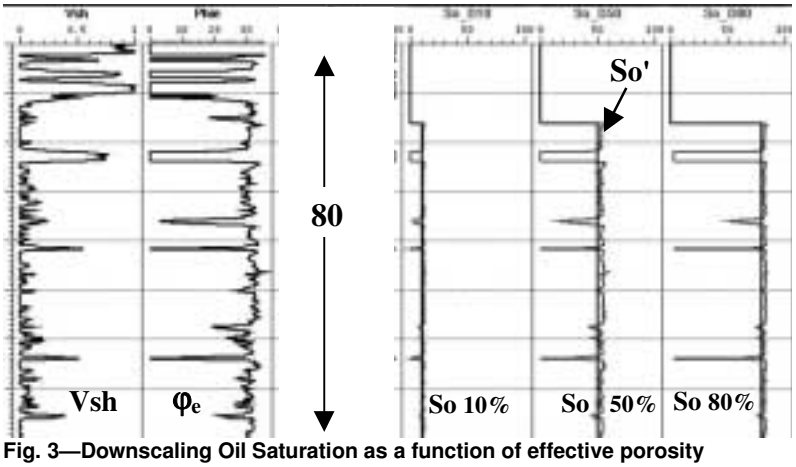

Fig. 3—Downscaling Oil Saturation as a function of effective porosity

Seismic Lithology

After approximate transforms relating rock matrix and fluid properties to velocity and density are derived, the synthetic seismic response as a function of incident angle is calculated for geocellular model.

Fig 4 is a view of the reservoir isopach contour map base-showing reservoir thinning associated with a channel cut-superimposed on the normal-incidence reflection coefficients of the reservoir base. **Fig 5** compares the filtered synthetic seismic volume to the 3D seismic data displayed as voxels on orthogonal axis, and interpolated on the stratigraphic framework of the geocellular model—the seismic volume showing similar shale body amplitude contrast as the synthetic seismic amplitudes.

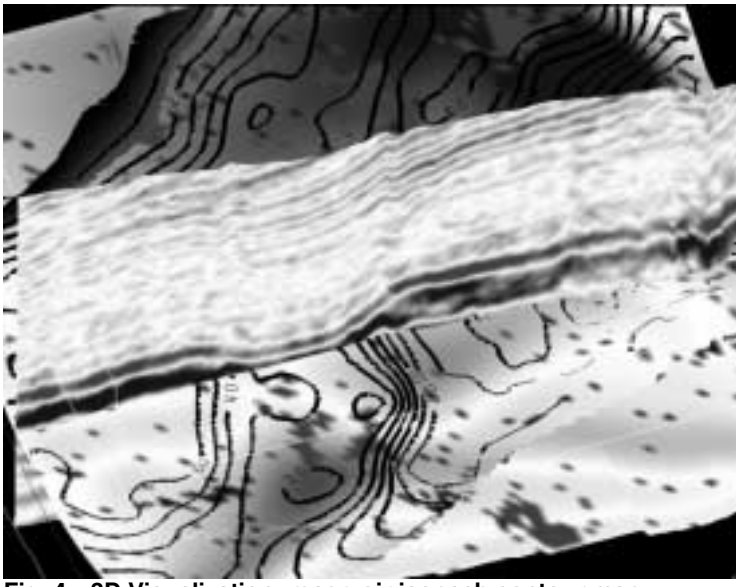

Fig. 4—3D Visualization: reservoir isopach contour map superimposed on the normal-incidence reflection coefficients of the reservoir base.

4D Seismic Analysis

In an attempt to optimize the relation of differential seismic attributes to production data, interpretive processing techniques are employed in a shared-earth-model environment on repeated 3D seismic surveys covering approximately six years of production. Using 4D seismic modeling as a guide, interpretive attribute processing involves suppressing acquisition & processing artifacts in the reservoir by finding a correction that minimizes differences outside the reservoir and applying a similar correction to the reservoir attribute. 3D ray-trace modeling is used to study potential artifacts on the differential attribute maps due to multiples and differences in seismic acquisition.

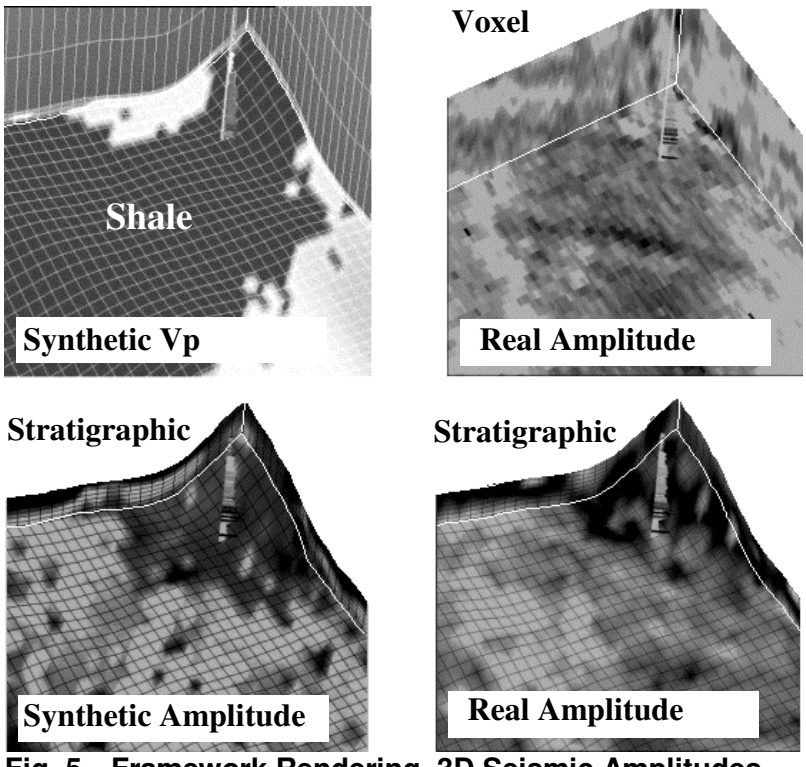

Fig. 5—Framework Rendering 3D Seismic Amplitudes

Fig. 6 compares the noise-free synthetic to the real change of the reservoir's average absolute amplitude after approximately six years of oil production: ΔAmplitude = survey before production minus survey after production. The 4D seismic model shows positive (black) for water displacing oil, and negative (white) for gas displacing oil. The real ΔAmplitude map shows that the region of largest positive values (body trending NW-SE) is in agreement with the model; however, due to the proximity of a fault passing just above this area, this could be a misleading positive correlation. Going away from the potential influence of the fault, there are several good correspondences near wells with large changes of oil saturation. To appreciate the potential effect of differences of X, Y location between the surveys—due to acquisition or processing—a relative shift 100m south is applied on the synthetic amplitude maps prior to subtraction.

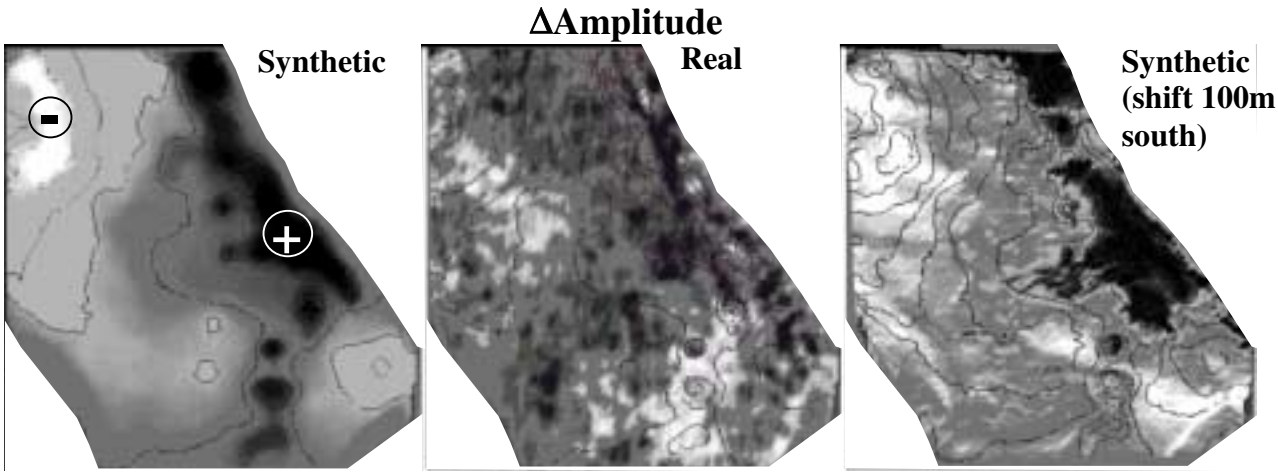

Fig. 6—ΔAmplitude = survey before production minus survey after production. The 4D synthetic shows positive (black) for water displacing oil, and negative (white) for gas displacing oil.

Change in reservoir velocity due to oil displacement by gas or water causes a change in seismic travel-time (ΔTime). **Fig. 7** shows a fair correlation between the modeled and real ΔTime (modeled ΔTime contours superimposed: negative values are due to gas displacing oil; positive, water displacing oil).

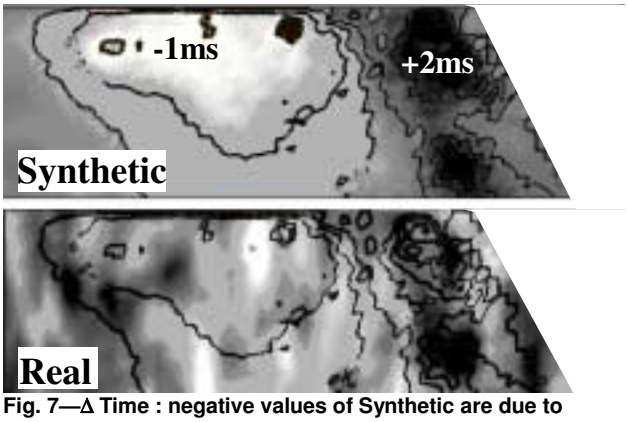

Fig. 7—Δ Time : negative values of Synthetic are due to gas displacing oil; positive, water displacing oil.

Concluding Remarks

Rapid analysis of 3D seismic information requires accurate velocity & density estimates of rock and fluids for time/depth transforms and seismic modeling.

Comparing in a shared-earth-model environment multidiscipline data using effective properties and domain transforms facilitates static and dynamic reservoir characterization—initial integration improving effectiveness for subsequent processes in the reservoir of the Campos Base.

Acknowledgments:

We thank PETROBRAS/R&D for permission to publish and especially Rogério Santos, PRAVAP 4D coordinator, for his support and contribution during the project.

Local porosity inversion of multiple geophysical data sets. Part I: using rock physics and geostatistical modeling

Luiz Geraldo Loures [†], *Fernando Moraes*[†]

Introduction

This is a first part of a two part paper investigating the problem of constructing a porosity model from multiple sources of information, considering a certain degree of uncertainty associated with each one of these sources. A methodology for porosity inference is developed using fundamental concepts of the Bayesian methodology, which is the direct use of probability theory as a method of inference. The main goal in Bayesian methodology is to obtain the posterior probability density function (PDF) for parameter under investigation, which serves to answer all questions of inference. The posterior is the product of two types of PDFs: prior PDF, which carries prior information about the unknown, and likelihood function, which carries data-fit information. In this part, we consider the combination of elastic seismic attributes and well log data. Then, in the next part (**?**), we discuss how to incorporate the seismic data (shot-gathers) directly into the formulation.

Seismic data have been the main source of information for determining reservoir properties in the interwell region. The most frequently employed methodologies are based on multivariate regression, which treat the data as spatially independent, or geostatistics. The latter is highly dependent on a model of spatial variability constructed from the data.

In this work, we follow the local approach of Moraes and Scales (2000), which yield marginal probabilities for porosity at a particular cell of the reservoir instead of the joint distribution. The final solution is a set of posterior distributions for interval porosities given the well log and seismic attribute data. Questions of inference such as estimates or associated uncertainty is addressed to these posteriors.

The posterior distribution for porosity is obtained, considering only prior information about bounds on porosity variation and data generated from seismic attributes, composed by P- and S-wave velocities (V_p and V_s, respectively) and density (ρ), and well logs (porosity, V_p, V_s, density and gamma ray). Equations from rock physics are used to relate seismic attributes to porosity. We assume that the seismic attributes are provided by a generic seismic inversion program without any kind of uncertainty analysis.

The application of the methodology follows a two step procedure. First, we run a separated inversion in each well, following the work described by Loures and Moraes (1999). Next, we propagate the well information to the interwell region, with the help of values of a variability measure and their corresponding formula. This information and the information derived from seismic attributes, both represented in terms of likelihood functions, are combined by simple use of Bayesian rules for deriving posterior probability distribution. A synthetic data example for reconstructing a slowly varing porosity model (Figure 1) illustrates how the methodology works.

Bayesian formulation

Consider a reservoir model composed by a set of N block cells with average porosity $\boldsymbol{\phi} \in R^M$. Our problem is to find the porosity of the ith cell ϕ_i, $i = 1, \ldots, M$, represented simply by ϕ, using data sets from elastic seismic attributes V_p, V_s and ρ, respectively represented by $\mathbf{s} = (\mathbf{s}_1, \mathbf{s}_2, \mathbf{s}_3)^T \in R^{3N}$, and some additional data $\mathbf{v} \in R^L$. To select $\mathbf{v}$, we focus on the role of the likelihood l_p (equation 1) which is to represent the well log data information at neighboring locations. The log data is summarized by an inversion procedure by Loures and Moraes (1999) yielding estimates $\hat{\phi}$. Then, our choice is to make $\mathbf{v}$ as experimental porosity-porosity variogram values computed from pairs of $\hat{\phi}$ at two different locations.

According to the Bayesian methodology, the solution to this problem is the posteriori PDF for porosity given the data $p(\phi \,|\, \mathbf{v}, \mathbf{s})$. This posterior distribution can be obtained by application of Bayes' Theorem which gives

$$p(\phi \,|\, \mathbf{v}, \mathbf{s}) \propto l(\mathbf{v}, \mathbf{s} \,|\, \phi) q(\phi), \qquad (1)$$

where $q(\phi)$ is the prior distribution and $l(\mathbf{v}, \mathbf{s} \,|\, \phi)$ is the likelihood function.

Assuming that the only relevant prior information comes from lower and upper bounds on porosity (ϕ_l and ϕ_u), a uniform distribution can

[†]Laboratório de Engenharia e Exploração de Petróleo/Universidade Estadual do Norte Fluminense (LENEP/UENF), Macaé, RJ, Brasil. (gera@lenep.uenf.br, fernando@lenep.uenf.br)

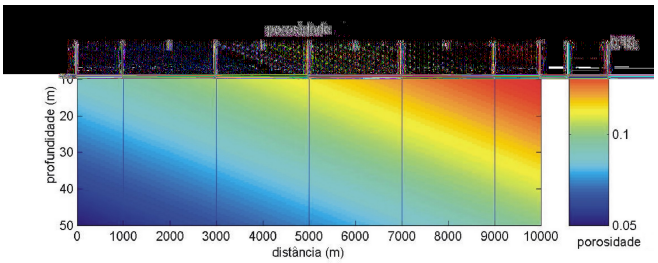

Figure 1: The image representing the true porosity model used in the synthetic data example. Vertical lines show the locations of 5 wells distributed across the model.

be assigned for the prior. In this case, a standard procedure in Bayesian inference is to incorporate the prior into a proportionality constant.

We rewrite the likelihood in terms of each type of attributes data $\mathbf{s}_1, \mathbf{s}_2$ and $\mathbf{s}_3$, considering all data vectors to be independent, the posterior becomes

$$p(\phi \mid \mathbf{v}, \mathbf{s}) \propto l_p(\mathbf{v} \mid \phi)\, l_{s_1}(\mathbf{s}_1 \mid \phi)\, l_{s_2}(\mathbf{s}_2 \mid \phi) \\ l_{s_3}(\mathbf{s}_3 \mid \phi), \text{ for } \phi_l \leq \phi \leq \phi_u \quad (2)$$

In this work, we assume lack of information regarding the method used to obtain seismic attributes making it an independent process. This is often the situation when using commercially available software to generate attribute volumes. Although we admit that correlations and higher order moments exist, they are not known. Neither are attribute uncertainties.

Assigning probabilities

Next task is to define mathematical forms for the likelihood functions l_p and l_s. To do that, it is first necessary to specify the relations between data and unknown porosity. In our case, assuming additive errors in the data, we may write

$$\mathbf{s}_i = \mathbf{f}_i(\phi) + \mathbf{e}_i, \text{ for } i = 1, 2, 3 \quad (3)$$

and

$$\mathbf{v} = \mathbf{f}_4(\phi) + \mathbf{e}_4, \quad (4)$$

In the case of f_i, for $i = 1, 2, 3$, we seek, respectively, for equations of seismic attribute V_p, V_s, and ρ as a function of porosity. These are available in the rock physics literatures. For instance, Eberhart-Phillips et al. (1989) derive empirical formulas for V_p and V_s, which are given by

$$f_1(\phi) \equiv V_p = 5.77 - 6.94\phi_i - 1.73\sqrt{c} \\ +0.446(P_e - e^{-16.7P_e}), \quad (5)$$

and

$$f_2(\phi) \equiv V_s = 3.70 - 4.94\phi - 1.57\sqrt{c} \\ +0.361(P_e - e^{-16.7P_e}), \quad (6)$$

where P_e is effective pressure and c is the clay content. For density, we use

$$f_3(\phi) \equiv \rho = (1-\phi)\rho_m + \phi\rho_f, \quad (7)$$

where ρ_m is the matrix density and ρ_f is the pore fluid density.

In the case of modeling operator f_4, our choice of data $\mathbf{v}$ makes f_4 the variogram function of pairs of well log porosity estimates $\hat{\phi}$ and the unknown cell porosity ϕ, which is given by

$$\gamma(h) \equiv f_4(\phi) = \frac{1}{2\,NP} \sum_{i=1}^{NP} \left[\hat{\phi}(\mathbf{r}_i) - \phi(\mathbf{r}_i + \mathbf{h})\right]^2, \quad (8)$$

where $\mathbf{r}_i$ and $\mathbf{r}_i + \mathbf{h}$ represent two different locations separated by a lag vector $\mathbf{h}$ of size h and NP is the number of pairs.

Next, we select the normal PDFs to describe the errors in equations (3) and (4). According to the maximum entropy criterion (Jaynes (1978)), this implies that first and second order moments are, for our purposes, appropriate to describe the uncertainty in the data.

Posterior distribution

Mathematically, normal distributions depend on two parameters, mean and variance. Consequently, choosing normal distributions to describe errors in the data introduces new parameters into the posterior distributions, the data variances. These are unknown parameters which we have no interest in infering. Marginalization of the posteriori distribution is a standard tool in Bayesian inference to eliminate parameters such as these. This marginalization process is an integration of the posterior distribution with respect to data variances. This procedure results on t-student distributions, which when combined gives the posteriori distribution

$$p(\phi \mid \mathbf{s}, \mathbf{v}) \propto \left\{[\mathbf{v} - \mathbf{f}_v(\phi)]^T\, [\mathbf{v} - \mathbf{f}_v(\phi)]\right\}^{-\frac{L}{2}} \\ \Pi_{i=1,\ldots,3} \left\{[\mathbf{s}_i - \mathbf{f}_i(\phi)]^T\, [\mathbf{s}_i - \mathbf{f}_i(\phi)]\right\}^{-\frac{N_i}{2}}. \quad (9)$$

Synthetic data example

Using a 2-D model of vertical and lateral changes in porosity (Figure 1) and the equations (5), (6) and

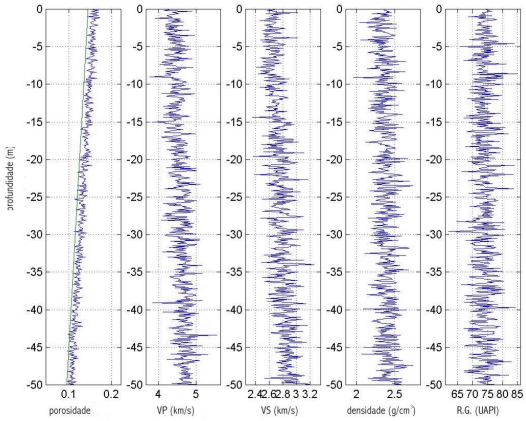

Figure 2: Well log data for the first well represented in the model of Figure 1. These are, from left to right, neutron porosity, sonic logs (P and S waves), density and gamma ray.

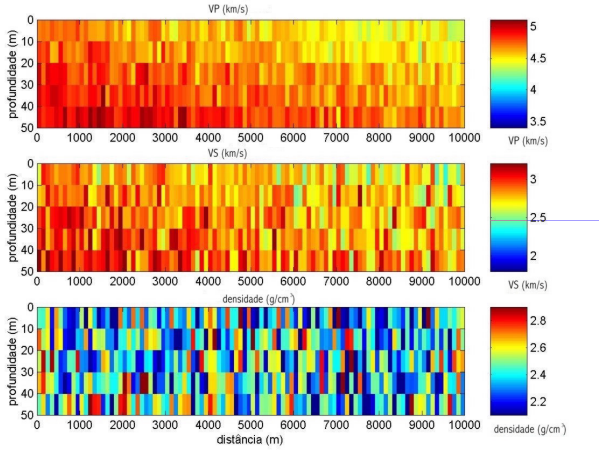

Figure 3: Seismic attributes V_p (top), V_s (middle) and density (bottom).

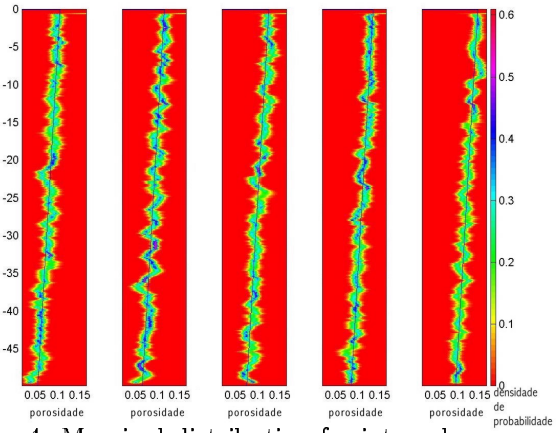

Figure 4: Marginal distribution for interval porosity resulting from application of the inversion procedure by Loures and Moraes (1999) using the well log data (Figure 2). The purple line represents the true porosity of the model.

(7), we simulated all required data: neutron porosity, P and S-wave sonics, density and gamma ray logs and seismic attributes of V_p, V_s and density. The gamma ray log is used to obtain information about clay content of the medium, that is required in equations (5) and (6). The clay content of the model is constant along the model and equal 0.5.

All simulated data are corrupted with 10 % pseudo-random Gaussian noise with zero mean. Additionally, the neutron porosity log, has a 10 % of the true porosity shift to simulate a systematic error. The noise corrupted logs are shown in Figure 2. In the case of seismic attributes, the standard deviation of the noise was defined based on examples of elastic inversion available at literature (e.g., Debski and Tarantola (1995)), respectively 10 %; 20 % and 30 % for V_p, V_s and density. The noise corrupted seismic attributes, which are shown in Figure 3, constitutes data vectors $\mathbf{s}_i$, for $i = 1, 2, 3$.

As described above, the first step in the application of the proposed methodology is to proceed the inversion of well log data. Figure 4 shows the resulting porosity PDFs for each depth interval along the wells. The mode of these PDFs are estimates for interval porosities at the wells. Data vector $\mathbf{v}$ is generated from these well porosities using experimental horizontal variogram calculated with a lag spacing of 2 km. Next we to evaluate both likelihoods l_s and l_p to compute the posterior as their product. To do that, we use a interpretative model composed of cells 100 m wide by 10 m thick. A moving 2-D window, covering three cells (10 x 300 m), is used to obtain the distribution the likelihoods in each cell of the reservoir. To evaluate the individual contributions of well information and seismic attributes data, the posterior distribution is computed using three different data combinations: using well and attribute data individually ($p \propto l_p$ and $p \propto l_s$) and both data sets combined ($p \propto l_s \times l_p$). The cell porosity posterior distribution is referenced to the position of the center of the window. The Fresnel Zone can be considered for defining the dimension of the window, allowing it to vary across the reservoir.

Figure 5 shows the porosity values corresponding to the modes of the posterior in each cell of the model using the three data combinations: just the variogram data (**a**), just seismic attributes (**b**) and both variogram and attribute data (**c**). Figure 6, following the same order of the mode images in Fig-

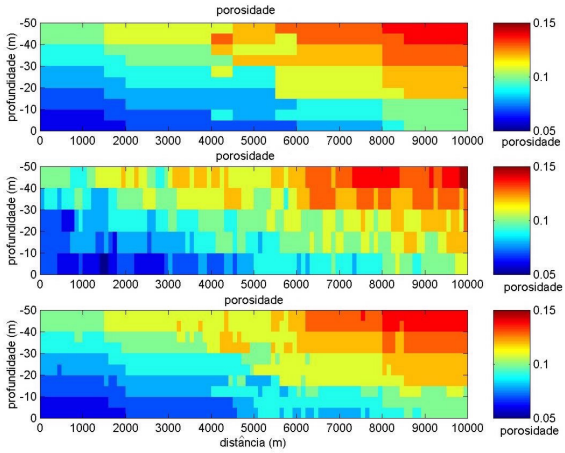

Figure 5: Images representing the modes of the posterior distributions obtained by the use of variogram data (a), seismic attributes (b) and both data sets (c).

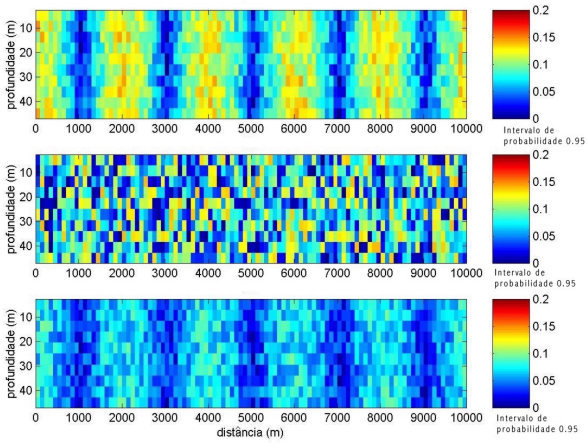

Figure 6: Length of the 0.95 probability interval of the posterior distributions obtained from the inversion of variogram values (a), seismic attributes data (b) and both data sets (c).

ure 5, represents the length of centered 0.95 probability interval. This gives the idea of the spread of the posterior and resolution for porosity of each cell of the reservoir.

Conclusion

We presented an approach to reservoir characterization fully based on inversion theory, which is capable to integrate multiple data sets in a straight forward way. The commonly employed formulations of the mathematical physics relating data and model parameters is replaced by empirical formulas of experimental rock physics. Geostatistics is also integrated through the experimental variogram and the corresponding formula, both used in the context of inversion theory. This procedure produced similar results as geostatistics without going trough the task of variogram modeling. A synthetic data test using a slowly varying model demonstrated the consistency of the proposed methodology.

Analysis of results show reasonable reconstructions of the true porosity model obtained from the mode of the posteriors. The associated uncertainty, represented by the length of 0.95 probability intervals, consistently vary depending on the amount of information available. Higher resolution is obtained at the wells. The variogram fitting procedure allowed to describe the information about the porosity from the wells at interwell location. For the inversion of seismic attributes alone the level of uncertainty varies homogeneously across the model. When combining variogram and attribute data, we observe that the overall uncertainty is reduced and the porosity model is better reconstructed.

References

Debski, W., and Tarantola, A., 1995, Information on elastic parameters obtained from the amplitudes of reflected waves: Geophysics, **60**, 1426–1436.

Eberhart-Phillips, D., Han, D., and Zoback, M. D., 1989, Empirical relationships among seismic velocity, effective pressure, porosity, and clay content in sandstone: Geophysics, **54**, 82–89.

Jaynes, E. T., 1978, Where do we stand on maximum entropy?:, *in* The maximum entropy formalism Cambrifge, Mass. M.I.T.

Loures, L. G., and Moraes, F., 1999, Inferência bayesiana de porosidade em poços: Inferência bayesiana de porosidade em poços:, Gociedade Brasileira de Geofísica, Annual Meeting Abstracts, SBGF33299.

Moraes, F. S., and Scales, J. A., 2000, Local bayesian inversion: theoretical developments: Geophys. J. Int., **141**, 713–723.

Local porosity inversion of multiple geophysical data sets. Part II: incorporating elastic seismic modeling

Luiz Geraldo Loures [†], *Fernando Moraes*[†]

Introduction

This work presents a methodology which incorporates seismic elastic inversion and equations from rock physics in a porosity reservoir characterization methodology by Loures and Moraes (2001). In part I, we presented a formulation for porosity inversion of well log data and seismic attributes. The latter was assumed to be obtained in an independent process by application of a generic inversion program without any uncertainty analysis. This led to naive statistical assumptions regarding the mutual dependency of the attributes to avoid additional inferences of the correlations.

Contrasting with Part I, here we formulate a method for performing a porosity inversion based on a Bayesian inversion of seismic data, which incorporates all the uncertainty analysis. The seismic inversion employs elastic reflectivity modeling and nonlinear conjugated gradients optimization to obtain a joint probability density function (PDF) for velocities and density of the medium. A change of variable is applied to produce posterior PDF for average layer porosity. A test using synthetic data is performed on a slowly varying porosity model (Figure 1) to show the impact of seismic data in the porosity estimates and their corresponding covariances.

Bayesian formulation

Consider a set of M layers with average porosity $\boldsymbol{\phi} \in R^M$. Our problem is to make inferences about model porosity from seismic data, represented by $\mathbf{d} \in R^N$. The Bayesian methodology is centered in obtaining a conditional PDF for the parameters under investigation $\boldsymbol{\phi}$, given the experimental data $\mathbf{d}$, which is the posterior distribution $p(\boldsymbol{\phi} \,|\, \mathbf{d})$.

According to Bayes' Theorem, the posterior distribution is obtained from the product of two other distributions: the prior distribution $q(\boldsymbol{\phi})$ and the distribution and the likelihood function $l(\mathbf{d} \,|\, \boldsymbol{\phi})$, which can be written as

$$p(\boldsymbol{\phi} \,|\, \mathbf{d}) \propto l(\mathbf{d} \,|\, \boldsymbol{\phi}) q(\boldsymbol{\phi}). \qquad (1)$$

We consider prior information about lower and upper bounds on $\boldsymbol{\phi}$ (respectively $\boldsymbol{\phi}_l$ and $\boldsymbol{\phi}_u$), in such a way that the prior distribution is uniform. In this case, the Bayesian formulation becomes

$$p(\boldsymbol{\phi} \,|\, \mathbf{d}) \propto l(\mathbf{d} \,|\, \boldsymbol{\phi}), \text{ for } \boldsymbol{\phi}_l \leq \boldsymbol{\phi} \leq \boldsymbol{\phi}_u. \qquad (2)$$

The next step is to define the likelihood function. Generally speaking, definition of a likelihood function involves two fundamental steps: the specification of the mathematical relationship between data and parameters and assignment of a statistical model (PDF) representing the uncertainty in the data. As far as we known there exists no mathematical formulation for seismic modeling as a function of porosity. There are, however, several rock physics studies, which provide formulas relating elastic seismic attributes to porosity. An isotropic elastic wavefield can be described by P- and S-wave velocities (respectively V_p and V_s) and density (ρ), which can be represented, respectively, in our layered medium by a set elements $\mathbf{s} = (\mathbf{s}_1, \mathbf{s}_2, \mathbf{s}_3)^T \in R^{3M}$. Using this representation, we may write that

$$\mathbf{s}_i = \mathbf{f}_i(\boldsymbol{\phi}) + \mathbf{e}_i, \text{ for } i = 1,2,3.$$

Following the same choices made in Part I, we select modeling operators f_i, for $i = 1,2,3$, respectively for V_p and V_s and ρ, as given by

$$V_p = 5.77 - 6.94\phi - 1.73\sqrt{c} + 0.446(P_e - e^{-16.7P_e}), \qquad (3)$$

$$V_s = 3.70 - 4.94\phi - 1.57\sqrt{c} + 0.361(P_e - e^{-16.7P_e}) \qquad (4)$$

(both from Eberhart-Phillips et al. (1989)), where P_e is the effective pressure and c is the clay content, and

$$\rho = (1 - \phi)\rho_m + \phi\rho_f, \qquad (5)$$

where ρ_m is density of the matrix and ρ_f is density of pore fluid.

At this point, we have obtained general form of the posterior for porosity given the seismic data (equation (2)) and established the relationships of seismic attributes to porosity (equations (3), (4) and (5)). The bridge between seismic data and porosity is still missing. This bridge may come from the analysis of the seismic inversion problem, which is done next.

[†]Laboratório de Engenharia e Exploração de Petróleo/Universidade Estadual do Norte Fluminense (LENEP/UENF), Macaé, RJ, Brasil. (gera@lenep.uenf.br, fernando@lenep.uenf.br)

Seismic elastic inference

We follow Gouveia and Scales (1998), who develop a Bayesian formulation of the seismic inverse problem. In their work, all uncertainties are described by normal distributions, but careful considerations are taken to construct the variance-covariance matrices. These matrices are responsible for expressing all uncertainties in a normal PDF.

According to Bayes' Theorem, the general formulation of the seismic inverse problem, can be written as

$$p_s(\mathbf{s} \,|\, \mathbf{d}) \propto r(\mathbf{d} \,|\, \mathbf{s})\, h(\mathbf{s}), \tag{6}$$

where p_s is the resulting PDF for the seismic attributes and r and h are, respectively, the likelihood function and the prior distribution.

In defining the probability models, one problem arrises due to the nonlinearity of the forward seismic problem $\mathbf{d} = \mathbf{g}(\mathbf{s})$, where $\mathbf{g}$ is the seismic modeling operator defined by the elastic reflectivity method (Muller (1985)). Even when the prior and the likelihood are Gaussian, the PDF for the seismic attributes p_s can not be obtained in closed form. Only in the case that the forward problem is linear, p_s is also Gaussian.

Standard solution is first to obtain optimum estimates for the seismic attributes, $\hat{\mathbf{s}}$. Then a Gaussian approximation for p_s is constructed on the basis of the linearization of the forward problem around point $\hat{\mathbf{s}}$. This optimization process is designed on the basis of equation (6) to yield the point of maximum probability density. When r and h are both Gaussian, maximizing probability density is equivalent to minimizing the argument of the Gaussian, leading to standard non linear least squares problem. In our case, we assume no prior information, which makes

$$p_s(\mathbf{s} \,|\, \mathbf{d}) \propto r(\mathbf{d} \,|\, \mathbf{s})\,. \tag{7}$$

and the argument of the likelihood

$$\arg(\mathbf{s}) = [\mathbf{d} - \mathbf{g}(\mathbf{s})]^T\, C_D^{-1}\, [\mathbf{d} - \mathbf{g}(\mathbf{s})] \tag{8}$$

The process of optimization by conjugated gradients used in Gouveia and Scales (1998), and adapted by our purposes, can be summarized by the following expression:

$$\mathbf{s}_{n+1} = \mathbf{s}_n + \alpha \boldsymbol{\delta}_n, \tag{9}$$

where $\boldsymbol{\delta}_n$ is the direction of the nth iteration step and α is the step length. The gradient of equation (8) is given by

$$\bigtriangledown\Theta = G(\mathbf{s})\, \mathbf{C}_D^{-1}(\mathbf{d} - \mathbf{g}(\mathbf{s})), \tag{10}$$

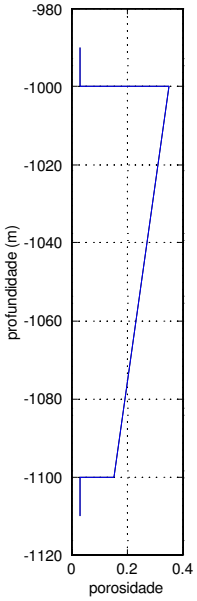

Figure 1: Porosity profile of the model.

where $G(\mathbf{s})$ is the matrix of Frechét derivatives (Gouveia (1996)) of the forward modeling term $\mathbf{g}(\mathbf{s})$. After completing the optimization process, the resulting Gaussian approximation for the seismic attributes around $\hat{\mathbf{s}}$ can be expressed by

$$p_s(\mathbf{s} \,|\, \mathbf{d}) \propto \exp\left\{-\frac{1}{2}\,[\mathbf{s} - \hat{\mathbf{s}}]^T\, \mathbf{C}_{\hat{\mathbf{s}}}^{-1}\, [\mathbf{s} - \hat{\mathbf{s}}]\right\}, \tag{11}$$

where the covariance matrix is $\mathbf{C}_{\hat{\mathbf{s}}} = \left[G_{\hat{\mathbf{s}}}^T C_D^{-1} G_{\hat{\mathbf{s}}}\right]^{-1}$ with the Frechét derivatives evaluated at $\hat{\mathbf{s}}$.

Posterior distribution

The missing bridge between seismic data and porosity, which is the key for assigning the likelihood r in equation (2), comes from the analysis of equations (2) and (7) and by expressing $\mathbf{s} = \mathbf{s}(\phi)$. The likelihood r of the seismic inverse problem is Gaussian and the dependency of $\mathbf{s}$ on ϕ is linear. In this case, by making a simple change of variables replacing the attributes for porosity yields a valid PDF, which is also Gaussian and can be used to represent the likelihood $l(\mathbf{d} \,|\, \phi)$ we have been looking for. In addition, in the case here where no prior information is been considered used, p_s itself can be used since it is the same as r.

Taking the above remarks into consideration, we may write the posterior distribution $p(\phi \,|\, \mathbf{d})$ as

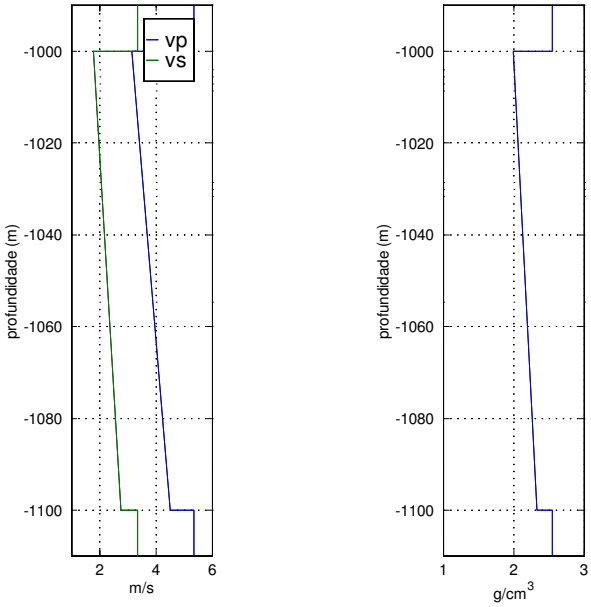

Figure 2: Elastic velocities and density for the model.

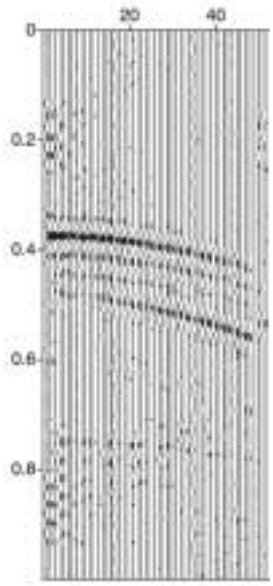

Figure 3: Vertical component of seismogram used in the inversion.

a Gaussian distribution given by

$$p(\phi \mid \mathbf{d}) \propto \exp\left\{-\frac{1}{2}\left[\phi-\hat{\phi}\right]^{T}\mathbf{C}_{\phi}^{-1}\left[\phi-\hat{\phi}\right]\right\}, \tag{12}$$

where $\hat{\phi}$ is the mean vector of porosity of the layered model and $\mathbf{C}_{\phi}^{-1}$ the inverse of covariance matrix. These elements are obtained from a simple change of variables applied in equation (11), after rearranging terms. Each element $\hat{\phi}_i$ from the vector $\hat{\phi}$ represents the porosity of the ith layer, which is given by

$$\hat{\phi}_i = -\sum_{j=1}^{3}\frac{1}{\beta_j}a_{j\times M-M+i}, \tag{13}$$

where β_j, for $j=1,2,3$, represent the angular coefficients from the equations (3), (4) and (5), respectively given by

$$\beta_1 = -6,94, \tag{14}$$

$$\beta_2 = -4,94 \tag{15}$$

and

$$\beta_3 = -(\rho_f - \rho_m). \tag{16}$$

The coefficients a_n, for $n=1,...,3M$ are obtained by the following expressions:

$$\begin{aligned} a_n &= 5,77 - 1,73\sqrt{c_i} + 0.446\,[P_{e_i} \\ &\quad -\exp(-16,7P_{e_i})] - \hat{s}_{j\times M-M+i}, \\ &\quad \text{for } n=1,...,M, \end{aligned} \tag{17}$$

$$\begin{aligned} a_n &= 3,70 - 1,57\sqrt{c_i} + 0,361\,[P_{e_i} \\ &\quad -\exp(-16,7P_{e_i})] - \hat{s}_{j\times M-M+i}, \\ &\quad \text{for } n=M+1,...,2M \end{aligned} \tag{18}$$

and

$$a_n = \rho_m - \hat{s}_{j\times M-M+i}, \text{ for } n=2M+1,...,3M, \tag{19}$$

where c_i and P_{e_i}, for $i=1,...,M$, are the clay content and the effective pressure, respectively, for the ith layer.

The elements $C'_{\phi_{k,l}}$ from $\mathbf{C}_{\phi}^{-1}$ are obtained by the following expression

$$C'_{\phi_{k,l}} = \sum_{j=1}^{3}\sum_{i=1}^{3}\beta_i\beta_j C_{\hat{\mathbf{s}}_{j\times M-M+k,\,j\times M-M+l\,i}}. \tag{20}$$

Synthetic data example

Consider a 1-D model of sandstone layer 100 m thick, under uniform pressure of 0,4 Kbar/cm^3 and saturated with oil pore fluid. The clay content of the model is constant and equal 0.05. The Figure 1 represents the porosity of the model. From the porosity model, using equations (3), (4) and (5) with the above values for pressure, fluid and clay content, we simulated the model velocities, which are represented in Figure 2.

A seismogram is computed using the reflectivity method. The geometry of the simulated experiment is defined on a line of 48 geophones with 25

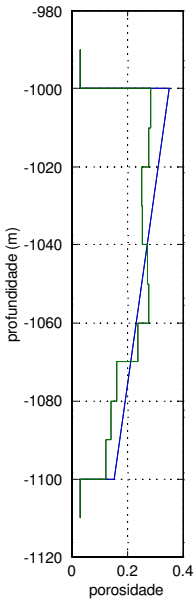

Figure 4: True porority and estimates given by the mean of the posterior distribution.

m spacing. The frequency range of the signal is 5 Hz and 50 Hz. The final seismogram, which is shown in Figure 3, has a component of a Gaussian pseudo-random noise yielding a signal/noise ratio equal of 20.

Estimates of seismic attributes $\hat{\mathbf{s}}$, resulting from the optimization process described above, are used to compute mean porosity by equation (13). The corresponding covariance matrix is obtained from $\mathbf{C}_{\hat{\mathbf{s}}}$ using equation (20). The mean and true value of porosity are shown in figure 4 and the posteriori covariance matrix $\mathbf{C}_{\phi}$ is shown in Figure 5.

Conclusion

The porosity variances and covariances are larger when porosity vary slowly between two adjacent layers. The top and bottom reflectors of the model are associated with high contrasts of impedances. Resolution analysis show that porosities from the top and bottom of the model are better resolved due to high impedance contrasts associated with top and bottom reflectors.

Acknowledgments

This work has the financial support from Finaciadora de Estudos e Projetos (FINEP), PETROBRAS and Fundação Estadual Norte Fluminense (FENORTE). We thank Dr. V. Priimenko for suggesting the change of variables used in this work.

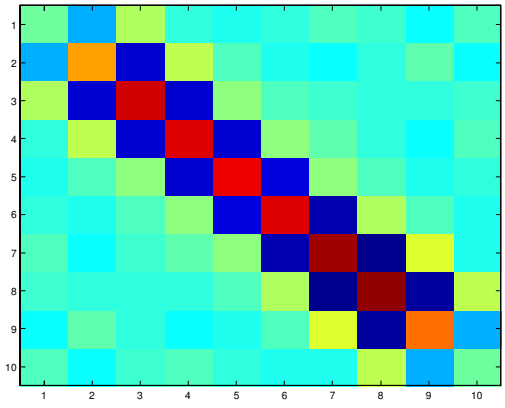

Figure 5: Porosity posterior covariance matrix.

References

Eberhart-Phillips, D., Han, D., and Zoback, M. D., 1989, Empirical relationships among seismic velocity, effective pressure, porosity, and clay content in sandstone: Geophysics, **54**, 82–89.

Gouveia, W. P., and Scales, J. A., 1998, Bayesian seismic waveform inversion: Parameter estimation and uncertainty analysis: J. Geophys. Res., **103**, 2759–2779.

Gouveia, W., 1996, Bayesian seismic waveform data inversion: Parameter estimation and uncertanty analysis: Ph. D. Thesis, Colorado School of Mines, Golden, CO, 145.

Loures, L. G., and Moraes, F., 2001, Local porosity inversion of multiple geophysical data sets. Part II: incorporating elastic seismic modeling: Sociedade Brasileira de Geofísica, Annual Meeting Abstracts.

Muller, G., 1985, The reflectivity method: a tutorial: Journal of Geophysics, **58**, 153–174.

One Step 3D Migration – A Tool to Improve Reservoir Pinch-Out Visualization

Amin Murad, & José Clauver de Aguiar Junior PETROBRAS S/A, Brazil

Abstract

One of the greatest difficulties found in reservoir geophysics is the lack of new seismic acquisition and pre-stack migration in 3D's acquired in the past. A way to improve the data image is to migrate the 3D data in one step in the PROMAX processing package. The response of it was excellent to get a good image from faults, making its traces better focused in the seismic sections, and so helping the mapping. This fact is very important in the location of development wells. The response was very satisfactory in positioning pinch-outs features of channels and/or lobes. It will be shown how this migration helped to solve some troubles in a Campos Basin oil field, where we have got a good amplitude response but only 10 meters of reservoir, or we could not define sand bodies limits.

One Step Migration in PROMAX

The one step 3-D migration algorithm uses extrapolators F-X-Y of finite differences with space variation. The data needs a square shaped mesh and one step migrated through McClellan transform that reduces the errors from two steps migration. The aperture angle was of 50^{o} and frequency band varied from 60 to 70 Hz in agreement with amplitude spectrum present in input data. In spite of needing a greater number of floating-point operations than that is used in two steps migration, the sharpness of final data and computational cost compensate as we obtained a good response in positioning events as well as improving the band of frequency of the migrated seismic data.

Fault Image

One step 3D migration acted in a way to locate better the fault planes facilitating its mapping, in relation the older processing and in relation to two steps processing (Fig. 1).

Features of Channels and/or Lobes Pinch-Outs

The one step 3D pos-stack migration facilitated the visualization of pinch-outs features of lobes and/or channels, in relation to the two steps 3D migration (Fig. 2).

Reservoir Characterization

This migration technique was employed to an oil field located in central portion of Campos Basin,

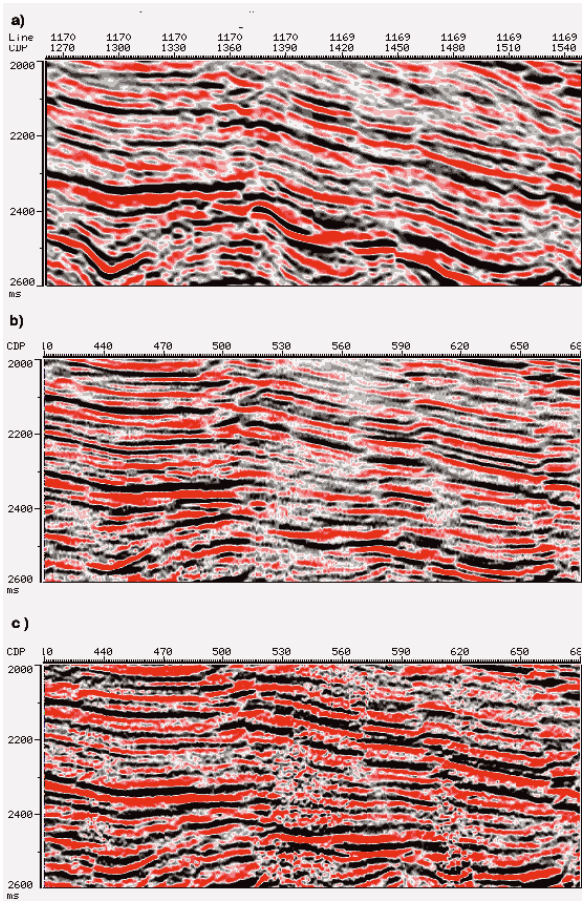

Figure 1 – Example of better fault image. a) Older seismic processing, b) Two step 3D migration, c) One step 3D migration

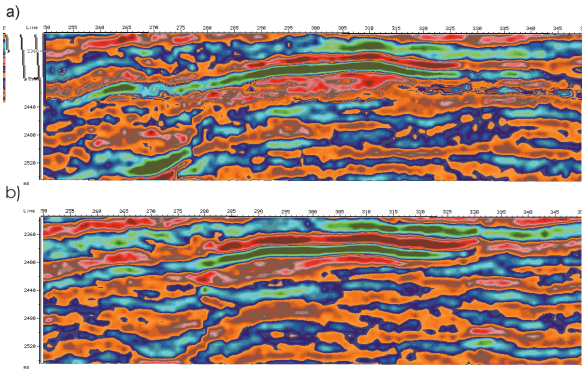

Figure 2 – Example of better pinch-out image. a) Two steps migration with weak definition of reservoir pinch-outs, around 2400 ms b) One step migration with good definition of pinch-outs.

southeastern offshore Brazil. The main reservoirs are Eocenic sandstones deposited in a channelized-turbidite system and characterized by a good to excellent reservoir properties, great lateral continuity and thickness in the depositional axis.

The one step 3D migration was a test as we were carrying along a greater reservoir characterization study, which involves inversion to obtain acoustic impedance data, which had showed better correlation with reservoir properties of interest

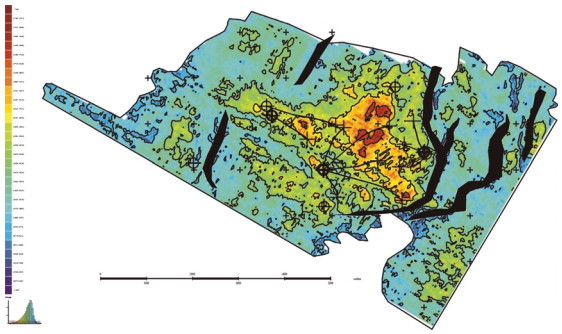

Figure 3 – Amplitude map showing good reservoir quality, even in NE extreme where the well has only 10 m of thickness.

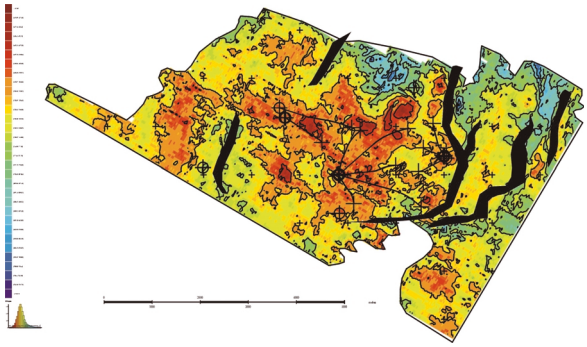

Figure 4 – Impedance map obtained between the top and bottom of reservoir. Showing in position of NE well, a reservoir quality corresponding to reality

The one step 3D migration helped to understand problems in the development of the field, where the amplitude map did not correspond the reality as the reservoir thinned around 10 meters to NE and amplitude response in this area corresponded to a good quality of reservoir (Fig.3). The impedance cube

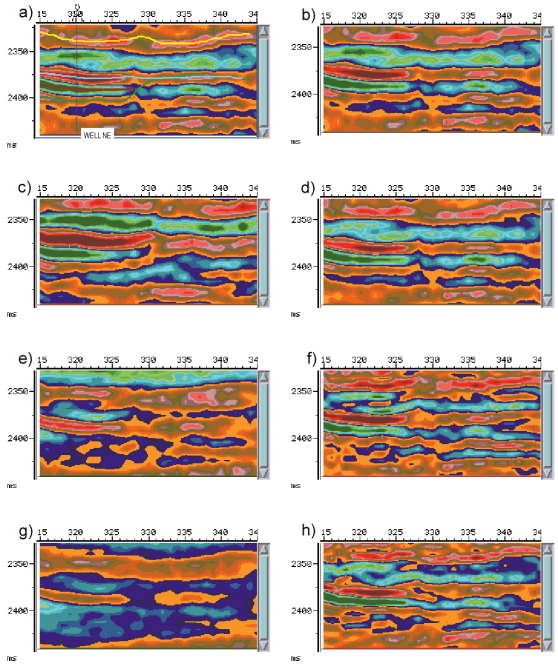

Figure 5 – Picture showing several seismic attributes, to demonstrate 3D one step migration efficiency. a) Two step migration in position of NE well. Brown line reservoir top yellow green line reservoir bottom. b) Same section without interpretation. c) One step migration, showing local pinch-out. d) Zero Phase Section. e) impedance section former interpretation. f) reflectivity section former interpretation. g) impedance section newer interpretation. h) reflectivity section newer interpretation.

shows similar features as one step 3D migration and strengthens it, as can be seen in impedance map (Fig. 4). The reservoir thinning is clearly seen in Fig. 5 where volumes of some other attributes in the position of the well of the NE extremity are shown. But the Fig 6 shows a section, in the same position of Fig 2, where we have two sand bodies of different ages in the southwestern (left) portion that even impedance data did not solve its limits very well.

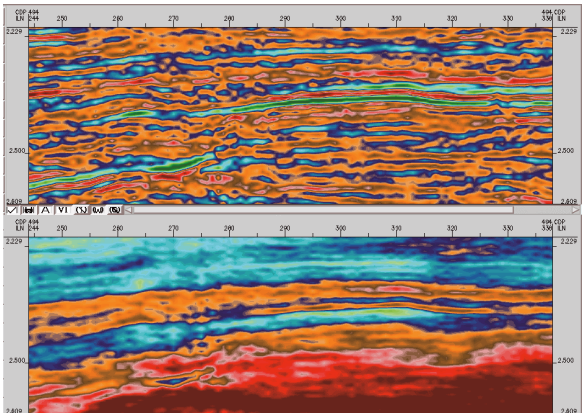

Figure 6 – Top. Amplitude section with two steps migration. Bottom. Impedance section without resolution to solve two sandstones reservoir. Compare with Fig.2.

Conclusions

The one step 3D migration supplies one better picture of seismic data helping to solve pinch-outs situations where we are not able to do seismic inversion or we do not have enough time to perform a pre-stack depth migration to solve troubles development of mature oil fields.

References

Hale, D., 1991. 3-D Depth Migration via McClellan Transformations. Geophysics, 56, 1178-1785.

Landmark, Manual of PROMAX

Schwedersky, G., Albertão, G. A., Mundim, E. C., Murad, A., 2000. Seismically constrained reservoir quality modeling – an example in Eocenic turbidites of Campos Basin, Brazil: SEG annual meeting, Calgary, Expanded Abstracts

Soubaras, R., 1992. Explicit 3-D Migration Using Equiripple Polynomial Expansion in Laplacian Synthesis: SEG annual meeting, New Orleans, Expanded Abstracts, 905-908

Seismic Delineation of Non-structurally Trapped Oil in Low Permeability Chalk

Nils L. Jacobsen, A. Uldall and Søren Priisholm,Mærsk Olie og Gas AS, 50 Esplanaden, DK-1263 Copenhagen K, Denmark, e-mail: nlj@maerskoil.dk

Abstract

Non equilibrium hydrocarbon distributions have recently been recognized representing a significant incremental development target within the low permeable Cretaceous Chalk reservoir off-shore Denmark. In the case of the Dan field, where production started in 1972 and more than 100 mainly crestal development wells have been drilled, the down flank area was based on a conventional hydrocarbon distribution model believed to have only limited development potential. Drilling of extensive long horizontal wells at the flank of the main structure, including one that set a world record horizontal section, found the oil in the better of the units extending down flank, and outside the structural closure far beyond what could be predicted from modelling of the saturation profiles observed in the crestal wells.

The availability of good quality 3D seismic data inverted to acoustic impedance has allowed mapping of high porosity streaks within the Upper Maastrichtian. These data have in combination with a more advanced hydrodynamic model proved essential in estimating the hydrocarbon distribution allowing the development of the flank area.

Introduction

The basis for the development of the Danish chalk fields has historically been pure structural hydrocarbon trapping given an initial field wide pressure equilibrium, including a flat free water level as modelled from the crestal exploration and development wells. Recent well evidences, however, suggest a significant more complex fluid distribution model. Re-evaluation of the low permeable chalk reservoir based on an integration of seismic attribute mapping with a revised, regional fluid distribution model has revealed a significant hydrocarbon upside potential suggesting that hydrocarbons on many structures extend far out on the flanks, below the structural closure, and that the free water level, and thus the fluid phases, are not in a state of equilibrium.

This paper demonstrates the value of 3D seismic data used to predict chalk matrix porosity that when combined with hydrocarbon saturation modelling from well data has resulted in delineation of a significant incremental volume of non-structurally trapped oil within low permeable chalk at the flank of the mature Dan Field offshore Denmark.

Field History

The Dan oil field (**Fig. 1**) is operated by Mærsk Olie og Gas AS on behalf of DUC (Dansk Undergrunds Consortium), and came as the first Danish oil field on production in 1972 and has since then been developed by more than 100 mainly crestal wells.

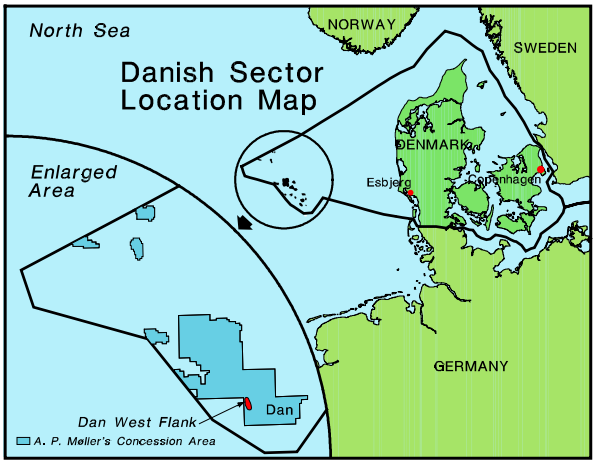

Fig. 1 Danish sector location map

The field has during the last years undergone extensive further development, latest the initiation of high rate water injection, where water is injected at pressure above the fracture propagation pressure. The daily production is currently over 100 Mstb. Part of the development program was to drill water injection wells at the flank of the field. This plan gave the opportunity to further appraise the lateral downdip extent of the hydrocarbon-bearing zone. As the field is uncompartmentalized, limited development potential was believed to remain at the flank with the reservoir strata being located several hundreds of feet downdip of the 50% Sw contour line predicted from data within the crestal part of the structure (**Fig. 2**). Drilling of a few long-reach horizontal wells in the flank area of this well investigated field thus provided new information important for an improved understanding of the mechanisms controlling the reservoir properties and hydrocarbon distribution within the low permeable chalk formation. Since 1998, nine up to 9 kilometers long horizontal wells have been drilled at the field's west and south flanks. These wells, that were completed with 4 to 6 kilometers long horizontal drain sections in Upper Cretaceous Maastrichtian chalk, consistently found the hydrocarbon zone extending far beyond expectations and with the best reservoir intervals being fully oil saturated.

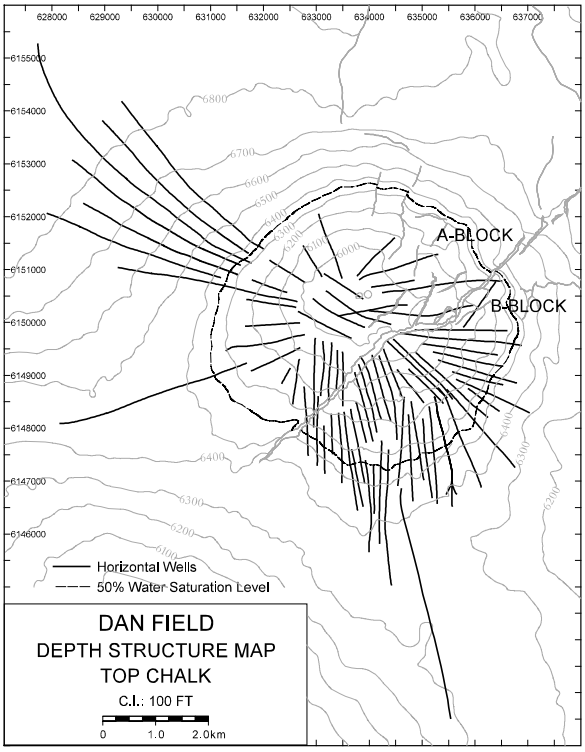

Fig.2 Dan Field depth structure map – Top Danian chalk showing the location of the long horizontal appraisal/production wells drilled outside the structural closure (6,400 ft contour). The 50%Sw line shown on the map is predicted from the crestal wells.

Saturation height modelling based on the reservoir information obtained from the wells estimates the free water level (FWL) to be strongly dipping at the flank, to a degree mimicking the present day structure towards the NW and SSE, and extending to a depth of about 2,200 m subsea or 200 meters deeper than observed in the crestal wells.

Reservoir Description

The Dan Field is a domal structure characterized by a major central fault, however from pressure data the field appears un-compartmentalized with vertical and lateral pressure continuity existing between the hydrocarbon and water bearing units on the field including the flank area. The reservoir is located at a depth of about 1,800m subsea, and the best properties are found within the Upper Maastrichtian interval where the chalk is formed as a predominantly pelagic sediment. The classical interpretation is that the porosity development of the autochthonous chalk is fairly predictable and dominated by a clear trend of porosity loss with depth[1]. The porosity at time of deposition was about 70% while it can decrease to as low as 15% at a reservoir depth of 2 to 3 kilometers. Early onset of overpressuring combined with hydrocarbon charging are believed to be among the main factors responsible for the present day high reservoir porosity of up to 40% found within the best reservoir intervals. In the case of Dan the reservoir chalk is characterized by high matrix porosity and a very low permeability (0.5 to 4mD) as is the case with many of the North Sea chalk fields. Natural fracturing appears limited[2]. Detailed geological studies on cores from all parts of the Dan Field have indicated the presence of a repetitive or cyclic bedding development in the Upper Maastrichtian[3]. Characteristic cycles of 1 to 10 meter scale can be stratigraphically correlated in cores as well as on wireline logs across the field[4]. Variations in the sedimentation rate and other processes affecting the sedimentary fabric are believed to be the main cause controlling the cyclicity. Each cycle consists of a high and low porosity interval and is thus responsible for the observed large vertical porosity variations. Laterally the porosity development of the units appears much more homogeneous.

Flank Appraisal

Drilling of the first flank well in 1998 to the west found the oil bearing Maastrichtian reservoir section extending far beyond the lowest closing contour at 6,350 ft SS (1,935 meters). Later appraisal by two horizontal wells drilled to the south-west and north-west respectively, confirmed the oil leg to be present on the entire west flank. Recent appraisal of the south flank has confirmed the existence of similar reservoir properties towards the south, while also indicating a more complex hydrocarbon distribution pattern, not only linked to the presence of a high porosity chalk matrix but in addition showing a likely overprint of the early hydrocarbon filling history. The northern and eastern flank appears of less interest as the best reservoir intervals seem to pinch out in that direction.

From pressure and fluid saturation measurements, vertical and lateral pressure continuity seems to exist between the hydrocarbon and water bearing units on the field including the flank area. The oil column observed by a long well to the North-west, could thus be traced within the main reservoir unit for more than six kilometers resulting in an oil saturation of 50-60% at the TD location of the well positioned more than 200 m structural deeper than the 50% Sw level modelled in the central part of the field.

The Maastrichtian pay zone at the flank of the field is 25 meters or less thick compared to the four times thicker column existing in the main field. It can be subdivided into a number of more homogeneous porosity units of which the best sub-unit, M1b1, is just 2 meters thick and with an average porosity of 33%.

Impact of 3D Seismic

Two generations of 3D seismic data exist across the Dan field comprising a 1988 and 2000 survey, and the well placement has thus been assisted and evaluated by these data. The availability of good quality 3D seismic data inverted to acoustic impedance has allowed mapping of high porosity streaks within the Upper Maastrichtian. The best reservoir units appear to pinch out towards the North and East and recognizing this the seismic data have thus proved essential, not only in the well planning, but also as an indicator of the likely lateral extent of the producible reservoir. Guided by the seismic data the now nine horizontal flank wells have thus all been completed successfully in the thin reservoir unit. The seismic data do not allow resolving all details of the stratigraphic column and steering of the wells during drilling is further supported by a combination of high resolution micro-palaeontological data from ditch cuttings, cyclostratigraphic correlation (where the horizontal well bore discordantly covers a stratigraphic interval) and saturation evaluation. In some of the wells real-time LWD data from the 'up-down' density tool have proved vital in determining when the well bore moved up or down stratigraphically during drilling.

Seismic Impedance Processing

Seismic acoustic impedance data are used to predict the porosity of the reservoir zones. As normal for properly zero phased seismic data where the necessary seismic wavelet is well determined, the data could be inverted to relative acoustic impedance using standard processing techniques. However, as the resolution is restricted to the seismic bandwidth, in this case of approximately 8 to 70 Hz, special provision is required to produce an accurate low frequency model. The dominant low frequency trend that needs to be added to the inversion result to obtain the correct absolute impedance level could in this case be derived from well data and interval velocities derived from regional horizon consistent seismic velocity data (HVA data). This process is relatively delicate and little software exists that can secure producing a reliable absolute porosity estimate. The quality and accuracy of the final absolute acoustic impedance volume therefore rely heavily on the experience of the interpreter.

Seismic Porosity Mapping

A good correlation exists between log derived acoustic impedance and porosity data and the seismic inverted absolute acoustic impedance volume could in this case be converted directly to apparent porosity.

The term apparent porosity is used, as the derived porosity does not take the distorting effect of possible gas or shale content into account. The chalk is generally quite clean, with about 3% clay and silica, and the effect of shale on the acoustic impedance is negligible. However, the presence of gas is a potential larger problem as the inversion derived apparent porosities are tuned to wells without gas and therefore tend to overestimate the porosity within any gas charged zone. The seismically derived apparent porosity volume was calibrated to regional well control represented by a substantial database of about 100 wells. The well porosity estimates are based on log-density measurements and consistently corrected for the effect of fluid fill. The distribution of the variations between the seismically derived porosity at the well location shows an overall standard deviation of 2.4 p.u. The prediction quality was tested against a number of wells not included in the calibration process. The mean error is -0.5 p.u. for the gas free wells with a standard deviation of 3 p.u. Gas bearing units have a mean error of 1.2 p.u. As expected the calibration process has resulted in a tendency of the seismic to slightly underestimate the porosity in the gas free zones while the porosity is over estimated by about 1 to 2 p.u. in the gas bearing part of the reservoir.

The porosity volume was depth converted using the inversion derived velocity field to provide a data cube populating the individual reservoir zones. As the high porosity intervals, above 25%, represent the potential target zones these could be identified directly using voxel based technology in this case suppressing values below 25%. Values above 50% are similarly excluded as these represent porosity overestimates due to the data not being corrected for gas effects. Maps representing individual reservoir zones are produced from the depth porosity cube (**Fig. 3**).

Reservoir Prediction

The mapped structural and stratigraphic model, including the seismic controlled porosity volume, combined with the modelled FWL that controls the hydrocarbon saturation, is used as input for reservoir simulation studies and in the estimate of the in-place volumes. The integrated reservoir modelling, strongly guided by the seismic data, thus concludes that a sizable volumetric upside exists on the West, North-west and South flank of the Dan field, and linked to the extent of the high porosity Maastrichtian M1b1 subunit. The main factors controlling the oil accumulation in the flank area are thus enhanced reservoir porosity combined with a significant deepening of the free water level towards the North-west and South.

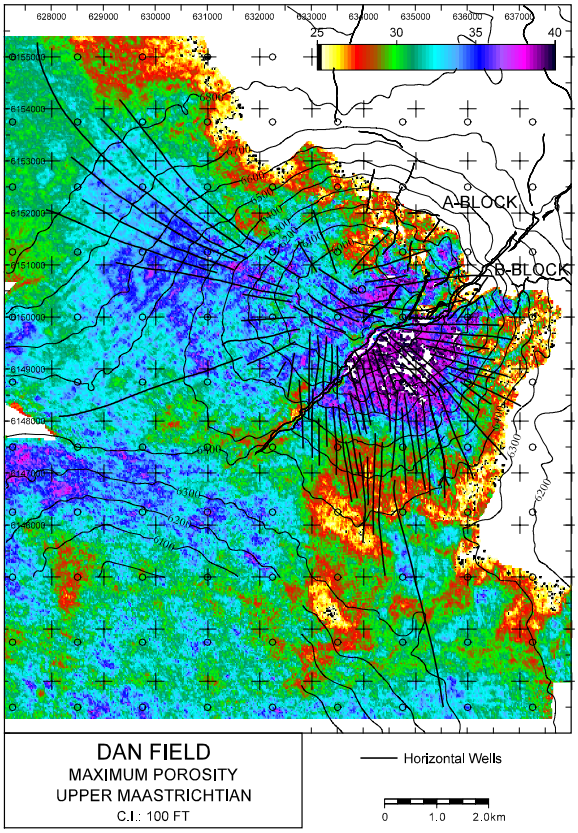

Fig. 3 Porosity Map at Upper Maastrichtian Level predicted on basis of inverted seismic Acoustic Impedance data. Depth contours are at Top Chalk Level.

Re-equilibration of the hydrocarbon accumulation in the tight low permeable chalk is an extreme slow process acting on a geological time scale and may thus be affected by late structural changes during the Tertiary period. In the case of the Dan Field gas-cap compaction combined with a continuing re-migration and possibly present-day charging of the area, are believed to be the main factors responsible for the significantly dipping fluid contacts. The outline of the fluid column shows some resemblance to the paleo-structure at time of hydrocarbon migration when considering also later structural changes. However, other parameters as the early charging history, that is not yet fully understood, may also be partly responsible for the present day relatively complex fluid pattern.

Conclusions

Drilling of excessive long horizontal development/appraisal wells with up to 6,000 meters long reservoir sections in the flank area of the mature Dan field and outside the mapped main field hydrocarbon accumulation has resulted in adding substantial extra reserves to the field. The availability of high resolution 3D seismic data inverted to porosity has proven to be one of the key parameters allowing successfully drilling of long horizontal production wells into the just few meters thick main reservoir zone. Saturation modelling based on data extrapolated from the crestal reservoir section suggests the distal flank to be substantially below the hydrocarbon zone. However, the wells found a continuos oil zone extending more than 200 meters vertically down flank from the FWL modelled in the crestal part of the field. The wells have thus provided the data necessary for an improved prediction of the regional FWL showing a continuous oil accumulation with a significantly more complex fluid distribution than could be mapped from well data obtained in the central part of the field. The lateral variations in the hydrocarbon saturation observed by the flank wells indicate a complicated charging and drainage history. In this case the availability of two generations of seismic 3D data are further being used in a pilot study investigating possibly 4D effects.

The observations made in the Dan field have renewed the exploration interest for the chalk looking not only at the obvious structural traps, but now focus more on the stratigraphic and hydrodynamic components including combinations of high porosity zones, paleo-structures and hydrodynamic flow patterns. A significant oil volume has thus been found trapped in a dynamic condition related to a low relief and non-closing structure. 3D seismic data have also in this case proven a key element guiding the development drilling by predicting zones of enhanced reservoir quality.

References:

1. Scholle, P.A., “Chalk Diagenesis and Its Relation to Petroleum Exploration: Oil From Chalk, a Modern miracle” AAPG Bulletin, 61:7, (1977), p 982-1009.
2. Jørgensen, L.N.: “Dan Field - Denmark, Central Graben, Danish North Sea”. In AAPG Treatise of Petroleum Geology - Atlas of Oil and Gas Fields. Structural Traps VI. Compiled by Norman H. Foster and Edward A. Beaumont (1992).
3. Scholle, P.A., Albrechtsen, T. & Tirsgaard, H., “Formation and diagenesis of bedding cycles in uppermost Cretaceous chalks of the Dan Field, Danish North Sea”, Sedimentology (1998), 45, 223-243.
4. Toft, J., Albrechtsen, T. & Tirsgaard, H.: “Use of cyclostratigraphy in Danish chalks for field development and appraisal.” In: Fifth North Sea Chalk Symposium (7-9 October 1996, Reims, France), Joint Chalk Research Program, TopicV (1996), p.1-8.

Acknowledgements

The authors like to thank Mærsk Olie og Gas AS and their partners in DUC; A.P. Møller, Shell Olie og Gasudvinding B.V. (Holland) and Texaco Denmark Inc. for their permission to publish this paper.

Seismically constrained reservoir quality modeling – an example in Eocenic turbidites of Campos Basin, Brazil.

*Guenther Schwedersky (Petrobras/Cenpes) **
Gilberto A. Albertão (Petrobras/EPBC)
Evaldo C. Mundim (Petrobras/Cenpes)
Amin Murad (Petrobras/EPBC)

Abstract

The integration of seismic data into the reservoir characterization process is very important in cases where the amount of well information is sparse. This is the case for most of the Campos Basin oil fields as well as for the field object of this study. Due to the large well spacing in this field, the use of seismic derived attributes to constrain the reservoir modeling is of paramount importance. For this case, the seismic amplitude, the most common seismic attribute used for reservoir characterization in Campos Basin, shows very weak correlation with the reservoir properties mainly due to strong impedance variations of the overlain beds. The alternative attribute chosen was the acoustic impedance derived from a post-stack seismic inversion. Such attribute showed better correlation with the reservoir properties of interest and it was then incorporated to the reservoir characterization process *via* geostatistical procedures. Stochastic simulation algorithms were used to generate facies and porosity models: the acoustic impedance was used as a soft constraint for the facies modeling and the facies distribution conditioned the porosity realizations. Based on the geological knowledge of the reservoir, some porosity models were selected to be the basis of the flow simulation model.

Introduction

The main objective of the present work was to obtain models for some reservoir properties, such as porosity and facies, with the purpose of (i) improving the understanding of spatial relations among the different facies and structural blocks, (ii) aiding in the location of future oil-producers and water-injectors wells and (iii) obtaining more realistic images from the drainage system to supply the flow simulator.

The studied area is related to an oil field located at the central portion of Campos Basin, southeastern offshore Brazil. The main reservoirs are Eocenic sandstones deposited in a channelized-turbidite system and characterized by good to excellent reservoir properties (average porosity and permeability of 29 % and 1400 mD respectively, for the main lithofacies), great lateral continuity (around 2 km) and thickness (40 m in average) in the depositional axis.

The structural context indicates the acting of listric faults as controlling factor for the canyon formation and further sandstone deposition. After that, salt movement and associated fault reactivation were responsible for a structural inversion, promoting coincidence between greater thickness and higher positions of the reservoir structural top.

Initially the idea was to obtain seismic maps presenting reservoir internal stratigraphic zones, which could be defined through log characteristics. Nevertheless limitations related to the quality of seismic data processing in some portions of the studied area and to the diminishing of thickness under the seismic resolution became impossible such task. For this reason only top and base of the reservoir were considered as surfaces to determine the volume to be modeled. By the other hand the seismic expression of those chosen surfaces, especially the reservoir top, showed enough quality for a confident mapping.

Core descriptions for sampled wells in the field and neighborhood allowed the characterization of 5 reservoir and 7 non-reservoir lithofacies. The reservoir facies were characterized based mainly on the clay content and sedimentary structures that determined the observed differences in reservoir properties. After performing a detailed core - log calibration, four reservoir and one non-reservoir electrofacies remained and they were determined for the total thickness of the reservoir and for all wells of the studied area.

Acoustic impedance

The seismic inversion for acoustic impedance was based on a baysian algorithm (Brac et. al., 1992). The low frequency component of the acoustic impedance was derived from the logs of 8 vertical wells. For the reservoir modeling, more 10 deviated wells were incorporated to the data basis. Figure 1 presents a 3D image of the acoustic impedance along

the reservoir. Information about the connection of different blocks of the reservoir were obtained.

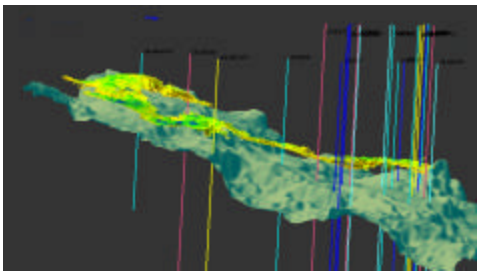

Figure 1: 3D image of the low acoustic impedance anomaly related to the reservoir.

Facies Modeling

To incorporate the seismic data into the facies modeling, the distribution of acoustic impedance (AI) for each reservoir facies was analyzed. Figure 2 shows the acoustic impedance Box & Whisker plot of AI against electrofacies (1 to 4). There is an overlap of events but if the facies are grouped (1-2 and 3-4) a reasonable discrimination of facies based on the AI is reached.

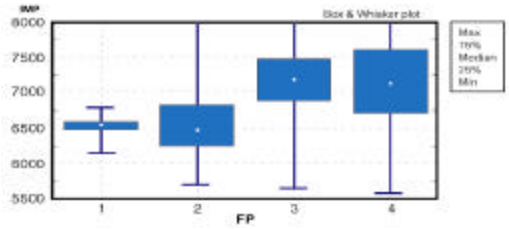

Figure 2: Acoustic impedance (IMP in g.m/cm^3.s) distribution for each electrofacies (FP).

Therefore two reservoir "AI" facies were defined: facies A related to the electrofacies 1 and 2 and facies B related to electrofacies 2 and 4. A third "AI" facies was defined as the grouping of non-reservoir rocks such as shales, diamictites and calcite-cemented sandstones. Figure 3 shows the calibration between these "AI" facies and the acoustic impedance. The AI cube was transformed into facies probability based on this calibration result.

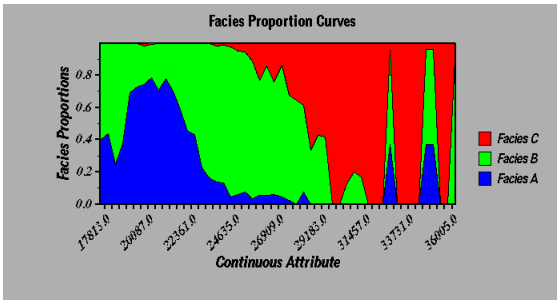

Figure 3: Relation between acoustic impedance (Continuous Attribute, in g.m/cm^3.s) and facies proportion.

To better explore the observed properties of the acoustic impedance-facies relation, a stochastic simulation was used in the facies modeling. Among many options of stochastic simulation, the P-field simulation (Deutsch and Journel, 1998) was selected. According to the concepts ot the conventional sequential simulations (i.e., sequential gaussian simulation), the covariance model reproduction is obtained considering each simulated value as a conditioning data for next simulation points. The conditional cumulative density function (ccdf) at each point to be simulated must be reconstructed at each realization. In the P-field simulation, these ccdf´s functions still the same from one realization to another, being conditioned only by the original data. The spatial correlation is obtained assuring the correlation between the probability values used to sample the ccdf´s. This procedure turns the P-field simulation algorithm much faster than the conventional stochastic simulation.

The speed characteristic of the P-field simulation algorithm allowed the generation of many facies models with different parameterization mainly related to the variogram. The "best" realizations were selected based on the geological knowledge about the reservoir.

The variogram parameters were estimated based on the well logs and seismic data. Due to the long distances between wells, the initial horizontal

ranges and anisotropy were estimated from the horizontal acoustic impedance variograms. These parameters were then changed and the results on the simulated facies model were validated also considering the geological knowledge of the reservoir. The vertical variogram was derived from the facies logs at the well locations. Figures 4 and 5 show a map and a cross section of one realization. These facies models were then used to constrain the porosity models generation.

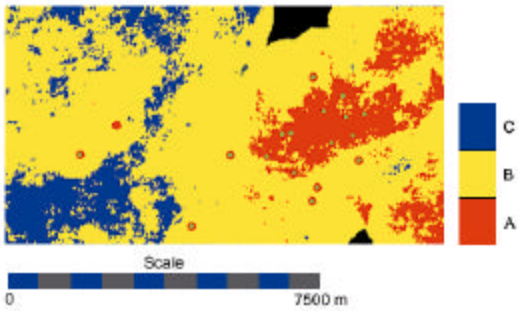

Figure 4: Example of one facies realization at an intermediate layer of the reservoir. Wells are represented as red-green dots.

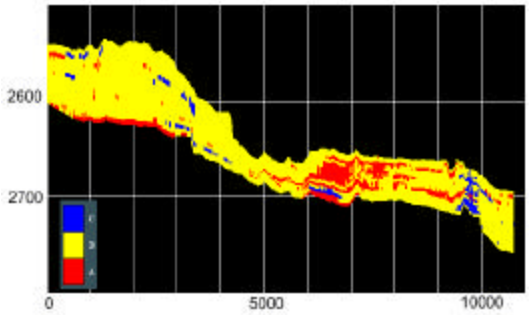

Figure 5: Example of one facies realization along a left to right cross section.

Porosity Modeling

Figure 6 is the Box & Whisker plot of effective porosity against facies. It comes from the plot that if the same facies grouping is used again each resulting facies (A to C) has a distinct porosity distribution. Based on that, a set of conditional sequential gaussian simulation of porosity was performed for each facies.

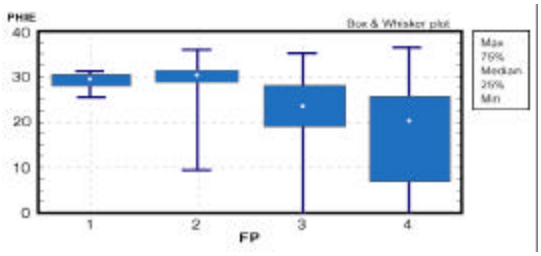

Figure 6: Effective Porosity (PHIE in %) distribution for each electrofacies (FP).

Figures 7 and 8 show one realization (map and cross-section) of porosity. From this set of porosity models, uncertainty maps were generated.

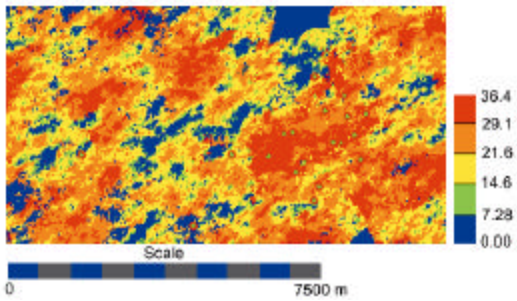

Figure 7: Example of one porosity realization at an intermediate layer (the same of figure 4) of the reservoir. Wells are represented as red-green dots.

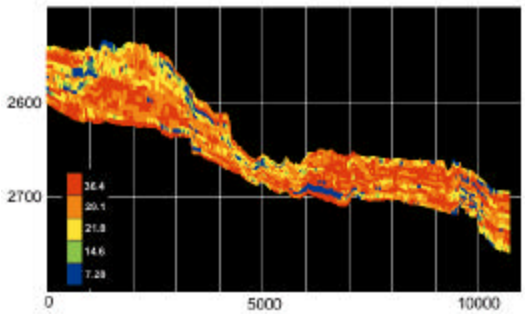

Figure 8: Example of one porosity realization along a left to right cross section (the same of figure 5).

Conclusions

At first, a better understanding of the connection between the two major production blocks was possible after analyzing the acoustic impedance data in 3D.

Facies definition and modeling were the key to incorporate the seismic information into the modeling procedure. Porosity models of the studied field were generated based on the acoustic impedance information, which by its turn derived from a seismic inversion procedure. The use of geostatistical tools allowed the evaluation of the uncertainties.

Next step will be to perform an upscale procedure where porosity and facies models will be the basis for the definition of flow simulation models.

References

BRAC, J., DEQUIREZ, P.Y., HERVE, F., JACQUES, C., LAILLY, P., RICHARD, V. and VANNHIEU, D. T., 1992. Inversion with a priori information: an approach to integrated stratigraphic interpretation. IN: *Reservoir Geophysics,* Sheriff, R.E. (ed), Soc. Expl. Geophy., Investigation in geophysics, vol. 7, pp. 251-258

DEUTSCH, C. V. and JOURNEL, A. G. 1998. *GSLIB – Geostatistical Software Library and User's Guide*. 2nd Edition, Oxford University Press. 369 p.

The 4D-4C at Teal South: what have we learned so far?

Simon Spitz, CGG Houston, Texas, US, sspitz@cgg.com
Roger Entralgo, ERCH, The Woodlands, Texas, US, roger@erch.org
William Haggard, CGG Houston, Texas, US, whaggard@cgg.com
James Hallin, CGG Houston, Texas, US, jhallin@cgg.com

Abstract

Acquisition and processing of repeated conventional seismic 3D surveys have demonstrated a positive impact on the management of reservoirs. The seismic time-lapse technology (4-D) is nowadays firmly established in the North Sea. Its own success points however at its financial limitation. Indeed, the need to better characterize and monitor the reservoir implies that there is a point beyond which the repetition of standard surveys becomes less economical than the installation of permanent arrays. The concept of the instrumented oil field that follows this simple economic observation opens the door to continuous, real time reservoir monitoring and makes possible the "smart" wells of the future.

Introduction

These last five years have seen a dramatic increase in the growth curve of conventional P-wave (acoustic mode) 3-D time-lapse surveys. The same pace has also characterized the number of multi-component 4-C surveys acquired on the sea floor. Combining the time lapse and the multi-component technology seems natural, yet until today no sea floor 4-D survey involving shear waves has been documented. Questions regarding seismic monitoring in the marine environment with multi-component technology remain therefore unanswered. Is the state of the art in acquiring and processing time lapse acoustic and converted shear waves adequate? If multi-component data are necessary to monitor fluid movement, is the acquisition and processing cost effective? What methodology will be needed in deep and ultra deep water?

The Houston based Energy Research Clearing House (ERCH) launched a multi million dollar consortium aimed at answering such questions. Eight oil companies (Agip, Anadarko, BP, Exxon-Mobil, Marathon, Petrobras, Shell and Texaco) joined the consortium as full participants, while eleven service companies (of which CGG was to perform the initial processing) joined as in-kind participants together with ten academic partners. The site chosen was Teal South, located off the Louisiana coast in Eugene Island Block 354, a field originally operated by Texaco and nowadays by Apache. The field produces oil with associated gas. The producing sands are located at a depth varying between 4500 and 7300 feet and the average porosity is circa 28%.

The sea bottom time-lapse layouts

The legacy data at Teal South concerns a 1996 surface (streamer) acquisition. In July 1997 Texaco acquired the 9 km sq. 4-C baseline survey. The cross spread configuration involved a primary vessel shooting with a single array source on a 25 by 25 m grid and the recording spread included four lines lying at a depth of 335 ft on the sea floor. The receiver lines were separated by 400 m and each line supported six 4-C receivers, spaced 200 m apart. The original layout was left in place for the second survey. Unfortunately, three original cables were lost, due to fishing trawler activity in the area. The acquisition of the second survey was completed in April 1999, with a similar shot geometry. Four cables were relaid and trenched as close as possible to the old locations. Three additional cables, that do not concern the 4-D study, were added to the field layout for further studies of the coupling conditions.

Processing the PP and PS modes

Data processing at Teal South had to solve several general problems related to:

- repeatability,
- fidelity of the recorded vector field,
- sparse receiver geometry.

As it can be easily imagined, these issues had a larger influence on the processing of the mode-converted data recorded by the horizontal geophones than on the processing of the acoustic data.

Repeatability, or rather the lack of it, was worrisome from the very beginning. Indeed, while the redeployment of the layout for the second survey led to an acceptable average mis-positioning of the 4-C receivers on the order of 20 m, two of them were found to be located more than 100 m away from their planned position. A receiver orientation QC of the PS mode detected errors in the orientation of the horizontal geophones in both acquisitions. These errors were corrected for in later processing. More importantly, the coupling condition between the geophones and the sea floor was found to be variable, not only between the two acquisitions, but also between geophones on the same survey. We did not

attempt to correct for that variability. Another important pre-processing stage was the removal of the cross-talk noise between channels. The orientation errors, the variability of the coupling conditions and the cross-talk noise were the major factors that affected the vector fidelity at Teal South.

While the processing of the acoustic mode raised no particular problem, that was not the case with the PS converted mode. After correcting for positioning and orientation errors, the data sets were rotated from the acquisition coordinate system to the radial-transverse coordinate system defined by the receiver-shot direction and the direction perpendicular to it. This new coordinate system is not only the natural one for processing the PS mode 3D data, but it is also the indispensable one for the study of any possible azimuthal anisotropy. Indeed, in a horizontally stratified and isotropic earth all the energy related to the converted mode lies on the vertical plane made by the radial and vertical receivers. In a horizontally stratified earth that contains at least one azimuthally anisotropic layer the transverse component vanishes each time the shot direction is along one of the two axes of azimuthal anisotropy.

Figure 1 shows the behavior of the data recorded by the horizontal components at Teal South. Such characteristic behavior cannot be ascribed to that of out of plane reflections. Because the direction of azimuthal anisotropy stayed constant at the various geophones, and because that direction was common to the two acquisitions, the data sets were rotated (as a first approximation) to the natural axes shown in Figure 1. For each acquisition, two volumes were constructed, the C1 and C2 volumes, that correspond to the wave fields propagating with respectively fast and slow velocities after the shear wave splitting induced by the birefringence phenomenon. At this stage of the discussion, the direction of natural axes of the azimuthal anisotropy at Teal South can be related to the regional directions of stress, parallel and perpendicular to the coast.

Processing resumed after analysis of the azimuthal anisotropy. The critical steps included shear static corrections for the leg propagating in the shear mode, deconvolution and velocity analyses combined with binning. The binning of the data itself was carried out in several stages. The first processing steps were based on an asymptotic binning with a Vp/Vs ratio of 2.8. The final binning was performed using a PS DMO algorithm, and involved an independent imaging of positive and negative offsets, followed by a focusing analysis for the determination of the optimal Vp/Vs ratios for the final binning (Herrmann et al., 1999).

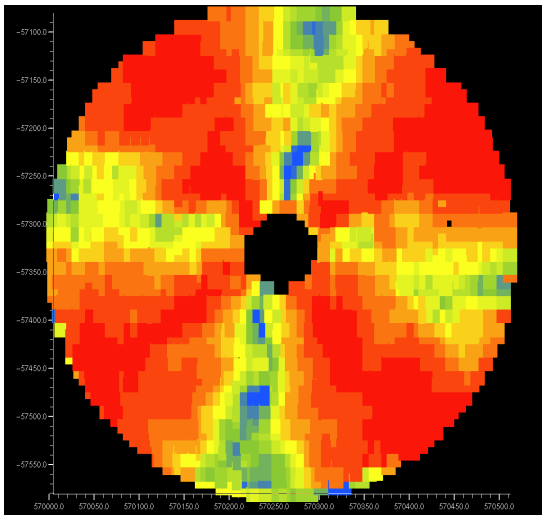

Figure 1 – The figure shows the ratio between the amplitudes recorded in the radial and transverse directions along one event on a geophone gather. The directions of the natural axes, defined by the high values of that ratio (in blue), can be easily seen. The NNE-SSW direction is the slow (C2) direction.

The presence of the birefringence at Teal South contributed to the multiplication of processed volumes. Besides the final results in the natural axes for both acquisitions, two other volumes were provided to the consortium members. For each acquisition, a 3D data set was constructed for which the effect of the azimuthal anisotropy was removed. This dataset (denoted by R') involved correcting the differences in velocity and amplitude of the fast and slow shear waves and rotating back from the natural axes to the radial component. The R' data sets generated (pre-stack) were carried through all the other processing steps to produce stack volumes.

Preliminary results

In the acoustic mode the non-repeatability and the various acquisition issues related to coupling had little impact on the quality and resolution of the final images. The acoustic 4-D signal was extracted after post stack cross-equalization of the second survey data volume (of higher quality) to the baseline data volume. Clear differences could be observed at the various reservoir levels, despite the relative short time lapse (18 months) between the two surveys. Figure 2 shows the 4D signal at the level of the 4500' sands. An expansion of the gas cap due to the release of free

gas from solution resulting from a pressure drop is a plausible explanation for the brightening and expansion of the amplitude anomaly between the baseline and the second survey. Time lapse amplitude changes concerning other anomalies are being investigated.

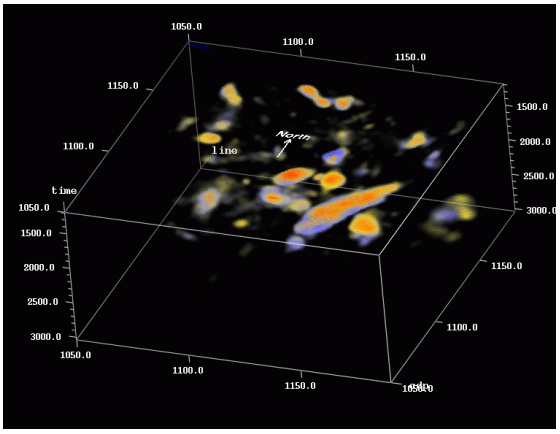

Figure 2 – The acoustic amplitude anomalies at the 4500' sand level (in the foreground). The acoustic amplitude anomalies recorded by the baseline survey (red), and by the subsequent survey (blue).

One troublesome aspect of the converted PS mode acquired data at Teal South is caused by the acquisition geometry itself. Optimized for the PP mode, the sparse geometry that characterizes the experiment, together with the tight mute zones defined at the processing stage, lead to an unsatisfactory distribution of offsets inside each bin. As a result, strong acquisition patterns can be observed in the shallow part of the data. Fortunately these acquisition footprints vanish at the depths of interest. Nevertheless, it is doubtful that the problem caused by missing offsets could allow a high spatial resolution PS AVO/AVA study.

As with the PP acoustic mode, the time lapse signal for the converted PS mode was estimated after stack, by matching the second survey volumes to the baseline survey. The fact that after cross equalization, time slices through the C1, C2, and the R' volumes display similar events recorded by the two surveys proves that the converted mode processing has actually preserved the relative amplitudes. Figure 3 illustrates this fact at the level of the 4500' sands. At that particular level, the lack of coherent PS mode events on the difference section (not shown) confirms the interpretation of the strong time lapse signal observed in the PP mode.

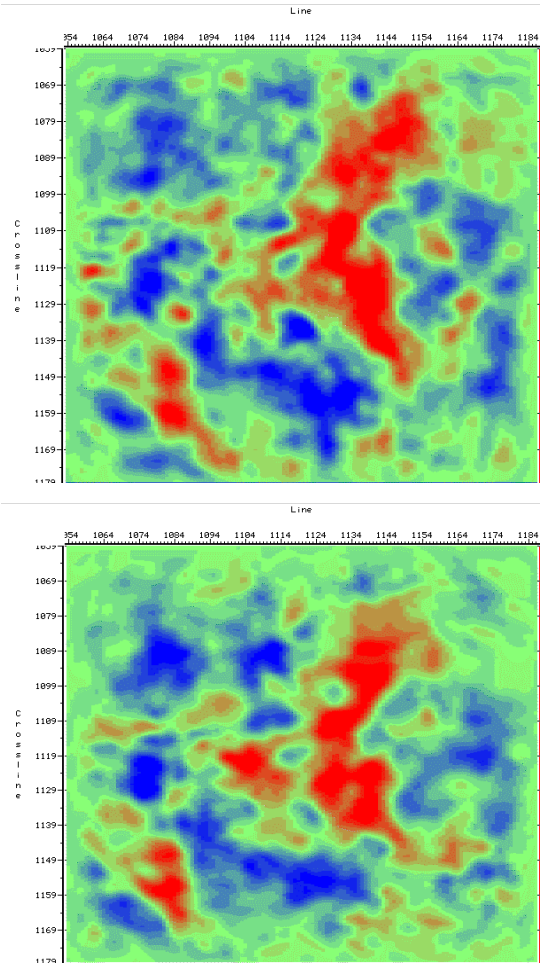

Figure 3 – Time slices through the C1 volumes at 3372 ms. Top: first acquisition. Bellow: Second acquisition.

Conclusions

The history of the seismic acquisitions on the sea floor at Teal South indicates the possibility of troubles at the processing and interptetation stages due to repeatability and coupling condition issues. A sparse 4C recording geometry is an additional concern; targeting the receiver layout to an optimal acquisition of the PS mode instead of the PP mode would certainly alleviate some processing problems. Finally, the Teal South experience proves that hasards due to sea currents should be carefully considered in deep waters: leaving the material simply lying on the sea floor can lead to disaster.

At this preliminary stage in the analysis, the experiment has shown that despite the repeatability issue and the relatively short time lapse between the two surveys, clear differences in the acoustic images could be observed due to the production at the various reservoir levels. In this respect, the Teal South experiment completes the information on sea bottom time-lapse acoustic seismic obtained from the Foinhaven 4D-2C experiment in the Nort Sea (see for instance Kristiansen et al., 2000). As expected, the differences between the two surveys in the PS mode are more subtle and their analysis is only just beginning. The PS differences are small and their random aspect is consistent with the interpretation of the fluid related changes observed in the PP mode between the first and second acquisition. Work is under way by other Teal South consortium members in order to extract more information from the PS data volumes.

Aknowledgments

The authors wish to express their gratitude to the Teal South consortium members for permission to present this paper.

References

Herrmann P., Michaud G. and Granger, P.Y., 1999, “Stacking P-S Converted Waves”, CSEG International Meeting, Calgary.

Kristiansen P, Christie P, Bouska J, O’Donovan A, Westwater P, Thorogood E, 2000, “Foinaven 4D: Processing and Analyssis of Two Designer 4Ds”, SEG International Meeting, Calgary.

Using Volumetric Visualization to Improve Reservoir Characterization

Carlos Eduardo Abreu, PETROBRAS Brasil
Márcio Spínola, Landmark Graphics Brasil
Walter B. Maciel, PETROBRAS Brasil
Marco S. Moraes, PETROBRAS Brasil

Abstract

This work discusses volumetric interpretation techniques of 3D seismic data. The main concern is on reservoir characterization processes and the way seismic can be integrated to well and other reservoir data, bringing new insights regarding the depositional models of the reservoir rocks, stratigraphic stacking patterns, structural geology and architecture.
Volumetric visualization techniques of 3D seismic data are presented, including color maps, histograms, opacity, attribute analysis, horizon, faults and voxel-based interpretation. Other advanced interpretation techniques, including image processing covering automated volume recognition (*Body Labeling*), morphology operations (*Morphology*), seismic volume math (useful for 4D seismic) and copy of seismic data using pre-defined *masks (Shape Cutter*) are also discussed.

Introduction

Volumetric interpretation techniques of 3D seismic data are presented, aiming on reservoir characterization processes, and the way seismic data can be integrated to well and other reservoir data to bring new new insights regarding the depositional models of the reservoir rocks, stratigraphic stacking patterns, structural geology and architecture.
Digital volumetric images can be generated from many different methods. Computer tomography (based on X-ray beans), magnetic resonance tomography, ultrasound, microscopy, and seismic acquisition and processing are some examples. These images play important role in medical imaging as well as in interpretation of geological bodies from tridimensional - 3D seismic volume, and are, actually, 3D image arrays corresponding to a stack of two-dimensional slices produced by some scanning technology (Lohmann, 1998). 3D seismic volumes are time or depth sequences of 2D images obtained from seismic acquisition and processing.
The building blocks of three-dimensional images are called *volume elements* or *voxels*[1]. A *voxel*, or volume pixel, is the smallest distinguishable box-shaped part of a three-dimensional image. *Voxels* are used to render seismic attributes like amplitude, impedance, coherence, etc.

For a true 3D image, voxels must undergo opacity transformation, which gives voxels different opacity values. This is important when it is crucial to expose interior details of an image that would, otherwise, be hidden by more opaque outside-layer voxels.
The most frequent visualization and volume interpretation techniques, including color maps, histograms, opacity, attribute analysis, horizon, faults and *Voxbody*[2] interpretation are presented. Then Advanced Volume Interpretation techniques are introduced, including image processing derived from medical industry.

3D Visualization Techniques

a) Color maps, histograms and opacity curves

Seismic interpreters highlight events on seismic data by simply addressing a color table to a range of attribute values. Usually, hot colors are used to emphasize seismic anomalies, such as those associated with oil bearing rocks, with high acoustic constrast with the embedded rocks. Generally, seismic anomalies of conventional P-wave data can be interpreted in terms of lithology changes, facies variation, and fluid content.
A typical histogram of an amplitude seismic data is show in Figure 1, with a normal distribution and zero mean. For other seismic values, such as acoustic impedance, other distribution should be expected. Histograms calculated from seismic data changes according to scale applied during data loading operations. Usually seismic data are stored in dynamic range format, from 8 to 32 bits.
For visualization and volumetric interpretation tasks, color tables are associated to a calculated histogram of seismic data, resulting in one specific color map or seismic view to express the distribution of that particular seismic attribute.
Opacity is a property of materials objects related to the transmissivity of light itself. For a true 3D image, *voxels* must undergo opacity transformation, which gives *voxels* different opacity values. We can think

[1] http://www.pcwebopedia.com/TERM/v/voxel.html

[2] Some definitions follow the Landmark's volume visualization tool EarthCube®.

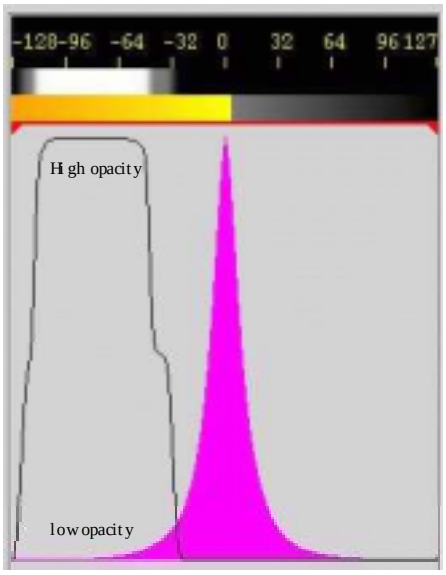

Figura 1 - Histogram, color map and opacity curve used for volumetric visualization of seismic data in Figure 2.

opacity in opposite terms: how transparent, for instance, a glass window is regarding the passage of light. In Figure 1, an opacity curve associates an opacity value for each amplitude value of the distribution. In this example, only the high negative values are viewable in the 3D seismic volume, resulting in the Figure 2 display, as show in the 8 bit scale in the top.

Opacity is an important visualization technique applied to seismic data. It enables interpreters to examine and comprehend the spatial relationship of seismic anomalies, whichever seismic data is under interpretation, amplitude, acoustic or elastic impedance, etc. Applying an opacity function (or transparency) to a seismic data, it is possible to filter the background noise values and focus on anomalies that may represent geological features, as show in Figure 2.

Since opacity is a pure visualization technique, from a top view perspective of earth model, we are stacking seismic anomalies in different time slices. Extreme amplitude values might be associated with zones of interest, for instance, carbonate or siliciclastic reservoirs, presence of fluids, etc.

Opacity leads interpreters to quickly focus on interest areas and furnish straight information on what is good to work on. Usually an amplitude analysis is performed observing how different the external geometry is, regarding opposite attribute values.

b) Horizon and Fault interpretation

Conventional horizon picking is usually carried out by manual or automatic picking in bidimensional vertical seismic sections at, for instance, each 5 or 10 inlines and/or crosslines, depending on the data signal-to-noise ratio. Then an interpolation followed by an automatic snaping to an onset (maximum, minumim, ou zero-crossing) is done. Quality control is performed by inspecting how interpreted horizons behave close to the well locations. Horizon interpretation is currently done after seismic-to-well tieing, and all geological markers and its corresponding reflectors in the seimic section are defined.

Horizon interpretation in the volumetric visualization approach is more dependent on the way interpreters select color scales and correspondent opacity curve, as show in Figures 1 and 2.

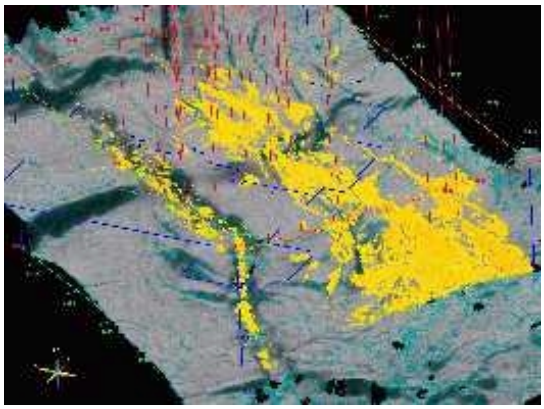

Figura 2 - Seismic volume rendered using parameters from Figure 1. In yellow, high negative amplitude values associated to reservoir rocks. The surface represents a tracked regional marker.

Opacity tracking enables interpreters to automatically extract horizons from seismic data based on opacity range values within which seed points lies. Tracking can be applied to particular data clusters that represent extreme continuous coherent reflectors and might be associated to the reservoir.

Regional geological markers, representing high impedance contrast, are more like to produce extensive horizon picking. In such cases, opacity tracking furnishes enormous advantage over the traditional interpretative workflow, done line by line and/or trace by trace. In areas with high structural or stratigraphical complexity, a closer inspection is done by using subvolumes, where a re-tracking is performed in this smaller volume.

The conventional fault interpretation methodology is carried out in a similar way, by inspecting bidimensional seismic profiles, where fault segments are

picked at each 5 or 10 inlines and crosslines, and then interpolated to generate fault planes. Fault interpretation is also strongly dependent on seismic quality.
Seismic plane animation is a suitable volumetric visualization technique to detect and identify faulted zones, and how it evolves through volume. Horizontal slice animation seems to be the best tool to quickly access the strucutural framework understanding.
Another valuable fault interpretation tool is based on post-stack seismic attributes analysis. During last decade, seismic coherence was one of the most intensively seismic attribute studied. Seismic coherence can be defined as the phase relationship maintenance through either a reflector or a set of reflectors (Damasceno, 2000). Combining horizontal coherence slices with previously interpreted fault planes reduces the risk of fault misinterpretation.
Ideally, fault plane interpretation should be done using the *opacity tracking* technique over a computed coherence volume. In this approach, an appropriate opacity curve should be used to enhance the low coherency values associated to the fault planes, in a computed coherence volume.

Voxbody and Volumetrics

Once reservoir targets were identified in particular zones, we can isolate different geologic intervals and compute hydrocarbon volumetrics through *Voxbody Interpretation*. *Voxbody* consists of a set of connected *voxels*, and can be generated by tracking or sculpting seismic volume.
Tracking consists in selecting parameters, such as amplitude range, neighbourhood criteria, and then picking a valid seed point (or multiple seed points) from the 3D seismic volume. Figure 3 shows a voxbody interpretation result from an amplitude anomaly.
Sculpting consists in defining an upper and lower surface (actually could be the same surface shifted in time/depth) and removing the seismic data above and below the bounding intervals. The result is a slab of seismic data that may contain, for instance, a parasequence.
Formation isolation via sculpting consists in a valuable technique that benefits interpretation. When combined with other techniques like opacity, an optical stacking furnishes valuable stratigraphic information. Hydrocarbon volumes can straight be calculated since interval velocity is given and each *voxel* represents line and trace intervals, for seismic in time. Also average porosity, net to gross and uncertainties associated can be addressed for quick volume estimation. Note however that care must be taken when calculating volumetrics specially because, seismic amplitudes may not correspond or resolve reservoir interval.

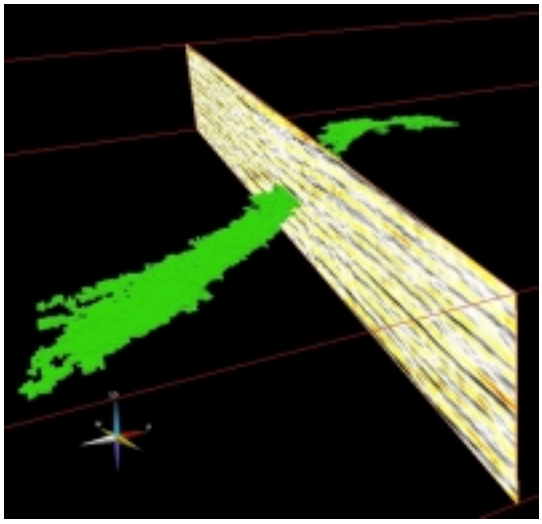

Figura 3 - Channel like feature interpreted in 3D through voxbody tracking.

Henry (1997) pointed out that without the understanding of wavelet as the filter through which geology is viewed when interpreting image provided by seismic data, there are many equally valid geological interpretations of the actual subsurface geology. Synthetic traces are compared to seismic data and the best correlation between them is determined. The main benefit brought by identifying high frequency well information (lithology, markers) on low frequency seismic information (high area coverage) is to provide the interpreter key links to identify reservoir facies.

Advanced Volume Interpretation

Advanced volume interpretation tools include image-processing techniques allowing *voxel* manipulation, automated feature (*Morphology*), seismic volume math (useful for 4D seismic) and copy of seismic data using pre-defined *masks (Shape Cutter*). Together all these tools can be combined to create structural or stratigraphic interpretation workflows. These tools enhance structural or stratigraphic interpretation workflows, enabling manipulation of multiple seismic attributes that combined with other types of information can be user to infer lithology, stratigraphy and other properties.
Body labeling is the first of these techniques, and allows interpreters to automated extract geological features without seed picking. It consists in defining volumetric criteria for isolating 3D features. Afer isolating reservoir bodies would be populating these regions with seismic data. One of the benefits of isolating seismic is working with seismic attributes of

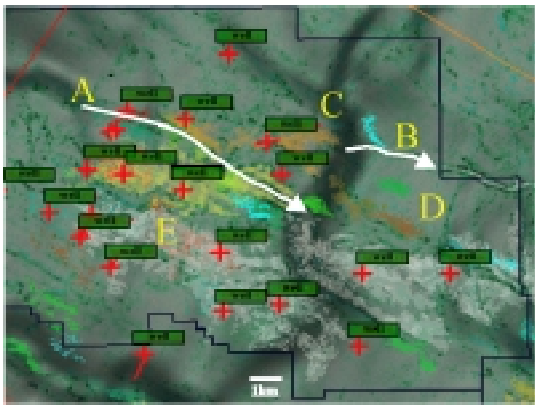

Figura 4 - Opacity tracked volumes over the strucutural map of a regional marker. Overlying this structural map, the coherence atribute extracted for this stratigraphic layer. (A) and (B) represents eroded and depositional channels. (C) and (D) main faults interpreted from coherence volume, and (E) the stacking pattern of turbidite sandstones. Wells are represented by red crosses, and tracked voxbodies are in white, green, blue, yellow and orange.

the interest zones, for volumetrics computation, horizon interpretation (voxbody wrapping) or body labeling. Figure 4 shows the result of body-labeling procedure applied on the Figure 2 data.

External Geometry and Reservoir Arquitecture

Volumetric interpretation with multi-attribute analyses is crucial when building geological model from seismic data. Important stratigraphic, depositional, diagnetic and structural features must be taken into account when building a consistent geological model. All these information, after a properly upscaling to a flow simulation model, will guide the decision-making process. Figure 4 shows how interpretation was greatly impacted by the large number of information simultaneously available in the same image, in a true 3D way. In (E), the low opacity value applied to the tracked Voxbodies enabled the visualization of a lower sand-body, in orange. The coherence attribute extracted over the interval of interest was superimposed to the structural map. Features assigned by C and D, representing some of the main faulting planes in the area, are also resulting from visualization process, with no previous interpretation.

The final reservoir model, represented by depth converted voxels, is show in Figure 5. The acoustic continuity between blocks, that controlled the tracking procedure, enables a good insight of possible hydraulic continuity. Considering this final voxel based model, all the estimates based on seismic properties and attributes were computed.

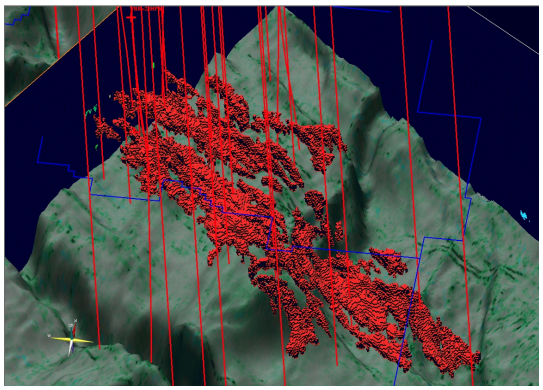

Figura 5 - Resulting depth converted voxbodies, from Figure 4, used to compute final volumetrics.

Conclusions

A review of volumetric visualization and interpretation techniques was presented. These tools combined enhanced reservoir characterization, bringing new insights in terms of depositional models, stacking patterns, structural geology and reservoir architecture in a giant turbidite oil-field off-shore Brazil, with a significant reduction in the seismic interpretation and geological modeling turnaround time. Another remarkable advantage of this approach is the work-team integration, enhancing the communication between geophysicists, geologists and reservoir and drilling engineers.

References

Damasceno, R. D., 2000. Aplicação da coerência sísmica à detecção de feições estratigráficas e estruturais. Tese de Mestrado, Universidade Federal da Bahia, Salvador, Brasil.

Henry, S., 2000, Pitfalls in Synthetics. The Leading Edge, June, 604-606.

Lohmann, G., 1998, Volumetric Image Analysis: Wiley & Teubner, 243p.

Landmark, OpenBooks. Postack Family Reference Manual. Marck 1999. Landmark Graphics Corp.

Woo M., Neider, J., Davis T., 1997. OpenGL Programming Guide. Addison-Wesley Developers Press. 2nd Ed. Massachusetts. 650p.

Acknowledgments

We would like to thank PETROBRAS and LANDMARK GRAPHICS for the courtesy to publish this work. We are also grateful to our colleagues from PETROBRAS-E&P, for valuable discussions.

Utilização da sísmica como deriva externa na krigagem do topo de um reservatório

Antônio Camilo Cruz Júnior – UNICAMP, Brasil.
Rui César Sansonowiski – UNICAMP, Brasil.
Sérgio Sacani Sancevero – UNICAMP, Brasil.

Resumo

O presente trabalho apresenta uma análise sobre o uso da krigagem com deriva externa para se obter uma melhor estimativa, por exemplo, do topo de um reservatório de petróleo. A vantagem da krigagem com deriva externa em relação à ordinária é que a variabilidade da variável secundária é assumida como deriva local da variável primária. A variável primária aqui é representada pela profundidade do topo de uma determinada zona do reservatório, obtida através de medidas realizadas em 53 poços. Como variáveis secundárias foram usadas, primeiro o imageamento sísmico, referente ao tempo duplo de trânsito (TDT) do topo da mesma zona do reservatório, e segundo,a mesma imagem do atributo sísmico porém processada e filtrada utilizando-se um filtro cúbico. Os objetivos deste trabalho são: realizar uma breve discussão sobre a metodologia utilizada para krigar o topo do reservatório com os dados de poço; analisar a estimativa feita através da krigagem ordinária e da krigagem com deriva externa; e comparar a utilização das duas variáveis secundárias citadas, como deriva externa.

Introdução teórica

A krigagem ordinária é o método de krigagem mais usado. Serve para estimar o valor de um ponto numa região cujo variograma é conhecido, usando dados de sua vizinhança, podendo também ser usada para estimar o valor de um bloco. Implicitamente avalia a média em uma vizinhança móvel. Na krigagem ordinária deseja-se estimar o valor de um ponto x_0 usando os valores dos dados de n vizinhos x_α e combinando-os linearmente com pesos ω_α.

$$Z^*(x_0) = \sum_{\alpha=1}^{n} \omega_\alpha \cdot Z(x_\alpha)$$

Assume-se que os dados são parte da realização de uma função aleatória intrínseca com um variograma γ (h). A característica de não viés da krigagem é garantida com a soma dos pesos sendo igual a zero. Minimizando a estimativa da variância com o controle nos pesos, obtemos então o sistema da krigagem ordinária:

$$\sum_{\beta=1}^{N} \omega_\beta \cdot \gamma(x_\alpha - x_\beta) + \mu_{KO} = \gamma(x_\alpha - x_\beta)$$

$$\sum_{\alpha=1}^{N} \omega_\alpha = 1$$

Onde, ω_α são os pesos a serem atribuídos para os dados, e μ_{KO} é o parâmetro de Lagrange.

O método de deriva externa consiste em integrar dentro do sistema de krigagem condições suplementares sobre uma ou mais variáveis de deriva externa S_i (x), i =1,...,N. A variável externa deve estar disponível em todas as locações onde a variável primária estiver bem como nos cruzamentos da malha a ser estimada. As condições:

$$\sum_{\alpha=1}^{n} \omega_\alpha \cdot S_i(x_\alpha) = S_i(x_0), \longrightarrow i = 1,..., N$$

são adicionadas ao sistema de krigagem.

Com esta definição de deriva externa, pode-se ter uma nova visão dos problemas de estimativa, na teoria da krigagem ordinária, a qual está ligada por funções aleatórias intrínsecas com um variograma γ (h).

A forma da deriva é definida implicitamente em cada ponto através da variável externa. Assim é necessário dispor da variável e que ela reflita a forma da variável primária. O sistema de krigagem com deriva externa, pode ser escrito:

$$\sum_{\beta=1}^{N} \omega_\beta \cdot \gamma(x_\alpha - x_\beta) - \sum_{i=1}^{N} \mu_i \cdot S_i(x_\alpha) = \gamma(x_\alpha - x_\beta)$$

$$\sum_{\beta=1}^{N} \omega_\beta \cdot S_i(x_\beta) = S_i(x_0)$$

Para: α = 1,...,N; i = 1,...,N.

Apresentação dos dados e Metodologia

Neste trabalho são considerados dois conjuntos de dados. O primeiro consiste da profundidade do topo de uma zona do reservatório, e o segundo dos dados sísmicos, duplo tempo de trânsito, relativo à mesma zona do reservatório.

A zona do reservatório a qual se referem os dados é um intervalo definido como Z3 em Mundim (1999), localizado num reservatório turbidítico na Bacia de Campos, Brasil. O reservatório está localizado na megasequência marinha transgressiva da margem continental leste. É formado por turbiditos depositados no paleocanyon cretáceo escavado em uma plataforma carbonática.

No intervalo Z3, a espessura de fácies reservatórios apresenta valor médio de 18,22m, variando de 0m a 64,40m. Pode ser identificado o caráter confinado das areias do reservatório que ocorrem em dois grandes bolsões.

Os dados referentes às cotas do topo da zona Z3 são originados de 53 poços localizados na mesma região. Os dados sísmicos de duplo tempo de trânsito da zona Z3, segundo Mundim (1999) são originados de perfis de 45 poços. A figura 1 mostra a localização dos 53 poços utilizados na krigagem do topo, juntamente com o sistema de falhas existente no reservatório.

Para a realização da krigagem dos dados referentes a profundidade do topo, procedeu-se uma análise geoestatística utilizando o software *ISATIS.*

O primeiro passo foi elaborar um mapa de variograma dos dados, para se identificar as direções preferenciais para a variografia, direções estas expressas em ângulos. A figura 2 mostra o mapa de variograma, utilizado para identificar as direções de anisotropia. O ângulo calculado para a direção de anisotropia mínima foi de 37º, sendo o de 127º calculado para a direção de anisotropia máxima.

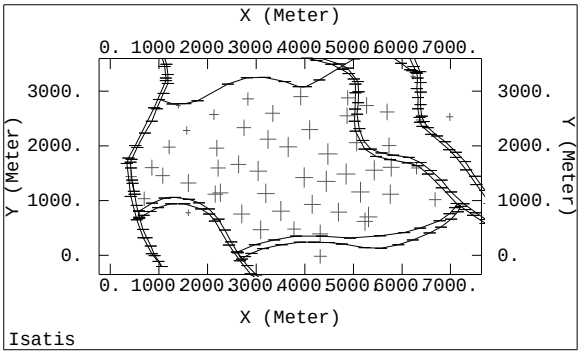

Figura 1: Mapa mostrando a localização dos 53 poços utilizados na krigagem do topo.

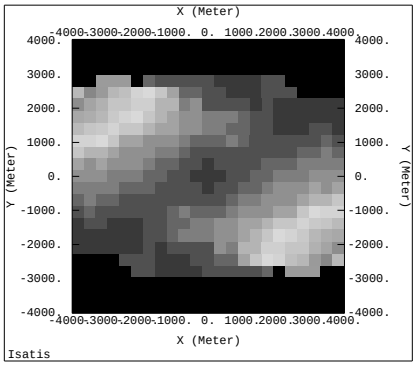

Figuras 2: Mapa de variograma dos dados.

Em seguida variografou-se os dados, juntamente a essa etapa foram modelados os variogramas experimentais. A figura 3 representa os variogramas experimentais, juntamente com o modelamento.

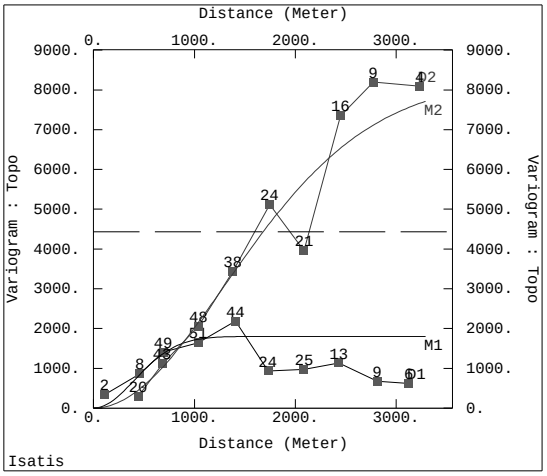

Figura 3: Variograma referente aos dados do topo.

Com os variogramas experimentais modelados, procedeu-se com a krigagem dos dados. A figura 4, mostra a imagem referente à krigagem do topo do reservatório utilizando-se os dados de profundidade dos 53 poços.

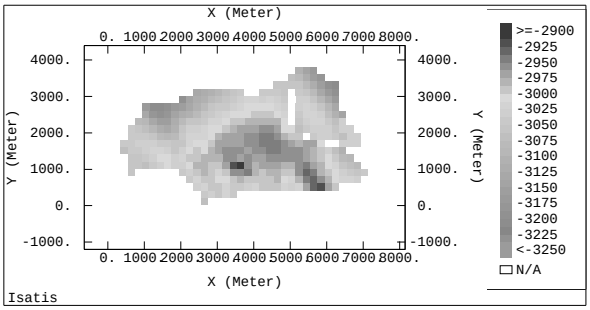

Figura 4: Krigagem do topo do reservatório.

Análise das imagens

A imagem representada na figura 4 será usada como base para as análises realizadas nesta seção do trabalho. Primeiramente uma krigagem do duplo tempo de trânsito, realizada por Mundim (1999), foi usada como variável secundária no procedimento da krigagem com deriva externa.Com isso obteve-se a krigagem do topo do reservatório usando como deriva o atributo sísmico TDT. Esta krigagem é representada na figura 5.

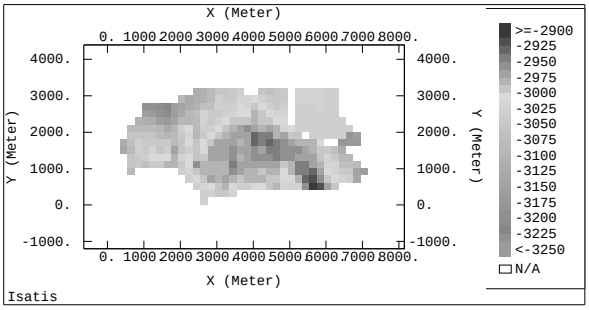

Figura 5: Krigagem com deriva externa, sendo a variável secundária o atributo sísmico TDT.

Quando se procede a comparação entre as figuras 4 e 5, o que se pode notar, primeiramente, é que a figura 5 está suavizada em relação à figura 4. Isso pode ser evidenciado ao notarmos a região localizada em X≅ 3500m,Y≅1000m. Na figura 4 esta região apresenta um valor muito elevado, destacando-se de sua vizinhança. Já na figura 5 este valor elevado foi suavizado igualando-se a sua vizinhança. Analisando região X≅5500, Y≅3000m o que se pode observar é que na figura 4 a queda nos valores é mais abrupta do que na figura 5. A região localizada na posição X ≅ 6000,Y≅500, não sofreu alteração, permanecendo com valores elevados.

Foi também utilizada como variável secundária para a deriva externa, a mesma imagem sísmica realizada por Mundim (1999), só que processada através de um filtro cúbico. A krigagem com deriva externa empregando o filtro cúbico como variável secundária é mostrada pela figura 6.

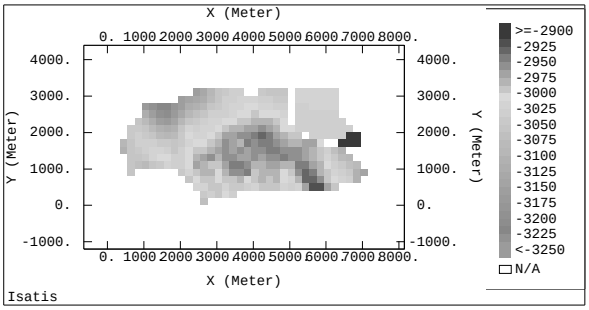

Figura 6: Krigagem com deriva externa, sendo a variável secundária o atributo sísmico TDT com filtro cúbico.

A suavização observada entre as figuras 4 e 5, manteve-se para a análise comparativa com a figura 6, porém deve-se destacar que a figura 6 é mais suavizada que a figura 5, levando-se em conta a região central do reservatório. Neste ponto vale a comparação entre as duas krigagens com deriva externa, ou seja, comparar as figuras 5 e 6. A região central do reservatório é mais contínua na figura 6, isso é evidenciado na região localizada em X≅4000m, Y≅2000m. Na figura 6 esta região apresenta valores mais uniformes, enquanto que a figura 5 mostra uma maior variação nos dados. A região localizada em X≅7000m, Y≅2000m, na figura 6 apresenta valores elevados, não mostrando suavização.

As comparações realizadas acima das figuras podem ser constatadas na análise da figura 7, que apresenta os gráficos de dispersão entre as três imagens geradas.

Ao se comparar os gráficos A e B nota-se que onde se empregou a deriva externa com filtro cúbico, a dispersão foi minimizada. Na análise do gráfico C, pode-se notar que as krigagens com deriva externa são bem correlacionadas, exceto na região não suavizada, citada anteriormente.

Nas imagens acima analisadas vale ressaltar que as regiões em branco se referem a pontos localizados em cima dos planos de falhas e que não tiveram seus valores krigados.

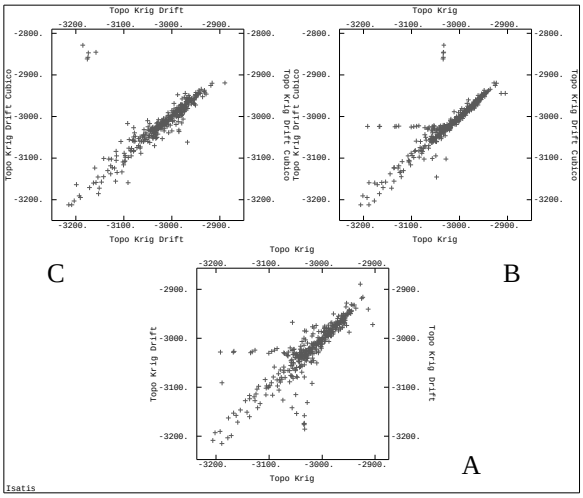

Figura 7: Gráficos de dispersão entre as três imagens geradas.

Conclusões

Após analisar as imagens e os gráficos de dispersão, alguns pontos devem ser discutidos. Com relação às imagens notou-se que a krigagem com deriva externa forneceu melhores estimativas para o topo do reservatório do que a krigagem ordinária realizada somente com os dados dos poços. Esta melhora na estimativa ocorreu, devido as variáveis secundárias controlarem as tendências tanto para os altos valores como para os baixos, suavizando a imagem krigada.

Ao se comparar as duas krigagens com deriva externa, nota-se que na região central do reservatório as duas fornecem estimativas próximas, sendo que a krigagem que utilizou o filtro cúbico como variável secundária, mostrou-se ligeiramente mais contínua nessa porção. Fato evidenciado nos gráficos de dispersão que apresentaram ótima correlação. As regiões localizadas em X≅6000m, Y≅500m e X≅7000m, Y≅2000m, apresentaram um valor elevado para a estimativa, que está relacionado ao fato da imagem krigada, não possuir dados nessa região. Ao se utilizar uma imagem como deriva externa, que possui valores nessa região, os valores são então extrapolados.

Sugere-se a utilização de imagens que utilizem filtros diferentes ou mesmo imagens de outros atributos sísmicos como variável secundária na krigagem com deriva externa, tentando suavizar mais os resultados.Para tentar solucionar o problema da região não suavizada deve se obter dados que alcancem limites além dos utilizados.

Referências Bibliográficas

- Wackernagel, H. Multivariate Geostatistics, Springer-Verlag, Berlin, 1995.
- Remacre, Z. A. Coestimativas, 1997.
- Mundim, C. E. Avaliação da krigagem fatorial na filtragem de atributos sísmicos: Um filtro geoestatísitico aplicado a caracterização de reservatórios, Dissertação de Mestrado, Unicamp 1999.
- Mundim, C. E.; Johann, P.; Remacre, Z. A. Factorial kriging analysis: Geoestatistical filtering applied to reservoir characterization, The Leading Edge, July 1999.
- Manual do programa *ISATIS*

VOLUMETRIC ESTIMATION – A CASE HISTORY TO EXPLAIN AN INTEGRATED METHODOLOGY

Jairo Rios Brandão Petrobras S.A / UN -ES - BRAZIL

Paulo Ernesto Vieira Petrobras S.A/ UN -ES - BRAZIL

Abstract

This study intends to demonstrate an application of a high-resolution method employed for volumetric estimation in complex reservoirs. The authors used a channelized turbiditic system that make up the Oligocene reservoirs of the offshore Peroá Field, located in the Espirito Santo basin, southeastern Brazil.

The focused reservoirs belong to a very complex system of turbiditic channels lying over a main Chattian unconformity. The turbiditic system was built by cut and fill processes produced by a braided subaqueous north- south trending channel system that created an autocyclic pattern over a complete low stand system tract facies.

The volumetric estimation employed two very common softwares in the petroleum industry, VoxelGeo® from Paradigm Geophysical and Seisworks® from Landmark.

Both these programs were applied as complementary tools to integrate data and to permit the use of the volumetric estimation method, which, roughly, has the following sequence:

(1) Seed detection of reflectors, (2) amplitude extraction, (3) calibration with well logs, (4) construction of grids and maps and (5) a volumetric estimation of individual and associated seismic reservoirs.

The application of this technique is useful in the sense of linking exploration tools in order to increase the critical capacity of interpreters to approach areas where complex stratigraphy may occur, such as those where channelized turbiditic fills are present.

Resumo

O objetivo deste trabalho é demonstrar um método alternativo de estimativa volumétrica em reservatórios complexos. O método foi aplicado no Campo de Peroá, região costa afora da Bacia do Espírito Santo, que consiste de reservatórios de arenitos turbidíticos depositados em um sistema canalizado tipo *braided*.

Estes arenitos por terem sido depositados em um sistema autocíclico, ocorrem segundo um padrão do tipo corte e preenchimento, o que torna difícil a sua correlação lateral, normalmente baseada em métodos convencionais com uso de poços e sísmica.

O trabalho utilizou dois *softwares* muito conhecidos o *Seisworks®* da *Landmark e* o *VoxelGeo®* da *Paradigm Geophysics*. Estes *softwares* foram empregados de modo complementar. O método consistiu das seguintes fases: (1) detecção de *voxels*, (3) extração de amplitude, (4) construção de grids e mapas e (5) estimativa volumétrica dos reservatórios, tanto individualmente como associados.

A aplicação desta técnica tem se mostrado útil, sobretudo em reservatórios complexos, onde existe dificuldade em estimar a continuidade e a geometria dos mesmos.

Os Princípios da Visualização Sísmica

A visualização sísmica tridimensional apresenta como característica a possibilidade de observar os dados de reflexão sísmica com vários níveis de transparência. O método de visualização é voltado à utilização do *Voxel*, que é um píxel tridimensional que representa uma amostra de dados. Cada *voxel* tem um valor que corresponde ao dado sísmico original, um valor de cor no padrão RGB e uma variável opacidade que permite ao usuário regular o seu grau de transparência. Cada traço sísmico é convertido em uma coluna de *voxels* (Kidd,1999). Desta forma, os píxels (*voxels)* são visualizados na tela do computador exibindo uma graduação de cor definida pelo usuário, o qual por sua vez, utiliza variações na opacidade das mesmas para obter o grau de visualização desejada. Na figura 1 pode-se observar como são tratados estes dados pelo usuário (Kidd, 1999; Becker, 2000).

O dado detectado através da visualização é observado aplicando-se diferentes níveis de opacidade e transparência. Este dado em conjunto com o dado sísmico permite a interpretação da distribuição espacial do objeto de estudo.

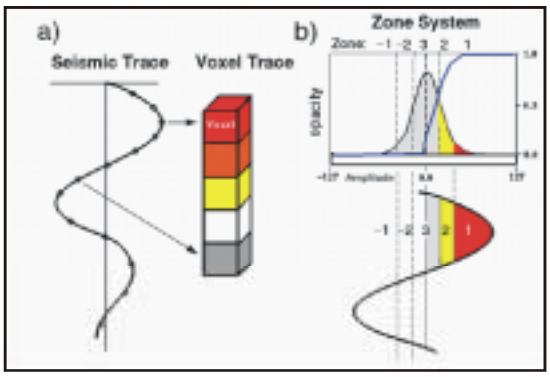

Figura 1 -a- Cada amostra de dados é convertida em um *voxel* com dimensões equivalentes às dimensões da cela e à razão de amostragem; **b-** Dados em 8 bits são mostrados em um histograma de distribuição normal com os valores dos *voxels* em relação às amplitudes. O recurso de opacidade permite filtrar as amplitudes desejadas em uma variável intensidade (Kidd, 1999; Becker, 2000).

Utilização dos Recursos de Amplitude Sísmica e Visualização

A variação entre as amplitudes sísmicas é dependente das diferenças de impedância acústicas entre os meios atravessados pela onda. Sabendo-se que a impedância acústica é o produto da densidade do meio pela velocidade de propagação da onda neste mesmo meio, pode-se concluir que a variação das amplitudes está intimamente ligada a atributos litológicos.

Os autores basearam-se neste princípio para aplicação dos dados obtidos na detecção sísmica no *VoxelGeo®* (figura 2) as quais representam volumes de amplitudes determinados dentro de um intervalo, que representa uma determinada espessura de reservatório turbidítico. A integração entre *Seisworks®* e *VoxelGeo®* torna-se mais facilmente realizável através do recurso *ULA* do *VoxelGeo®* que serve para exportar e importar dados de ambos *softwares*.

Os dados visualizados e detectados são convertidos em horizontes e carregados interpretados no *Seisworks®*. De cada horizonte reservatório obtém-se uma extração de amplitude em um intervalo determinado de tempo sísmico, que por sua vez representa uma determinada espessura.

A extração de amplitude é utilizada como critério determinístico para estimativa litológica. Dados de poços de correlação permitem a calibração das amplitudes com espessuras de reservatórios. Um gráfico como o mostrado na figura 2C permite obter a equação de calibração que deve ser utilizada na conversão de amplitude para espessura de rocha.

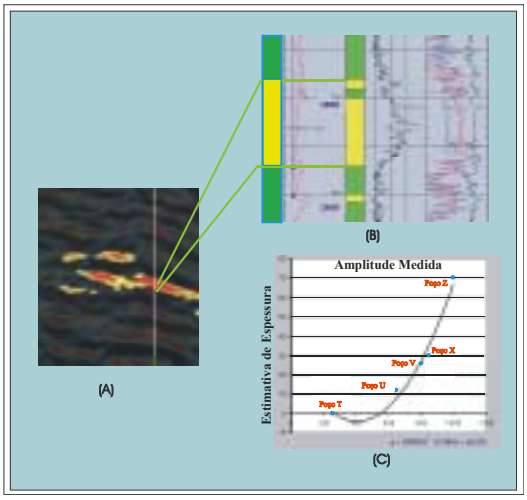

Figura 2 – Estimativa de espessura de reservatórios utilizando-se os recursos do *VoxelGeo®* e *Seisworks®*. Em (a) observa-se à detecção de um sinal correspondente a reservatório produtor no campo. Este reservatório apresenta uma espessura de 30 metros conforme determinado após a perfuração do poço X. A extração de amplitude entre este poço e os demais perfurados na área mostra uma correlação polinomial conforme mostrado em (c).

Conclusões

A técnica utilizada permitiu uma definição arquitetural dos depósitos estudados, dos limites e espessuras de rochas reservatórios e o controle de capeamento dos folhelhos adjacentes.

Foi comprovada a idéia inicialmente proposta por estudos em testemunhos e mapeamentos anteriores do modelo canalizado. A aplicação da técnica aqui discutida permitiu a interpretação do modelo deposicional e a compreensão de sua distribuição de noroeste para sudeste, originando-se em um cânion alimentador construído na borda da região paleoplataformal durante o início do Oligoceno Superior.

O reconhecimento do sistema deposicional, da arquitetura resultante do mesmo e das espessuras dos reservatórios, finalmente permitiu o cálculo da estimativa de volume do Campo de Peroá.

Embora este trabalho certamente não seja a palavra final em relação a volumetria do campo, visto que utiliza um método indireto para avaliação (método sísmico), ao menos representa um grande

avanço em relação ao trabalho até o momento realizado.

Pretende-se desta forma, demonstrar a importância da interação entre as várias ferramentas de interpretação exploratória existentes, tais como as de visualização sísmica e de interpretação convencionais, com o objetivo de obter uma interpretação mais confiável sobretudo em termos de confiabilidade de reservas, um atributo estratégico na exploração de petróleo.

Referências Bibliográficas

Becker, C. R., Grell A. P. , Hoerlle, M. R. 2000. Uso de Visualização Sísmica Tridimensional para Definição Estratigráfica e Geométrica de uma Acumulação Petrolífera na Bacia De Campos. Rio Oil & Gas Expo and Conference. RJ.Brazil.

Biassusi, A. S , Brandão, J.R., Vieira, P.E. 1999. Salt Tectonics and structural styles in the Province of the Foz do Rio Doce. 6th Int. Congr. Brazilian Geoph. Soc. Rio de Janeiro, 1999 Brasil.

Biassusi, A. S., Vieira, P. E., Brandão, J. R. 2000. Tectonostratigraphic Depositional Sequences of the Paleogene of Espirito Santo Basin, Brasil. Int. Geolog. Congr. Rio de Janeiro, 1999 Brasil.

Kidd, G. D. 1999. 1999. Fundamentals of 3-D Seismic Volume Visualization. The Leading Edge, June, p.702-712.

Vieira, P.E., Biassusi, A., Brandão, J.R.,1999. Arcabouço Preditivo de Fácies Arenosas no Terciário Offshore da Bacia do Espírito Santo. II Simpósio sobre Turbiditos. Petrobrás SA . Censud. Rio de Janeiro.